The Effect of Vertical Internals on the Hydrodynamics and Phase Dispersions in Bubble Columns: CFD Simulation and Population Balance Model

by

Siamak Agahzamin

Supervisor: Dr. Leila Pakzad

A thesis submitted in partial
fulfillment of the requirements for the
degree of Master of Science

Environmental Engineering Program
Department of Chemical Engineering
Lakehead University
Thunder Bay, Ontario, Canada, 2018

Abstract

The Effect of Vertical Internals on the Hydrodynamics and Phase Dispersions in Bubble Columns: CFD Simulation and Population Balance Model

Siamak Agahzamin

Vertical internals are widely installed in the bubble columns as heat exchangers or illuminating tubes. This research aims to investigate the effect of dense vertical internals (rods) on the performance of bubble columns. The Eulerian-Eulerian model coupled with the population balance model was used to develop the CFD simulation. The effect of interfacial forces on the results was studied by applying different models. The results indicated that just by choosing the appropriate interfacial forces, the numerical model agrees well with the experimental data. A sharper gas holdup, a stronger gas velocity gradient, and a more intense liquid recirculation were observed as important impacts of the internals. Moreover, three circular internals' arrangements were considered to study the effect of wall and core clearance distances on the bubble column hydrodynamics. The results revealed that by increasing the wall clearance distance, flatter gas holdup and velocity distributions could be achieved. Furthermore, the capability of the population balance model in the prediction of the bubble size distribution in the presence of internals was assessed, and a modification factor for the population balance kernels was proposed. Moreover, the impulse tracer injection was applied to study the gas dispersion in the bubble column. The results showed that the presence of internals has a notable effect on the gas behavior. Less turbulence and dispersion were found in the presence of internals. To study the liquid mixing, the tracer technique was applied. The presence of internals reduced the fluctuating liquid velocities, which led to a lower mixing performance in the bubble column.

Keywords: Bubble column, vertical internals, population balance model, gas dispersion, liquid mixing, CFD.

Acknowledgment

To My Family

Table of Contents

List of Figures

List of Tables

1. Introduction

Bubble column reactors are used in a wide variety of industries such as biochemistry, petrochemical, wastewater treatment, etc. Bubble columns can provide desirable mass and heat transfer in the absence of moving parts. Their simple structure and low maintenance cost have made them a popular type of multiphase reactors. On the other hand, the significant phase back-mixing and difficult scale up and design are their drawbacks (Youssef, 2010).

In the presence of suspended catalysts, the bubble columns are called slurry/bubble column reactors, which are associated with reduced plugging, high catalyst durability and online catalyst addition and withdrawal (Degaleesan et al., 2001, George, 2015). The slurry/bubble column reactors have gained great attention since they are considered as the best choice of the reactor for Fischer-Tropsch reactions (Krishna and Sie, 2000). Moreover, they can also be considered as a solution to enhance the performance of conventional methanol process. In the conventional methanol reactors, the catalysts are arranged in a fixed bed (gas cooled reactor) or the tubular forms (water-cooled reactor) (Agahzamin et al., 2016). In these kinds of reactors to avoid pressure drop, the catalyst particles with the diameters of over 3 mm are usually used, which led to a certain inner mass transfer resistance (Salehi et al., 2014). On the other hand, in the slurry bubble columns, usage of very fine catalyst particles ranging from 5 to 100 μm, (Degaleesan et al., 2001) reduce the mass transfer resistance. Moreover, a malfunctioning in the flow distribution or partially deactivation of the catalysts can cause an unexpected temperature drop in the catalyst bed (see Mirvakili et al., 2018). However, in the slurry bubble columns because of high mixing performance, a uniform heat transfer can be achieved to avoid cold spots.

In industrial bubble columns, the heat transfer is carried out by the installation of vertical heat exchanging tubes inside the bubble column reactors. The specification of the internals is determined regarding the heat of reactions, operating conditions, and construction issues. For processes with high heat of reactions, the higher internals' surface area is needed. For example, in a Fischer-Tropsch reactor with an annual capacity of 78000 T, a number of 1530 tubes with diameters of 38 mm are proposed (Casanave, 1999). In the literature, the presence of a high number of tubes per cross-section area is referred to dense internals (about 20% coverage of total cross-section area). On the other hand, the reactors with a low percentage of the covered area are referred to the sparse internals. For example, for methanol reactors, the 8% coverage of the area by internals

was found sufficient to maintain the desired temperature (Youssef, 2010). The presence of internals affect the hydrodynamics, bubble size distribution, and mixing performance in bubble columns (Chen et al., 1999; Forret et al., 2003; Youssef, 2010; Hamed, 2012; Al Mesfer et al., 2016; Kalaga et al., 2017).

Bubble columns can also be used as photobioreactors. In the photobioreactors, light is an essential source of nutrient for culture, so providing sufficient illumination is an import factor in the design of such reactors. For most commercial applications, sunlight is used as the light source (Miron et al., 2000). In these reactors (outdoor reactors), the cultivation of microorganisms is limited by the penetration depth of light into the reactor (Sutor et al., 2014). On the other hand, the light needed of phototrophic cultures can also be supplied by internal illuminating tubes. The efficiency of photobioreactors can be enhanced by providing uniform and sufficient light distribution over entire columns. The arrangement of internals not only affect the light distribution but also, can affect the hydrodynamics and mixing performance. Good mixing is required to minimize the dead zone and provide microalgae with desired carbon dioxide and nutrition (Muharam et al., 2017).

Bubble columns can also be exploited to study the nuclear reactors (Kalaga et al., 2017a; Yin et al., 2015). In the typical nuclear power generation plant, the fuel tubes, where the nuclear reactions take place, are surrounded by water to absorb the heat of reactions. Since the reactions are extremely exothermic, the water partially evaporates and forms bubbles. In this regard, bubble columns are widely studied as nuclear reactors in terms of bubble size distribution and fluid hydrodynamics. Bubble columns with internals have also been employed to study the physical effect of fuel tubes on the turbulence, mixing, and fluid behavior in heat exchangers of nuclear power plants (Kalaga et al., 2017a,b).

 Although in industries, bubble columns are commonly equipped with internals, the number of studies devoted to the bubble columns with internals is limited compared to the hollow bubble columns (with no internals). At the early stage, the focus of studies was on the impact of internals on the overall gas holdup (Yamashita et al., 1987; Pradhan et al., 1993; Saxena et al., 1992). Lately, optical probes were used to determine local properties such as radial gas holdup, bubble chord length (Youssef, 2010; Kagumba and Al Dahhan, 2015), and radial gas velocity (Hamed, 2012). The computed tomography (CT) techniques have also been applied to measure liquid velocity, turbulence parameters (Chen et al., 1999), and gas holdup (Al Mesfer et al., 2016) in the presence

of internals. Furthermore, radioactive particle tracking techniques were employed to investigate the hydrodynamics of obstructed bubble columns (Al Mesfer et al., 2017; Kalaga et al., 2017a,b). The effect of internals has also been the subject of numerical studies. Larachi et al. (2006) performed the first simulation of bubble columns with internals, where considerable changes in liquid velocity profiles and turbulent parameters were observed. Bhusare et al. (2017) presented the modeling and numerical development of a bubble column with internals. Guan and Yang (2017) discussed the role of interfacial forces in the simulations of bubble columns with internals. Guo and Chen (2017) coupled the population balance model with the CFD simulation to study bubble columns with different numbers of rods.

This study aims to investigate the effect of dense vertical internals (22% internals' coverage area) on the hydrodynamics of bubble columns. The development of the CFD simulation of bubble columns with and without internals are explained. The gas and liquid velocities, local and overall gas holdup, and turbulence parameters (e.g. k and ε) in the presence of internals are analyzed. The applicability of the population balance model in the bubble column with internals is discussed. Then, the impacts of the internals on the gas dispersion and liquid mixing are presented.

The next chapters of this dissertation are organized as follows:

Chapter 2, Literature Review: In this section, the important parameters in the study of bubble columns are reviewed; gas holdup, gas and liquid velocities, bubble size distribution, the presence of internals, and dispersion in gas and liquid phases are discussed. At the end of this section, the objective of this research is stated in detail.

Chapter 3, Multiphase Modeling: In this section, the numerical models to study the multiphase flows are reviewed. The principles of the multiphase and turbulence models are explained. The fundamental of population balance model and the breakage and coalescence kernels are summarized. Then, different frameworks to solve the equations of models are mentioned.

Chapter 4, Effect of the Vertical Internals on the Hydrodynamics and Population Balance Model in Bubble Columns: In this section, the development of CFD simulation to study the presence of internals are thoroughly explained. Afterward, the results of the simulation are presented. The complete discussion on the results is provided by comparing bubble columns with and without internals.

Chapter 5, Effect of the Vertical Internals on the Gas Dispersion and Liquid Mixing in Bubble Columns: In this section, the numerical methods to study dispersions in gas and liquid phases are explained. Then, the effect of the internals on the dispersion parameters are studied, and the results are compared with the hollow bubble columns.

Chapter 6, Overall Conclusions and Recommendations: In this section, the summary of results from the previous sections and the overall conclusions are given. Moreover, the author's recommendations for future work are presented.

2. Literature Review

Bubble columns, in their simplest structure, consist of a vertical cylinder equipped with a sparger at the bottom. The liquid phase in bubble columns can be in the batch mode, have a concurrent up-flow, or a countercurrent down-flow. The spargers, where through the gas phase enters the column, have different types such as perforated plate, ring shape, spider shape, etc. The effect of the sparger type on the gas holdup was found negligible in bubble columns with a diameter larger than 0.15 m, height to diameter ratio larger than 5, and a sparger with hole diameters larger than 1-2 mm (Wilkinson et al., 1992). The effect of sparger characteristics on initial bubble size and regime transition can be found in such studies as Kazakis et al. (2008) and Besagni et al. (2018), respectively.

In industries, bubble columns are commonly equipped with horizontal or vertical internals. Generally, in the case of horizontal internals, perforated plates are implemented in the perpendicular direction of the flow, which can cover 0.5-53% of the cross-sectional area (Youssef et al. 2013). This type of bubble column is also called sectionalized bubble column. More information about the effect of horizontal plates on the performance of bubble columns can be found in the study done by Doshi and Pandit (2005). On the other hands, vertical internals can be implemented in bubble columns. The Fischer-Tropsch and slurry/bubble column reactors, where vertical tubes used as a heat exchanger systems, are the examples of vertical internals in industries. A complete review on the presence of vertical internals in bubble columns is presented in Section 2.4. In the following subsections, important parameters including gas holdup, liquid and gas velocities, bubble size distribution, and dispersion of gas and liquid phases are reviewed.

2.1 Gas Holdup in Bubble Columns

Gas holdup or gas volume fraction is a dimensionless parameter defined as the volume ratio of gas to the total volume of fluid:

$$gas\ holdup = \frac{volume\ of\ gas}{volume\ of\ gas + volume\ of\ liquid} \tag{2.1}$$

This ratio also represents the gas residence time in the liquid phase. In industries, where usually a high gas residence time is desired, a higher gas holdup must be achieved. Moreover, the value of

5

gas holdup can be a bridge to the size distribution of bubbles, which is the key factor in the determination of the interfacial area, and consequently, mass transfer rates (Shah et al., 1982). In this subsection, common techniques for measuring gas holdup are introduced, and then, the effect of different parameters on the gas holdup is reviewed.

2.1.1 Gas Holdup Measurement Techniques

- Bed Expansion Technique

One of the most common techniques to find the overall gas holdup in bubble columns is bed expansion technique. In this technique, the static head (H_S) and hydrodynamic (H_D) head of the fluid are measured. A static head of fluid (H_S) is the height of the initial liquid in the system before sparging the gas phase. With sparging the gas into the system, the liquid phase expands in the axial direction of the column, and reaches the new height that is called the hydrodynamic or dispersion height (H_D). The overall gas holdup (α_g^T) can be calculated as follows (Krishna and Ellenberger, 1996):

$$\alpha_g^T = \frac{H_D - H_S}{H_D} \tag{2.2}$$

The main challenge in this method is accurately measuring the hydrodynamic head of the fluid because of the high fluctuations or foam formations on the top free surface. To address this issue, the average value of hydrodynamic heights can be obtained by repeating the experiments several times.

- Pressure-Based Methods

Another method to calculate the overall gas holdup is measuring the pressure difference along the height of the column (z-direction). The general formulation between pressure and overall gas holdup (α_g^T) was suggested by Merchuk and Stein (1981) as follows:

$$\alpha_g^T = \left(1 + \frac{1}{\rho_l \vec{g}} \frac{dP}{dz}\right) + \frac{U_l^2}{\vec{g}} \frac{1}{\left(1 - \alpha_g^T\right)^2} \frac{d\alpha_g^T}{dz} + \frac{4\tau_w}{\rho_l D_c \vec{g}} \tag{2.3}$$

where P is the pressure, $\vec{g}$ is gravitational acceleration, ρ_l is the liquid density, z is direction along the height of the column, U_l is the superficial liquid velocity, D_c is the column diameter, and τ_w is the wall shear stress. The first term on the right-hand side is the pressure drop, the second term is fluid acceleration due to the change of volume fraction, and the third term is wall shear effects. In the case of semi-batch operations ($U_l = 0$), the second term is eliminated. Even for the systems with a current of liquid flow, this term can be neglected because of its minor effect (Merchuk and Stein, 1981; Hills, 1976). For further simplification, the third term (wall effect) can be also neglected, which results in the following equation (Tang and Heindel, 2006):

$$\alpha_g^T = 1 - \frac{1}{\rho_l \vec{g}} \frac{\Delta P}{\Delta z} \tag{2.4}$$

For slurry bubble columns, where solid particles are suspended in the fluid as the third phase, the pressure drop can be used to estimate the overall gas holdup as follows (Li and Prakash, 2000):

$$\Delta p = (\rho_s \alpha_s^T + \rho_l \alpha_l^T + \rho_g \alpha_g^T) \vec{g} \Delta z \tag{2.5}$$

where ρ_s and ρ_g are the densities of solid particles and gas, respectively. α_s^T and α_l^T are the volume fractions of solid and liquid, respectively.

- **Electrical Tomography Methods**

Electrical resistance tomography (ERT) (Dickin and Wang, 1995; Toye et al., 2005) and electrical capacitance tomography (ECT) (Yang et al., 1995; Makkawi and Wright, 2002) are the well-known techniques to measure the variations in the conductivity and permittivity of fluids, respectively. In a fluid, the presence of gas in the liquid phase changes local properties such as local density, viscosity, conductivity, and so on. Therefore, measuring changes of these properties with the variation of volume fractions can be used to calculate the gas holdup in multiphase systems. Electrodes can be employed to measure the differences governed by conductance or the capacitance or both (Kumar et al., 1997). ERT devices consist of multiple electrodes located around the bubble column, a data acquisition system, and a controller associated with software to analyze data (Pakzad et al., 2008). In the ERT technique, the Maxwell correlation (Maxwell, 1873) is commonly used to convert electrical data to gas holdup:

$$\alpha_g = \frac{2\sigma_l^c + \sigma_g^c - 2\sigma_m^c - \sigma_m^c\sigma_g^c/\sigma_l^c}{\sigma_m^c - \sigma_g^c/\sigma_l^c + 2(\sigma_l^c - \sigma_g^c)} \tag{2.6}$$

where α_g is the local gas holdup. σ_l^c, σ_g^c, and σ_m^c are the conductivities of liquid, gas and the mixture, respectively. By assuming the gas phase as a nonconductive material, Equation (2.6) can be simplified as follows:

$$\alpha_g = \frac{2\sigma_l^c - 2\sigma_m^c}{2\sigma_l^c + 2\sigma_m^c} \tag{2.7}$$

The ERT technique is noninvasive, which can also be used for opaque solutions. Because the ERT devices measure gas holdup on cross-sectional surfaces, the calculated gas holdups are slightly different with pressure-based or fluid expansion-based methods (Fransolet et al., 2005). In order to use the ERT technique, the primary phase must be conductive, e.g., the gas-solid phase cannot be studied by this method. Also, calibrations are an important step in the ERT methods since, the initial conductivity of liquid influences the results significantly (Jin et al., 2009).

- Radiation Methods

Radiation techniques are widely used to measure gas holdup in multiphase systems. These techniques are completely nonintrusive, which do not even need to have contact with the system. The computed tomography (CT) methods provide images from the system by emitting radiation from different angles. The X-rays (Misawa et al., 1990; Maurer et al., 2015) and γ-rays (gamma ray) (Kumar et al., 1997; Chen et al., 1999; Sultan et al., 2017) are commonly employed to create cross-sectional images from bubble columns. Due to the higher energy of γ-rays, they can penetrate deeply to the object, for example, γ-rays can penetrate into the metal whereas X-rays cannot (Al Mesfer et al., 2016). This feature of γ-rays makes them an appropriate choice for systems with metal walls, though increases the safety challenges (Varma, 2008).

- Intrusive Probes

Conductivity (electrical impedance) probes and optical probes are widely used to investigate bubble columns. They are intrusive tools as the measuring probes are located inside the column. The conductivity probes sense the conductivity, electrical capacity, or resistance differences

between gas and liquid phases to determine the volume fractions. The gas holdup is measured from the time that probes spends in the gas phase compared to the total experiment time. On the other hand, the optical probes use the differences in the reflection index of phases. Generally, this kind of probes is applicable in the transparent systems with low gas holdups at moderate temperatures (Kumar et al., 1997). The optical probes can be used in both conductive and non-conductive mediums and have a more sensitivity compared to the conductivity probes (Xue et al., 2003).

The numerical approaches to study the gas distribution in bubble columns are explained in Chapter 3.

2.1.2 Effect of Different Parameters on Gas Holdup

- Effect of Dimensions of Bubble Columns

The effect of bubble column diameter on gas holdup has been the subject of numerous studies. As one of the earliest work, Yoshida and Akita (1965) investigated the impact of bubble column diameter on the overall gas holdup at different superficial gas velocities. The experiments were performed once with an electrolyte liquid and once with water in bubble columns with diameters of 0.077, 0.0152, 0.31, and 0.60 m. The results showed that for both liquids, the overall gas holdup in the three larger bubble columns are equal and did not change with the column diameter. However, the gas holdup in the smallest bubble column (D_c=0.077m) was higher than the ones in the other cases. That difference among the values of gas holdup increased with increasing the superficial gas velocity. Similarly, in the experiments of Zahradnik et al. (1997), a noticeable increase in the gas holdup by decreasing the column diameter from 0.29 to 0.14 m was observed. This observation was linked to the effect of the column wall on the bubble-bed instabilities. Their visual inspection showed that the developing macro-scale eddies in the larger bubble column disrupted the homogenous structure, leading to the transition of flow regime. This argument is in line with the fact that turbulence scales are proportional to column dimensions (the column diameter) (Joshi and Lali, 1984). The change of gas holdup with column diameter was found to be limited to the bubble columns with diameters smaller than 0.1-0.15 m in some literature (Wilkinson et al., 1992; Hikita et al., 1980; Kastánek et al., 1993; Bando et al., 1988). However, Zahradnik et al. (1997) claimed that the independence of gas holdup upon column diameter in large bubble columns just valid for the heterogeneous regimes, and it cannot be extended to the homogenous regime. Using CFD simulation, Krishna et al. (2001) showed that for homogeneous

regimes, intense liquid recirculation in the large bubble columns accelerated the bubbles in the upward direction, which led to the lower gas holdups. For the heterogeneous regime, Krishna et al. (1997) defined two imaginary phases: a dense phase composed of small bubbles, and a dilute phase composed of large bubbles. They showed that the gas holdup of the dense phase is independent of the column diameter while the gas holdup of the dilute phase is proportional to $(\frac{1}{D_C^{N_1}})$, where N_1=0.18 (Krishna and Ellenberger, 1996).

The height of the bubble column is the other geometrical parameter affecting the gas holdup. Tsuchiya and Nakanishi (1992) conducted experiments in bubble columns (D_c=0.15 m) with heights of 3.9 and 7.7 m. The results showed that the gas holdup is almost independent of liquid height. The experiments by Thaker and Rao (2007) showed a weak function of gas holdup to the liquid static head (H_S) as $\alpha_g^T \sim \left(\frac{H_S}{D_C}\right)^{0.09}$ for $3 \leq \left(\frac{H_S}{D_C}\right) \leq 7$.

- Effect of Superficial Gas Velocity

Superficial gas velocity is defined based on the gas flow rate and the cross-sectional area of bubble columns. By increasing the superficial gas velocity, the gas holdup increases as shown in several studies (Schumpe and Grund, 1986; Saxena et al., 1990; Daly et al., 1992; Prakash et al., 2001; Sivasubramanian and Prasad, 2009). In a homogenous flow regime, gas holdup increases linearly with increasing superficial gas velocity (Wilkinson et al., 1992):

$$\alpha_g^T = AV_{sf,g} \tag{2.8}$$

where $V_{sf,g}$ is superficial gas velocity, and A is a constant which was proposed as 4 by Krishna et al. (1991).

In the heterogeneous regime, the dependence of gas holdup on the gas velocity becomes weaker. The gas holdup can be calculated by the following correlation (Wilkinson et al., 1992):

$$\alpha_g^T == AV_{trans,g} + B_1\left(V_{sf,g} - V_{trans,g}\right)^{0.8} \tag{2.9}$$

where $V_{trans,g}$ is the superficial gas velocity which the flow regime changes from homogenous to heterogeneous. C is the experiment fitting parameter. In this correlation, the total gas holdup is decomposed into two portions: one portion is for the small bubbles, and the other one is for the large bubbles. This concept can be used to study the flow regime transition in bubble columns. In the homogenous regime, the gas holdup changes proportionally with superficial gas velocity while in the heterogeneous regime this trend changes. One can mark the point where the slop of gas holdup profile vs. superficial gas velocity changes as the regime transition point.

- Effect of Operating Conditions

In industries, bubble columns are usually operated at evaluated pressures and temperatures far from the normal ambient condition. Therefore, the effects of pressure and temperature on gas holdup were the subject of many studies. For example, Tarmy et al. (1984) measured the gas holdup in an evaluated pressure bubble column at condition near coal liquefaction reactors. The gas holdup was found almost 350% higher than the one at the ambient conditions. A similar observation has also reported for Fischer-Tropsch reactors (Clark et al., 1983). Clark (1990) performed experiments in a 0.075 m diameter and 3 m height bubble column to investigate the effect of pressure on the gas holdup. They observed a considerable increase in the gas holdup with increasing pressure. They attributed this increase to two factors: (1) the decrease in the diameters of bubbles leaving the sparger, and (2) the decrease in surface tension with increasing pressure, which caused a reduction in the coalescence rates. In addition to these two factors, Lin et al. (1998) claimed that increasing pressure led to an increase in the fluid viscosity. The increased viscosity caused less turbulence in the system, which reduced the collision rate of bubbles. A lower collision rate means smaller bubbles (a larger gas holdup) due to the less coalescence rate. Also, they observed that the effect of pressure was more pronounced at high superficial gas velocities.

The effect of temperature is the other parameter that has been studied in the literature. Deckwer et al. (1980) investigated the effect of temperature on the gas holdup through the experiments in two slurry bubble columns with diameters of 0.041 and 0.1 m. They tried to mimic the conditions of the Fischer-Tropsch process. The molten paraffin was used as the liquid phase while the temperature was increased up to 300 °C. The results showed that the temperature significantly affected the performance of the smaller bubble column (D_c=0.041 m). In the smaller column, the total gas holdup continuously decreased with increasing temperature up to 240 °C while in the

11

higher temperature, the gas holdup did not change. On the other hand, in the larger column, the gas holdup was found independent of temperature. They linked this difference to the wall effect without further explanation. Grover et al. (1986) performed their experiments in a bubble column with a diameter of 0.1 m. For water-air systems, they observed a decrease in the gas holdup with increasing temperature up to a certain point where after the gas holdup was found temperature-independent. However, for the systems with the electrolyte liquids, the gas holdup was found highly sensitive to temperature variations. The results showed that the gas holdup increased with increasing temperature at low velocities. However, at high velocities, the gas holdup decreased with temperature. Zou et al. (1988) conducted several experiments in the bubble column (D_c=0.1 m) with different three liquids (water, alcohol, and an aqueous solution of NaCl) at the temperature ranging 25-96.56 °C. They observed that the overall gas holdup increased with increasing temperature in all liquids. In addition, the results indicated a significant effect of temperature on the local gas holdup, i.e., sharper radial gas holdup profiles were observed at the lower temperatures. The inconsistent conclusions among the aforementioned studies show that in the studies on the impact of temperature, such operating parameters as bubble column diameter, liquid properties, the range of temperatures and so on must be considered.

- Effect of Liquid Properties

The other parameter affecting the gas holdup is liquid properties. Tap water is the most common liquid used as the carrier phase in experiments. However, the quality of tap water affect the results mainly because of the inhabitation impact of impurities on the bubble coalescence (Maruyama et al., 1981; Tang and Heindel, 2004). Moreover, additives in the liquid phase can affect the gas holdup. For example, alcohol acts as a coalescence inhabitation agent by reducing the surface tension (Akosman et al., 2004). It has been shown that only 1% volume aqueous ethanol solution led to 2.2 times higher gas holdup compared to pure deionized water (Rollbusch et al., 2015).

Ruzicka et al. (2003) summarized the effect of liquid viscosity as follows: at low gas superficial velocities, increasing liquid viscosity leads to a higher drag force (as a resistance force for bubbles ascending through the column). Therefore, the gas holdup increases with increasing liquid viscosity. On the other hand, at high superficial gas velocities, a high liquid viscosity contributes to higher bubble coalescence rates and larger bubbles. Therefore, the gas holdup decreases with increasing liquid viscosity. In another study, Eissa and Schugerl (1975) showed that the effect of

viscosity is negligible in systems with a liquid viscosity (μ_l)> 14 if the viscosity of water equals to one.

Several authors (Haque et al., 1988; Pradhan et al., 1993) tried to derive a correlation between the gas holdup and liquid viscosity. For example, gas holdup and liquid viscosity can be correlated as follows (Fransolet et al., 2005):

$$\alpha_g^T == aV_{sf}^b\mu_l^{-c} \tag{2.10}$$

where a, b, and c are the fitting parameters, and μ_l is the liquid viscosity.

The carrier phase in the bubble columns might be a non-Newtonian fluid. In this case, the liquid viscosity is not constant and changes with the flow condition. As a solution, the apparent viscosity is usually considered, which can be estimated by the power-law formulation:

$$\mu_a = K_\mu \dot{\gamma}^{(n_\mu - 1)} \tag{2.11}$$

where K_μ and n_μ are the consistency and power-law index, respectively. $\dot{\gamma}$ is the shear rate which can be calculated by empirical correlations such as:

$$\dot{\gamma} = C_\gamma V_{sf,g} \tag{2.12}$$

where C_γ is the constant parameter which was suggested as 5000 (Nishikawa et al., 1977) and 2800 (Eickenbusch et al., 1995) depending upon conditions. In the other method, Anastasiou et al. (2013) used CFD and analogy with Equation (2.12) to develop a correlation for the mean shear rate $\dot{\gamma}$ in aqueous glycerin–xanthan solutions:

$$\dot{\gamma} = 70V_{sf}^{0.48} \tag{2.13}$$

2.2 Gas and Liquid Velocities in Bubble Columns

The gas and liquid velocities are a key parameter in the determination of mixing and residence time in bubble column reactors. In addition, the instantaneous velocities can be used to estimate the turbulent parameters such as turbulent kinetic energy and Reynolds stress tensors (Degaleesan, 1997). In this section, three common velocity-measuring methods of particle image velocimetry (PIV), laser Doppler anemometry (LDA), and computer automated radioactive particle tracking (CARPT) are briefly introduced. In Chapter 3, the numerical approaches to study the velocity distributions in bubble columns are explained.

- Laser Doppler Anemometry (LDA):

LDA (Laser Doppler Anemometry) is a nonintrusive technique, categorized as an optical method. The LDA technique used laser beams to produce images from the velocity field (flow visualization). This method was first developed by Yeh and Cumins (1964), based on the Doppler effect. The Doppler effect is the change in the frequency of a wave due to the relative motion. The relative motion can be caused by the movement of the wave source, or the receiver, or both. In multiphase flows, laser beams are emitted to the system, and the detectors receive them. The emitted beams scattered through penetrating the system that causes changes in their frequencies. For the detectors, the scattering bubbles/particles act as the moving receivers, and for the detector, the scattering bubbles/particles act as the moving sources (Chaouki et al., 1997). This method is only applicable to transparent fluids in columns with transparent walls. In bubble column reactors, this transparency is disturbed because of the presence of bubbles, especially at high volume fractions. Moreover, in the LDA method, it is not clear that the measured velocity is of the liquid phase or the bubbles (Mudde et al., 1997). In other words, this method cannot discriminate between measured velocities data obtained from the two phases.

- Particle Image Velocimetry (PIV):

The PIV (particle image velocimetry) method is more recent compared to the LDA method. It can provide two-dimensional (Chen et al., 1989) and three-dimensional (Reese et al., 1995) images from the flow. In this method, the fluid is seeded with particles which become visible by illuminating light (laser) on them. The tracer particles must be sufficiently small that can move freely with along the fluid. To fulfill this condition, the characteristic time of particles have to be

much smaller (τ_p) than the characteristic time of the flow (τ_f). This condition can be represented by stokes number:

$$St = \frac{\tau_p}{\tau_f} \qquad (2\text{-}14)$$

An advantage of the PIV method is the ability to measure the velocities of each phase simultaneously, which is not possible in the LDA method as a single point measurement technique (Deen et al., 2000). In the PIV method, an algorithm is required to discriminate between the gas velocity and liquid velocity. Oakley et al. (1997) developed an algorithm that requires identification of individual bubbles. Delnoij et al. (1999) proposed an algorithm based on the slip velocity between the bubbles and their surrounding liquid. The PIV method, (same as the LDA method) requires transparent wall, and are not applicable in opaque fluids (Baroni et al., 2011).

- Computer Automated Radioactive Particle Tracking (CARPT)

This nonintrusive method was first developed by Lin et al. (1985). In the CARPT technique, a radioactive particle is added to the fluid. The particles used in CARPT contain scandium-46 isotope coated with different materials to match the system characteristics. For instance, enamel paint can be used to enhance the wetting characteristic of the tracer particle in bubble columns (Moslmian et al., 1992). The density of these particles must be close to the fluid phase (neutrally buoyant) so that particles can move easily within the fluid. The movement of the single particle is tracked by an array of scintillation detector around the column. The frequency of gamma rays arriving at each detector decreases with increasing distance between the source and the detector (Devanathan et al., 1990). In this way, the detectors can measure the distance of each particle over time. The data of measured distances are used to calculate the instantaneous velocities (Devanathan, 1991; Yang et al., 1993).

2.3. Bubble Size Distribution

In multiphase flows, the size of bubbles is very important because of its role in the determination of residence time, fluid hydrodynamics, and interfacial area of phases. Moreover, bubble size distributions offer valuable information about the regime of the flow since larger bubbles and a wider range of bubble sizes show up at the transition of the homogenous regime to the

heterogeneous regime (Wang et al., 2005). The bubble size can be obtained directly in various ways, such as acoustic techniques (Pandit et al., 1992), liquid scattering methods (Vera et al., 2001), and laser techniques (Leifer et al., 2003). On the other hand, indirect techniques can also be employed to estimate the bubble size distribution. The gas disengagement method is an indirect technique, which was originally developed by Sriram and Mann (1977). This technique is simple and very similar to the bed-expansion method in measuring overall gas holdup. This technique is based on the idea that bubbles of different sizes leave the bubble column with different speeds. In this method, after the bubble column reached pseudo-steady condition, the inlet gas flow is disconnected completely. Consequently, the expansion head of fluid decreases gradually to reach the static head. The drop in the height of the liquid is monitored to create the plot of fluid height (or gas holdup) vs. time (refer to Schumpe and Grund, 1986). The plot is divided into two parts with different slopes. The first part of the plot with the higher slope (faster decrease of fluid height with time) is attributed to the contribution of large bubbles. It is assumed that by shutting off the inlet gas, the large bubbles, because of their larger velocities, are the first group of bubbles leaving the column. The second part of the plot with the lower slope is considered as the contribution of small bubbles. In this regard, the populations of the large and small bubbles are estimated. The most difficulty with this technique is accurate measuring of changes in the head of fluid, especially in the first part of the plot because of the fast disengagement of large bubbles. Moreover, this method was built on some assumptions that impair the model validity. For example, considering the same rising velocity for the swarm of bubbles and the isolated bubble. Also, the consideration of bimodal size distribution limits the application of this technique. More explanation and proposed modifications can be found in the studies by Lee et al. (1985) and Daly et al. (1992).

Advancements in CFD modeling and power of computers provide opportunities for development of numerical models for the bubble size distribution. The population balance model (PBM) is explained in Section 3.3.

2.4 Vertical Internals in Bubble Columns

The bubble column hydrodynamics, in contrast to their simple geometry, can be very complex and include a wide range of bubble sizes and three-dimensional and vortical flows. The implantation of the heat exchanging internals in the bubble columns adds further complexity to their hydrodynamics. Moreover, vertical internals are used in photobioreactors to provide the required

light for the cultivation of the culture. In the industrial scope, the vertical tubes are widely used to remove the heat from reactions and ensure desirable and uniform temperatures throughout the reactors. Due to the growing attention to slurry bubble columns, especially for the methanol and Fischer-Tropsch processes, the number of investigations on the effect of internals on the bubble columns has also increased. These investigations can be categorized into experimental and computational studies.

At the primary stage, Yamashita et al. (1987) investigated the effect of internals on the overall gas holdup in bubble columns. They proposed correlations between the superficial gas velocity and overall gas holdup for columns with small and large diameters. Their correlations were based on the concept that the area occluded by the internals results in higher gas velocities throughout the bubble columns. Pradhan et al. (1993) employed a similar idea to drive the correlation for the gas holdup in non-Newtonian liquids. Saxena et al. (1992) performed their experiments at different temperatures, ranging from 24 to 90°C. They demonstrated that the impact of internals became more pronounced at high temperatures and high superficial gas velocities. Besides investigating the effect of sparse internals on gas holdup, Chen et al. (1999) studied axial liquid velocity, liquid recirculation, and turbulent parameters. The experiments were designed to simulate the methanol slurry columns where 5% of the cross-section area is occupied by vertical rods. The results showed that sparse internals did not significantly change the liquid recirculation flow pattern. In the case of dense internals, Forret et al. (2003) studied a bubble column equipped with 56 vertical tubes (22% coverage). They developed one and two-dimensional models to calculate axial liquid velocity and axial dispersion coefficient. The results showed that the internals significantly reduced the fluctuations while intensifying the liquid recirculation. The most comprehensive experimental studies on air-water systems in the presence of vertical internals were performed by Youssef and Al-Dahhan (2009) and Youssef (2010). In these studies, gas holdup, bubble chord length, averaged bubble velocity, liquid mixing, and scale up methodologies were investigated. The experiments were conducted in laboratory and pilot plant scales with various internal configurations when the superficial gas velocities were based on the total cross-section area. Hamed (2012), Kagumba and Al Dahhan (2015), and Jasmin (2016), however, considered the superficial gas velocities based on the free cross-section area of the bubble column. The experiments performed by Hamed (2012) on the bubble columns with diameters of 0.19 and 0.45 m showed that the internals altered the gas velocity profiles significantly. For a bubble column

with 0.14 m diameter, Kagumba and Al Dahhan (2015) and Jasmin (2016) demonstrated that the impact of the internals on the overall gas holdup was negligible, except at the high superficial gas velocity of 0.45 m/s where a slight increase in the total gas holdup was observed. They also examined the effect of circular, hexagonal internal configurations, and the tubes' diameter on the performance of bubble columns. The results indicated that although all internal configurations occupied a same fraction of the cross-section area, their effects were different on the bubble size and column hydrodynamics. Guan et al. (2015) compared the impact of pin-fin and plain tubes on gas holdup and liquid velocity with ones in the hollow bubble column. They showed that the overall gas holdup in the presence of pin-fin tubes was higher compared to the plain tubes. Al Mesfer et al. (2016) used the gamma-ray computed tomography (CT) to investigate overall and local gas holdup in the presence of dense internals (for the Fischer-Tropsch process). Al Mesfer et al. (2017) and Kalaga et al. (2017) used the radioactive particle tracking (RPT) technique to study the effect of dense vertical internals at different gas velocities. Al Mesfer et al. (2017) showed that the liquid recirculation increased in bubble columns while turbulent stress and turbulent kinetic energy was reduced. Kalaga et al. (2017) measured gas holdup, liquid velocity, turbulence and mixing parameters in the concurrent upward flows at different superficial gas velocities. The results showed that the internals significantly increased the liquid dispersion coefficient and liquid mixing.

In the numerical modeling scheme, although hollow bubble columns have been extensively investigated, the literature devoted to obstructed bubble columns was very limited. However, in recent years, the simulation of bubble columns with internals has received a great amount of attention. Guan et al. (2014) investigated the impact of vertical internals on the bubble shape and bubble rise velocity in small cuboids by using the volume of fluid (VOF) method. They showed that bubble rise velocity decreased almost linearly with the increase of the fraction of the area occluded by internals. Bhusare et al. (2017) discussed the numerical setup for co-current up flow bubble columns with internals. In their simulation, one of the columns was equipped with a large centric rod and the other one, in addition to the centric rod, had a concentric bundle with four rods. They achieved a better liquid mixing by adding the number of internals. Guan and Yang (2017) investigated the influence of interfacial closures in the modeling of a bubble column with sparse internals (5% coverage). Their study revealed the importance of wall-lubrication force in the simulation of bubble columns with internals.

However, the mentioned numerical investigations were limited to the effect of sparse internals. The CFD simulations in the presence of dense internals are very limited. Larachi et al. (2006) employed 2D and 3D geometries with the time-transient solver to investigate the effect of different internals configurations. They considered single bubble sizes, and because of the uncertainty about the choice of the bubble size, two sizes of 5 mm and 19 mm were tested separately. By applying each bubble size, the simulations resulted in different outcomes and flow patterns. The results, however, were not validated by experimental data, and even some liquid behavior was not in agreement (Guan et al., 2015) with the experiments of Forret et al. (2003) and Zhang et al. (2009). Guo and Chen (2017) applied the population balance model to reproduce the bubble size distribution. They showed that the bubble size distribution evolved faster in the presence of internals. Moreover, results showed that the effect of the internals on the liquid circulation was different at low and high superficial gas velocities.

2.5 Dispersion in Gas and Liquid Phases

Generally, three "ideal" states of ideally batch, plug flow, and mixed flow reactors can be considered to study mixing behavior in reactors. However, the real reactors are far from those ideal states. In bubble column reactors, the bubbles experience different residence times in the system. Also, the batch phases are associated with recirculation, non-uniform distribution, and molecular and turbulent diffusions. In the basic models for the study of mixing in bubble columns, the liquid is generally considered as an ideally mixed phase while the gas phase is taken as an ideal plug flow. However, with these assumptions, the model deviates from the real bubble column. For instance, the assumption of ideally mixed for the liquid phase can lead to overestimating the reactor size, especially at high conversions of reactants (Myers et al., 1987; Degaleesan and Duduković, 1998).

Considering nonidealities in the liquid phase of bubble columns, several models have been proposed in the literature; some were summarized by Shah et al. (1987). Among the proposed models, the axial dispersion model (ADM) has gained great attention because of its simplicity. In this model, all nonidealities are lumped into a single parameter named axial dispersion coefficient ($D_{a,l}$). In a theoretical attempt to calculate $D_{a,l}$, Baird and Rice (1975) derived a correlation based on Kolmogorov's (1941) theory and dimensionless analysis as follows:

$$D_{a,l} = K_D l_D^{4/3} \varepsilon^{1/3} \tag{2-15}$$

where K_D and ε are dimensionless constant and specific energy dissipation rate, respectively. l_D is the primary length parameter which can be approximated by the column diameter)in the case of no internals(.The axial dispersion coefficient $(D_{a,l})$ was also derived based on the column diameter (D_C), superficial gas velocity $(V_{sf,g})$, and kinematic viscosity $(\mu_{k,l})$ in the typical form of (Ekambara and Joshi, 2003):

$$D_{a,l} = K_1 D_c^{b1} V_{sf,g}^{c1} \mu_{k,l}^{d1} \tag{2-16}$$

where K_1, $b1, c1$, and $d1$ are empirical constants that vary with the experimental conditions. The axial dispersion can also be correlated based on the local properties of the bubble column e.g. $D_{a,l}$ can be given by the liquid centerline velocity, $U_l(0)$ as follows (Krishna et al., 2000):

$$D_{a,l} = 0.31 U_l(0) D_c \tag{2-17}$$

Further correlations for liquid mixing were tabulated by Majumder (2008).

In contrast to the liquid phase, fewer studies have been devoted to the dispersion in the gas phase, mainly because of challenges in measuring the extent of the gas dispersion (Kantak et al., 1995). As an early work, Vermeer and Krishna (1981) reported the gas residence time distribution (RTD) by the impulse tracer technique. Kantak et al. (1995) investigated the effect of liquid and gas properties on the gas phase dispersion through an experimental technique developed by Shetty et al. (1992). Joshi (1982) derived a correlation (Equation 2.18) for the axial gas dispersion coefficient $(D_{a,g})$ based on the Taylor's model (Taylor, 1953) and several experimental data (Kölbel et al., 1962; Carleton et al., 1967; Towell and Acherman, 1972; Men'shchikov, 1967; Mangatz and Pilhofer, 1981; Seher and Schumacher, 1979):

$$D_{a,g} = 110 \frac{V_{sf,g}^2}{\alpha_g^T} D_c^2 \tag{2-18}$$

where α_g^T is gas volume fraction. For the scale up purposes, Wachi et al. (1990) derived a correlation for $D_{a,g}$ in two bubble columns with diameters of 0.5 and 2 m as follows:

$$D_{a,g} \propto V_{sf,g} D_c^{\frac{3}{2}} \qquad (2\text{-}19)$$

As other empirical correlations for gas axial dispersion coefficient, the correlations by Pilhofer et al. (1978), and Field and Davidson (1980) can be named.

Numerical modeling has also employed to study the dispersion of phases in bubble columns. Thakre et al. (1999) developed a CFD model to investigate liquid mixing in semi-batch bubble columns. The results showed a continuous decrease of mixing time with increasing superficial gas velocity. However, Rampure et al. (2007) showed that decreasing mixing time with superficial gas velocity just continued up to a certain gas velocity. This behavior was linked to the formation of a large number of circulation loops in the system without further explanation. Thakre et al. (1999), Ranada and Taylaia (2001), and Ekambara and Joshi (2003) showed that mixing time was practically independent of the detector and tracer injection positions. However, different results were obtained by McCulre et al. (2015). In their experiments, three probes were considered at the top, middle, and bottom (beneath the sparger) of the bubble column to monitor the tracer concentration. The mixing time calculated from the bottom probe was found much larger compared to others. Moreover, a great dependency of mixing time upon the distance between the tracer injection point and detector point was observed. Also, In the CFD study by Gholamzadehdevin and Pakzad (2018), the shortest mixing time was achieved when the tracer injected at the middle of the bubble column.

Ranada and Taylaia (2001) employed a CFD model to study the effect of sparger design on the liquid mixing in shallow bubble columns (height to diameter ratio of 2). They found that a single ring sparger generated a stronger overall liquid circulation, and therefore a more efficient liquid mixing. The effect of spargers was also investigated by Li et al. (2009). In their simulation, the sparger with an asymmetric geometry resulted in the lowest mixing time because of the presence of a stronger liquid circulation.

Buwa and Ranada (2003) calculated mixing time once based on the time-averaged parameters and once through the full transient solver. The comparison of the two cases showed a considerable overestimation of mixing time in the time-averaged model.

The dimensions of bubble columns were also subject of numerical studies. Van Baten and Krishna (2001) showed that a larger column diameter led to a larger liquid mixing time. Roy and Joshi (2007) showed a considerable increase in liquid mixing time by increasing the ratio of height to column diameter. For the gas phase in bubble columns, using CFD simulation, Van Baten and Krishna (2001) found that larger bubbles leave the column with a lower degree of dispersion compared to the small bubbles. They argued that the small bubbles circulating along with the liquid cause the deviation of the gas phase from a straight flow. Bai et al. (2011) studied the gas dispersion at low superficial gas velocities (up to 0.025 m/s) in a flat bubble column in the Lagrangian framework. The results showed an increase in gas dispersion with increasing superficial gas velocity.

All the above studies considered hollow bubble columns with no internals. The effects of internals on the liquid mixing and gas dispersion have rarely been investigated. Forret et al. (2003) studied liquid mixing in a large-diameter bubble column with internals where the superficial gas velocity was based on the free cross-section area (CSA). They found an increase in liquid mixing time in the presence of internals. This result was related to the reduction of turbulence by internals. Kalaga et al. (2017b) observed the opposite results in a bubble column with the co-current up flow, where both turbulence and mixing performance enhanced in the presence of internals. Youssef et al. (2010) also observed an improvement of mixing performance in the presence of internals in the co-current up flow. George et al. (2017) studied the presence of baffles in the sparger zone of bubble columns with vertical rods. They concluded that the implementation of the baffles could reduce liquid back mixing in the system. However, they did not compare the mixing time measured in bubble columns with or without internals. For the effect of the internals on gas dispersion, the only study was conducted by Hamed (2012). They showed a considerable reduction of axial gas dispersion due to the reduction of turbulence intensity in the presence of internals.

2.6. Research Objectives

This study aims to investigate the effect of dense vertical internals (rods) on the different aspects of bubble columns. The numerical modeling of gas/liquid systems is explained in Chapter 3. Then, the simulation of the bubble column with vertical internals is developed in Chapter 4, with the following discussion:

- The effect of different interfacial forces (i.e. lift force and wall lubrication force) on the modeling results are studied.

- The effect of hexagonal arrangement on gas holdup, liquid and gas velocities, and turbulence parameters are investigated.

- Three circular internals' arrangements are considered to study the effect of distance of internals from the column's wall and concentration of internals at the core.

- The implementation of population balance model (PBM) in the presence of internals are explained, and a modification factor is proposed.

Furthermore, the effect of the internals on the gas dispersion and liquid mixing are studied in Chapter 5:

- The gas tracer technique to calculate the degree of dispersion in the gas phase is developed.

- The effect of superficial gas velocity and vertical internals on gas dispersion is studied.

- The liquid mixing was studied through tracer technique.

- The effect of tracer positions and tracer detectors on the mixing time was studied.

- The effect of the vertical internals on liquid mixing was investigated.

3. Multiphase Modeling

In fluid dynamics, the fluid field can be described with two frameworks of Lagrangian or Eulerian. The Lagrangian representative moves with the individual fluid elements. In this reference, the dynamical quantities of the flow are defined based on time and the choice of martial of the fluid element of the fluid (Batchelor, 2000). On the other hand, in the Eulerian framework, the properties of the flow are monitored through a specific position in the space (a fixed coordinate system). In this framework, the vector velocity is the primary flow quantity that can be written as a function of space and time (Batchelor, 2000). Most of the theoretical formulations have been based on the Eulerian framework. In multiphase modeling, the Lagrangian-Eulerian (L-E) and Eulerian-Eulerian (E-E) models are two popular approaches, developed based on the above-mentioned frameworks.

In the L-E (Lagrangian-Eulerian) model, the dispersed phases are treated in a Lagrangian reference, while the continuous phase is treated in the Eulerian reference. The conservation equations are solved for the continuous phase while the dispersed phase is determined by solving Newton's second law for each particle. The interaction between phases can be expressed by the different levels of complexity. The simplest one is one-way coupling where the dispersed phase is assumed not to affect the continuous phase. The next level is two-way coupling where the effects of dispersed phase and continuous phase on each other are taken to account. And in the most complicated approach, four-way coupling, the momentum exchange among dispersed particles has also been considered. The detail of phase coupling can be found in the study by Elghobashi (1991). The L-E model needs very fine grids to capture particle movements, and for smaller particle sizes the model requires finer grids. Moreover, the number of particles in the system is very important in the simulation's runtime, since each particle must be tracked and solved individually. Therefore, the application of this model (Lagrangian-Eulerian) is limited to small systems with a dilute concentration of dispersed phase. On the other hand, the E-E (Eulerian-Eulerian) model can handle large systems containing small particles with no needs of very large storage memory and computational time. In the following section, the Eulerian-Eulerian model is explained in more detail.

3.1. Eulerian-Eulerian Approach

In the E-E (Eulerian-Eulerian) approach, the different phases are mathematically treated as interpenetrating continua. This assumption is the first stage that can be problematic; in many systems, such as bubble columns, considering dispersed phase as a continuum is far from the reality. However, this assumption rids us from tracking a huge number of bubbles, droplets, and particles that can exist in multiphase systems. In the E-E model, a same framework and a control volume are assumed for all phases. As an instance, in a bubble column, both liquid and gas phases are considered as continua in a same framework. In this method, because a volume could not be occupied by two or more phases at the same time, the concept of phasic volume fraction was defined. The volume fractions are continuous functions of time and space, and their summation is unity. In this method, the continuity and momentum equations are written and solved for each phase.

The way of handling interactions of phases depends on the kind of phases that are involved; granular (fluid-solid) flows are handled in the different way than non-granular (fluid-fluid) flows. For granular flows, the parameters are attained from the application of the kinetic theory (Gidaspow, 1994). For non-granular systems, the continuity equation is written as follows:

$$\frac{\partial}{\partial t}\left(\alpha_\varphi \rho_\varphi\right) + \nabla.\left(\alpha_\varphi \rho_\varphi \, \vec{u}_\varphi\right) = 0 \qquad (3.1)$$

φ is the phase index. For liquid and gas systems, φ can be g for gas and l for liquid. In the above equation mass transfer between phases are neglected. As the summation of all phasic volume fractions must be unity, for a system with N_φ phases:

$$\sum_{\varphi=1}^{N_\varphi} (\alpha_\varphi) = 1 \qquad (3.2)$$

The momentum balance equation is given as:

$$\frac{\partial}{\partial t}\left(\alpha_\varphi \rho_\varphi \, \vec{u}_\varphi\right) + \nabla.\left(\alpha_\varphi \rho_\varphi \, \vec{u}_\varphi \vec{u}_\varphi\right) = -\alpha_\varphi \nabla P + \nabla.\left(\bar{\bar{\tau}}_{\text{eff}}\right) + \vec{M}_I + \rho_\varphi \alpha_\varphi \vec{g} \qquad (3.3)$$

The terms on the right-hand side represent, from left to right, the pressure gradient (∇P), effective stress ($\bar{\bar{\tau}}_{\text{eff}}$), interfacial momentum exchange ($\vec{M}_I$), and gravitational force ($\vec{g}$). This equation needs two closures: one for turbulence modeling ($\bar{\bar{\tau}}_{\text{eff}}$) and another for interfacial forces ($\vec{M}_I$).

3.2 Turbulence Modeling

One of the difficulties in dealing with multiphase systems is solving turbulence of the flow. Even in a single-phase flow, understanding of turbulence is very complicated because of the stochastic and fluctuating nature of turbulence. The main elements of turbulence are three-dimensional structures, time-dependent characteristics, and the existence of a wide range of time and length scales. Richardson (1922) introduced the concept of energy cascade which refers to the transfer of energy from the larger eddies to the smaller eddies. The larger eddies, which can be as large as the flow geometry, extract energy from the mean flow and pass it to the smaller eddies. It is assumed that no energy losses through the energy cascade (statistically steady), and all the energy dissipated to the flow only by the smallest eddies. At the smallest scale, which is named Kolmogorov length scale (Kolmogorov, 1941), the kinetic energy transfers to the flow in the form of heat through molecular viscosity. Therefore, a turbulent flow needs a source of energy to maintain active. If there is no energy supply, turbulence decays, and finally, the inertia forces is no longer large enough to keep the turbulence (Mathieu and Scott, 2000). All energy from the mean flow is extracted by the larger eddies while dissipated at the smallest scale. So, the amount of energy dissipation is determined by the largest eddies, and the scale of dissipation is determined by the Kolmogorov length scale. The dissipation rate (ε) is defined as energy dissipated by viscosity (or energy supplied to the fluid) per unit mass and unit time. In the turbulence flows, the instantaneous variables, such as velocities, can be decomposed into two parts as follows:

$$V_i = \bar{V}_i + V_i' \qquad (3.4)$$

This representation of variable is called Reynolds decomposition where V_i is the instantaneous velocity, $\bar{V}_i$ is the mean velocity, and V_i' is the fluctuation velocity in i direction. In the steady state condition, the mean value of velocity is a time-independent variable.

One of the inherent features of turbulence flows is that the fluctuation velocities cannot be predicted and formulated because of their random and stochastic behavior. Therefore, the turbulence can be studied with the statistical methods (Salas et al., 1999). In the statistical investigation of fluctuations, the standard deviation ($sdev(V)$) of an instantaneous velocity (V) from the mean velocity over a time span of t can be defined as follows:

$$sdev(V) = \sqrt{\frac{1}{t} \int_0^t V_i'^2 \, dt} \qquad (3.5)$$

If we show the probability by notation of P, the cumulative distribution function (cdf) of velocity V is defined as

$$cdf_V = P\{u < V\} \qquad (3.6)$$

where u is the velocity. The cdf_V gives us the probability of occurrence velocities smaller than V. So, the probability of occurrence of velocities between V and $V + dV$ can be given as follows:

$$P\{V \leq u \leq V + dV\} = cdf_{(V+dv)} - cdf_{(V)} \qquad (3.7)$$

The probability density function of velocity V can be shown by the notation of (PDF_V). PDF_V is defined as the derivative of $cdf_{(V)}$:

$$PDF_V = \frac{d(cdf_V)}{dV} \qquad (3.8)$$

The PDF_V can be built by the histogram of the velocities. One of the most common probability distribution functions is the Gaussian distribution:

$$PDF_V = \frac{1}{\sqrt{2\pi. \, sdev(V)}} \, e^{-0.5\left(\frac{(V-\bar{V})}{sdev(V)}\right)^2} \qquad (3.9)$$

To this conjuncture, it is explained how the fluctuation velocities can be represented through statistics. Now, by substituting the Reynolds decomposition into the instantaneous Navier-Stokes equations, the ensemble forms of the equations can be obtained. After the substitution, the Navier-Stokes equation in the x-direction (in Cartesian coordinate) is written as follows:

$$\rho\left(\bar{V}_x \frac{\partial \bar{V}_x}{\partial x} + \bar{V}_y \frac{\partial \bar{V}_x}{\partial y} + \bar{V}_z \frac{\partial \bar{V}_x}{\partial z}\right) = -\frac{\partial \bar{P}}{\partial x} + \mu \nabla^2 \bar{V}_x + \left(\frac{\partial \rho \overline{\acute{V}_x \acute{V}_x}}{\partial x} + \frac{\partial \overline{\acute{V}_x \acute{V}_y}}{\partial y} + \frac{\partial \overline{\acute{V}_x \acute{V}_z}}{\partial z}\right) \qquad (3.10)$$

where ∇^2 is the Laplace operator with the following form:

$$\nabla^2 \bar{V}_x = \frac{\partial^2 \bar{V}_x}{\partial x^2} + \frac{\partial^2 \bar{V}_x}{\partial y^2} + \frac{\partial^2 \bar{V}_x}{\partial z^2} \qquad (3.11)$$

The bar sign over the parameters shows the averaged values. The ensemble-averaged equations in y- and z- directions can be written similarly. As can be seen, all instantons parameters in the original Navier-Stokes equation are changed to the ensemble-averaged forms, except for $\overline{\acute{V}_x \acute{V}_x}$, $\overline{\acute{V}_x \acute{V}_y}$, and $\overline{\acute{V}_x \acute{V}_z}$.

These terms are named Reynolds turbulent stress that can be presented in the matrix form (tensor):

$$\tau_{ij}^t = \begin{bmatrix} \overline{\acute{V}_x \acute{V}_x} & \overline{\acute{V}_x \acute{V}_y} & \overline{\acute{V}_x \acute{V}_z} \\ \overline{\acute{V}_y \acute{V}_x} & \overline{\acute{V}_y \acute{V}_y} & \overline{\acute{V}_y \acute{V}_z} \\ \overline{\acute{V}_z \acute{V}_x} & \overline{\acute{V}_z \acute{V}_y} & \overline{\acute{V}_z \acute{V}_z} \end{bmatrix} = \begin{bmatrix} \sigma_{xx}^n & \overline{\acute{V}_x \acute{V}_y} & \overline{\acute{V}_x \acute{V}_z} \\ \overline{\acute{V}_y \acute{V}_x} & \sigma_{yy}^n & \overline{\acute{V}_y \acute{V}_z} \\ \overline{\acute{V}_z \acute{V}_x} & \overline{\acute{V}_z \acute{V}_y} & \sigma_{zz}^n \end{bmatrix} \qquad (3.12)$$

where σ_{xx}^n, σ_{yy}^n, and σ_{zz}^n are called Reynolds normal stress. In homogenous turbulent flows, Reynolds normal stress terms have a constant summation, which gives the mean turbulent kinetic energy:

$$k = \frac{1}{2}\rho(\sigma_{xx}^{n} + \sigma_{yy}^{n} + \sigma_{zz}^{n}) \tag{3.13}$$

It is good to mention that for a flow described by the Gaussian probability distribution function, each normal stress is equal to the square of the respective standard deviation (Zhang, 2010). Several approaches have been proposed to solve the Reynolds stress (τ_{ij}^{t}) such as the RANS model (Reynolds-averaged Navier-Stokes equations) and RSM models (Reynolds stress model). In this study, the RSM model was used, which is explained in the CFD Model Development in Chapters 4 through Sections 4.2.

3.3 Population Balance Model

This section explains the population balance model (PBM) originally developed by Ramkrishna, (2000). In this model, each dependent variable is defined by the external coordinate and internal coordinate. The external coordinate (r_{ex}) is the spatial coordinate that represents the position vector of the particle in the physical space. On the other hand, the internal coordinate (x_{in}) is an abstract coordinate that indicates the different quantities associated with the particle such as size, volume, age, etc. Therefore, the state of a particle can be determined by defining a vector accounting external coordinate, internal coordinate, and time. This vector is called the particle state vector. A particle is also affected by its surrounding liquid, so the continuous phase vector (Y_c) is defined to account for the effect of primary phase. This vector (Y_c) only is a function of the external coordinate and time, so $Y_C = Y_C(r_{ex}, t)$. Then, the velocity vectors are defined for each coordinate (external and internal coordinates). The vectors are functions of internal coordinate, external coordinate, continuous phase vector, and time; $U_r(x_{in}, r_{ex}, Y_c, t)$ and $U_x(x_{in}, r_{ex}, Y_c, t)$ denote for velocity in external space and internal space, respectively. The continuous density function (f_1) is defined as the number of bubbles per unit volume (volume of gas phase), which is a function of r_{ex}, x_{in} and t. The differential form of the population balance model is given as follows (Ramkrishna, 2000):

$$\frac{\partial f_1}{\partial t} + \nabla.(U_c f_1) = S_{f_1} \tag{3.14}$$

where U_C is the combined velocity of internal and external coordinates as $U_c \equiv U_x + U_r$. S_{f_1} is the source/sink term of bubbles, which is a function of $S_{f_1}(x_{in}, r_{ex}, Y_c, t)$. In another format, the population balance model can be written as follows (Yeoh, 2013):

$$\frac{\partial f_1(x_{in}, r_{ex}, t)}{\partial t} + \nabla_{r_{ex}} \cdot \left(U_r(x_{in}, r_{ex}, Y, t) f_1(x_{in}, r_{ex}, t) \right) \\ + \nabla_{x_{in}} \left(U_x(x_{in}, r_{ex}, Y, t) f_1(x_{in}, r_{ex}, t) \right) = S_{f_1}(x_{in}, r_{ex}, Y, t) \tag{3.15}$$

The terms from left to right are local changes of the bubble number density (f_1) with time, the change of the number density due to advection in the external coordinates, and the change of the number density due to advection in the internal coordinates (growth phenomena). And the term in the right-hand side is the source/sink rate. As the average number of particle in the infinitesimal volume of internal space ($dV_{x_{in}}$) is given by $f_1(x_{in}, r_{ex}, t)dV_{x_{in}}$, the local average number density in the internal space (the total number of particle in the physical space, external coordinate, per volume of physical space) can be given as follows (Yeoh, 2013):

$$N(r_{ex}, t) = \int_{X_{in}} f_1 dV_{x_{in}} \tag{3.16}$$

If it is assumed that the internal coordinate is equal to the volume of the bubble (V_b), the local volume fraction of all bubbles with different sizes (α_g) is given as follows:

$$\alpha_g(r_{ex}, t) = \int_{X_{in}} V_b f_1 dV_{x_{in}} \tag{3.17}$$

To solve Equation (3.16), the method of moments (MOM) developed by Hulburt and Katz (1964) can be employed. The moment of f_1 is defined as

$$m^J(r_{ex}, t) = \int_{V_b} V_b^J f_1(V_b, r_{ex}, t) dV_b \tag{3.18}$$

For $j = 0$, the moment is called the zeroth moment, which is equals to Equation (3.16). It is worth mentioning that $j = 1$ and $j = 2$ are the first and second moments, which offer mean and variance values, respectively. By considering the first moment ($N(r_{ex}, t)$) and neglecting the growth rate of bubbles, the transport equation of population balance can be given as follows (Yeoh, 2013):

$$\frac{\partial N(r_{ex}, t)}{\partial t} + \nabla_{r_{ex}}(U_b(r_{ex}, Y_c, t)N(r_{ex}, t)) = S_N(r_{ex}, Y, t) \tag{3.19}$$

where U_b is the average local bubble velocity. This equation (Equation 3.19) is not closed, and needs a closure for the right-hand side term (S_N), which accounts for the birth and death rates of bubbles. A bubble can be born by the breakage of bigger bubbles (B_{br}), or the coalescence of smaller bubbles (B_{co}). On the other hand, a bubble can die as the result of the breakage into smaller bubbles (D_{br}), or coalescing with other bubbles to form a bigger bubble (D_{co}) (Liao and Lucas, 2009):

$$S_N = B_{br} - D_{br} + B_{co} - D_{co} \tag{3.20}$$

Therefore, formulas for breakage and coalescence rates are necessary.

3.3.1 Breakage Rate

Breakage phenomenon can occur through four mechanisms of viscous shear stress, shearing-off, interfacial instabilities, and turbulence (Wang, 2011). The viscous shear forces in the liquid phase cause a velocity gradient around the surface of bubbles and deformation of the interface (Liao and Lucas, 2009). If the forces exceed a critical value, they break the bubbles down into two parts. It is assumed that the viscous force can cause a break up if overcomes the surface tension of the bubble. The viscous force relies on the value of viscosity in the continuous phase; a large viscosity leads to a larger force and enhances the chance of bubble break up.

The other breakage mechanism is shearing-off which is common in the case of slug and churn turbulent flows (Fu and Ishii, 2003b). The gas inside the slug bubble moves globally at the terminal velocity of the bubble while on the rim of the slug, the gas velocity is same as the surrounding liquid (Fu and Ishii, 2003a). Therefore, the gas entrains to the liquid through the thin boundary

layer between the two phases. In a bulk of a still liquid, the equivalent diameter of such bubbles is about 0.05-0.06 m, and their horizontal sizes reach 0.09-0.11 m (Avdeev, 2016). It is worth mentioning that since the tangential stress on the gas-liquid interface is almost negligible, the term "shearing" is not quite appropriate, and this phenomenon is called erosive breakage in some literature (Avdeev, 2016). In order to account for different sizes and shapes of bubbles, the bubbles are classified into two groups of spherical/distorted bubbles (named group-1) and cap/slug/churn-turbulent bubbles (named group-2) (Sun et al., 2004). In the shearing-off breakage, a bubble from group-2 results in a bubble from group-2 and a multiple numbers of bubbles from group-1. The average diameter of sheared-off bubbles (d_{sh}) can be given as follows (Sun, 2001):

$$d_{sh} = \frac{2\sigma}{C_S C_{fi} \rho_l v_{rb}^2} \tag{3.21}$$

where C_S is the interfacial friction factor, and C_{fi} is a proportional coefficient between the skirt of cap/slug bubble length and d_{sh}. The v_{br} is the relative velocity of the cap/slug bubble with respect to the liquid film near the cap bubble base.

Another mechanism of breakage is interfacial instability. A phenomenon is considered stable if the infinitesimal disturbance is not amplified spontaneously. For example, a ball on the flat surface is stable against small hit while the same ball on the top of a convex surface is unstable as it starts to go down by a very small hit. In multiphase flows, the difference between phases can lead to the instabilities. For instance, if a heavy liquid is located on the top of a lighter liquid, the heavy one penetrates and moves downward while the light phase moves in the upward direction. This difference in densities leads to Rayleigh-Taylor instability that occurs at the interface of two fluids of different densities when the lighter fluid pushes the heavier fluid (Zufiria, 1988). In bubble columns, the Rayleigh-Taylor instability (Komaboyashi et al., 1964) plays an important role in the determination of flow regimes. In small bubble columns (e.g., pipe), the bubbles form slugs at high superficial gas velocities. However, the formation of the slug cannot be observed in large bubble columns. In large bubble columns, the slug is not stable anymore because of Rayleigh-Taylor instability. In this conditions, the slugs are replaced by the coalescence-induced bubbles or cluster of bubbles (Besagni et al., 2017). The other instability is called Kelvin–Helmholtz instability (Kitscha and Kocamustafaogullari, 1989). This instability occurs at the interface between two

horizontal parallel streams of different velocities. More generally, it takes place over a finite thickness where variations of velocity and density are continuous (Kundu and Cohen, 2004). In the Kelvin–Helmholtz instability the viscous effects are negligible, so the Reynolds number does not have any role in this instability (Ishii and Hibiki, 2010). Although the relative motion between fluids is always destabilizing, gravitational force is destabilizing only if the upper fluid is heavier than the lower fluid (Ishii and Hibiki, 2010).

In turbulent flows, the turbulence is considered as the dominant breakage mechanism among the above mechanisms (Liao and Lucas, 2009). Most of the breakage models were based on the Hinze's theory (Hinze, 1955). This theory assumes that the bubble breakup occurs through collisions of bubbles and turbulent eddies which are approximately equal to the size of the bubble. The larger eddies tend to transport the bubbles rather than break it while very small eddies do not carry the sufficient energy to break up the bubbles (Chen, 2004). The minimum size of eddies that can contribute to breaking up a bubble was reported as the 20% of the bubble size (Prince and Blanch, 1990). Prince and Blanch (1990) defined the breakup frequency (Ω) as the product of collision frequency (w_{br}) and breakup efficiency ($P_{eff,br}$) as follows:

$$\Omega(V_{b,i}) = w_{br}(d_{b,i}, \lambda). P_{eff,br}(d_{b,i}, \lambda) \tag{3.22}$$

The collision frequency (w_{br}) of eddies of a size between λ and $\lambda + d\lambda$ with bubbles with size of $d_{b,i}$ is written as follows:

$$w_{br}(d_{b,i}, \lambda) = \int_{\dot{n}_\lambda} \frac{\pi}{4}(d_{b,i} + \lambda)^2 (v_{b,i}^2 + v_\lambda'^2)^{1/2} d\dot{n}_\lambda \tag{3.23}$$

where $\dot{n}_\lambda$ is the number of eddies in the range of λ to $\lambda + d\lambda$ per unit volume, which can be calculated by the relation proposed by Azbel and Athanasios (1983). $v_{b,i}$ is the discrete absolute mean velocity of the bubble with a diameter of $d_{b,i}$.

The breakup efficiency ($P_{eff,br}$) is defined as the probability of turbulent eddies with enough energy for breakage of the bubbles. In the model proposed by Luo and Svendsen (1996) (Luo model), the energy carried by an eddy must exceed the energy required by the surface area

increased due to the bubble fragmentation, $e_{s(d_{b,i})}$. The energy of an eddy $e(\lambda)$ is proportional to the squared turbulent velocity of the eddy, $v_\lambda'^2$, which is given as

$$e(\lambda) = \rho_l \frac{4}{3} \pi \lambda^3 \frac{v_\lambda'^2}{2} \tag{3.24}$$

The turbulent velocity of an eddy with size λ in inertial subrange is given by the following equation (Luo and Svendsen 1996):

$$v_\lambda' = C_\lambda^{1/2} (\varepsilon\lambda)^{1/3} \tag{3.25}$$

In this model, it is assumed that the turbulent velocity of an eddy in liquid flows could be approximated as the velocity of neutrally buoyant droplets in the same flow. In the Luo model, C_λ was set as 2 from the experimental data of Kuboi et al. (1972a,b).

In the binary breakage, a bubble with the volume of V_b breaks into two bubbles with the volumes of $V_{b,I}$ and $V_{b,II}$. Then, the size of daughter bubbles can be expressed by breakage volume fraction (f_{BV}):

$$f_{BV} = \frac{V_{b,I}}{V_b} \tag{3.26}$$

The increased surface energy due to the breakup of a bubble of volume $V_{b,I}$ with the given f_{BV} can be calculated as follows:

$$e_s(d_{b,i}) = c_{fs}\pi d_{b,i}^2 \sigma \tag{3.27}$$

where c_{fs} is the increase coefficient of surface area:

$$C_{fs} = f_{BV}^{2/3} + (1 - f_{BV})^{2/3} - 2 \tag{3.28}$$

Finally, the breakup efficiency ($P_{eff,br}$) is given as follows (Prince and Blanch, 1990):

$$P_{eff,br}(d_{b,i}, \lambda) = \exp(-\frac{e_s(d_{b,i})}{e(\lambda)}) \qquad (3.29)$$

To predict the size of bubbles resulted from the breakage rate, the daughter particle size probability density function is required. In the models proposed by Luo and Svendsen (1996) and Lehr et al. (2002), the breakage kernels include both breakage frequency and the daughter size distribution. However, if the breakage model does not contain daughter size distribution, either it can be determined by empirical models, phenomenological models, or statistical models (see Liao and Lucas, 2009).

3.3.2 Coalescence Rate

There are two general approaches of empirical and physical models to study coalescence in multiphase flows. The empirical models are developed based on the experimental data and fitting parameters. On the other hand, in the physical models, the coalescence frequency is obtained from the product of coalescence collusion frequency ($P_{eff,co}$) and collision efficiency (w_{co}). The coalescence mechanism (coalescence collusion frequency) can be explained by three following theories (Yeoh et al., 2013):

1- In the film-draining model developed by Shinnar and Church (1960), when two particles come together, a thin film of liquid trap between them. Then, the attractive forces between the two particles squeeze the liquid film to drain out. Eventually, the surfaces collapse and the two particles form a new larger particle. The coalescence can occur only if the interaction time between the two particles is sufficient for the liquid film to drain out to its critical rupture thickness. The simplified version of coalescence efficiency ($P_{eff,co}$) proposed by Ross (1971) is given as follows (Coulaloglou, 1975):

$$P_{eff,co}(d_{b,1}, d_{b,2}) = \exp(-\frac{t_{drainage}}{t_{contact}}) \qquad (3.30)$$

where $t_{drainage}$ and $t_{contact}$ are the drainage time and contact time, respectively. In this model, the particle surface can be considered as deformable surface or non-deformable surface, and the mobility of contact interfaces can be assumed immobile, partially mobile, and fully mobile (Lee

and Hodgson, 1968; Liao and Lucas, 2010). Luo (1993) considered deformable particles with fully mobile interfaces, which is the most complicated form, and proposed the drainage time as follows:

$$t_{drainage} = 0.5 \frac{v_{12} \rho_l d_{b,eq}^2}{\sigma} \tag{3.31}$$

where the $d_{b,eq}$ is the equivalent diameter of colliding bubbles of $d_{b,1}$ and $d_{b,2}$:

$$d_{b,eq} = \frac{d_{b,1} \cdot d_{b,2}}{(d_{b,1} + d_{b,2})} \tag{3.32}$$

$v_{b,12}$ is the characteristic velocity of collision of two bubbles with diameters of $d_{b,1}$, $d_{b,2}$:

$$v_{b,12} = (v_{b,1} + v_{b,2})^{1/2} \tag{3.33}$$

Luo (1993) assumed that the colliding bubbles have the same velocity with the eddy of equal size, so the velocities of $v_{b,1}$ and $v_{b,2}$ can be calculated by Equation (3.25).

The contact time (interaction time), can be calculated by the expression proposed by Luo (1993) as follows:

$$t_{contact} = \left(1 + \frac{d_{b,1}}{d_{b,2}}\right) \left(\frac{\left(\frac{\rho_g}{\rho_l} + C_{vm}\right) \rho_l d_{b,1}^3}{3\left(1 + \left(\frac{d_{b,1}}{d_{b,2}}\right)^2\right)\left(1 + \left(\frac{d_{b,1}}{d_{b,2}}\right)^3\right)\sigma}\right)^{1/2} \tag{3.34}$$

where C_{vm} and σ are the virtual mass coefficient and the surface tension coefficient, respectively.

2- In theory introduced by Howarth (1964), when the approach velocity of two colliding particles exceeds a critical value, coalescence will occur without film capturing and thinning. This model is also called the energy model, which was confirmed by optical records by Park and Blair (1975) and Kuboi et al. (1972b). The coalescence efficiency can be model as follows (Sovova, 1981):

36

$$P_{eff,Co}(V_{b,1}, V_{b,2}) = \exp(-C_{En}\frac{E_{int}}{E_{kin}}) \qquad (3.35)$$

where $P_{eff,Co}(V_{b,1}, V_{b,2})$ is the coalescence efficiency for the two colliding bubbles with volumes of $V_{b,1}$ and $V_{b,2}$. E_{int} and E_{kin} are the kinetic collision energy and interfacial energy, respectively. C_{En} is a model constant.

2- In the theory by Lehr and Mewes, (2001), two colliding bubbles will coalesce if their approaching velocities is less than a critical value. Hence, the smaller approach velocities lead to higher coalescence efficiencies.

The collision frequency (w_{co}) is defined as the number of collusion between two bubbles. It should be mentioned that collision of three or more bubbles at the same time is too rare, so it is mostly ignored in the literature. The different possible collision mechanism can be mentioned as follows (Liao and Lucas, 2010):

1- turbulent random motion-induced collisions,

2- velocity gradient-induced collisions,

3- capture in a turbulent eddy,

4- buoyancy-induced collision, and

5- wake entrainment.

The collision frequency (w_{co}) can be approximated with the help of kinetic gas theory (Kennard, 1938) as follows (Luo, 1993):

$$w_{co}(V_{b,1}, V_{b,2}) = A_{12}v_{b,12} \qquad (3.36)$$

where A_{12} is collision-sectional area:

$$A_{12} = \frac{\pi}{4}(d_{b,1} + d_{b,2})^2 \qquad (3.37)$$

By substituting Equations (3.33) and (3.37) in Equation (3.36), the collision frequency can be given as follows:

$$w_{co}(V_{b,1}, V_{b,2}) = C_{wf}(d_{b,1} + d_{b,2})^2 (d_{b,1}^{2/3} + d_{b,2}^{2/3})^{1/2} \varepsilon^{1/3} \qquad (3.38)$$

where C_{wf} is a constant.

3.4. Numerical Techniques

In the previous sections, some of the major equations used to deal with multiphase flow problems are mentioned. Finding the analytical solutions for those equations is impossible because of their complicity and nonlinearity. Therefore, the numerical approaches have to be employed. Trying to solve partial differential equations derived in the fluid analysis is recognized as computational fluid dynamics (CFD). Three major steps for CFD calculations can be mentioned as (1) pre-processing where the geometry of a problem is created, suitable grid (meshes) are generated, and finally, the boundary conditions are assigned; (2) flow solving where the driving equations of the flow are solved regarding the conditions introduced in the first step; and (3) post-processing where the results are interpreted and represented in graphical formats. In CFD simulation, discretization is applied to convert the continuous flow into a number of finite divisions so that they can be used in numerical calculations. The three main discretization methods are explained as follows:

3.4.1 The Finite Difference Method (FDM)

The finite difference method (FDM) is based on Taylor's series expansion to solve differential equations. For instance, the first derivative of an arbitrary function $fu(x)$ in the forward finit difference is given as:

$$fu'(x) = \lim_{h_T \to \Delta x} \left(\frac{fu(x + h_T) - fu(x)}{h_T} \right) \qquad (3.39)$$

It should be noted that h_T (interval) is approaching zero, but not be vanished. In this method, we have fix and limited values for h_T as it is named "finite" difference method. Although this method is simple, its implementation in case of complex geometries or unconventional boundary conditions is difficult (even impossible) because the grids are usually have to be defined in orthogonal ways (topologically square network) (Peiró and Sherwin, 2005).

3.4.2 The Finite Element Method (FEM)

In contrary to FDM, the finite element method (FEM) is appropriate for complex geometries because of its flexible dividing ability. This method consists of six steps (Chapra and Canale, 2015): (1) Discretization: in this step, the domain is divided into finite elements. (2) Driving element equations: developing equations for approximately solving each element. In this step, it is tried to optimize the equations regarding the original partial equations. The most common approaches are the direct approach, weighted residuals, and the variational approach. (3) Assembly: after driving equations for each individual element, they are combined and linked together. (4) Boundary conditions: boundary conditions are taken into account. (5) Solve: the equations are written in matrix formats and solved. (6) Post processing: the results can be displayed in a tubular or graphically forms. In summary, the FEM has strong and complex mathematics, and it can deal with complex and arbitrary shapes.

3.4.3 The Finite Volume Method (FVM)

The finite volume method (FVM) is widely used in computational software packages. This method is well suited for solving of different types of conservation laws (elliptic, parabolic or hyperbolic) (Eymard et al., 2000). Some of the key features of FVM are same as those of the finite element method: it can be applied on arbitrary and complex geometries, using both structured and unstructured meshes, and it leads to strong schemes. Moreover, because the finite volume method is based on the "balance" approach, the local conservativity of the numerical fluxes are guaranteed. It means that the conservation of a numerical flux from one discretization cell to its neighbor is constant. This feature makes the finite volume method very attractive, especially in the modeling problems where the flux is important, such as heat transfer and fluid mechanics problems (Eymard et al., 2000).

The first step in the FVM is dividing the domain into finite-sized subdomains called control volume or cell, which is represented by a grid point. The next key step is the integration of the governing equations over the control volume to yield a discretized equation at its nodal point (Versteeg and Malalasekera, 2007). Afterward, the profiles of variables within each control volume are derived. The integral form of the conservation law for a variable Φ can be written as (Garg, 1998):

$$\frac{\partial}{\partial t}\int_{\Psi} \Phi d\Psi + \oint_{S_A} F_A . dS_A = \int_{\Psi} Q d\Psi \qquad (3.40)$$

where F_A is the flux of variable Φ which crosses the control surface S_A that encloses the control volume Ψ. Q is the source/sink term for the parameter Φ in the control volume. The most important advantage of FVM is that this method guarantees conservativeness because it is based on material derivative ($\frac{D}{Dt}$) and divergence theorem (Equation 3.40). However, in the FVM, the definition of derivatives is not simple since the computational grid is not necessarily orthogonal and equally spaced (Garg, 1998). In addition, there is no mechanism to convert higher-order derivatives into lower ones (Garg, 1998).

3.4.5 Solution Algorithms

The SIMPLE algorithm (semi-implicit method for pressure-linked equations) is a common solution method in CFD tools, which was originally developed by Patankar and Spalding (1983). To solve the continuity (Equation 3.1) and momentum equations (Equation 3.3), we face nonlinearity and coupled equations. For example, the term of velocity in the *x*-direction is present in all momentum and continuity equations (coupled equation). Moreover, we have no individual equation for the pressure gradient terms. In the SIMPLE algorithm, a pressure gradient is guessed as the first step, and then, the momentum equations are solved. In the next step, the solved velocities are used in the continuity equation to modify the first guess. This procedure will continue until the reasonable residuals are achieved. It should be mentioned that in this method, the staggered grid (using different nodes for calculations of different variables) is employed. The velocities are computed at the cell faces while pressure is computed at the cell centers. To avoid exaggerated values from each iterative step, under-relaxation factor ($F_{rl,under}$) (to slow down the

changes) is used. For example, a new pressure (P_{new}) in the iterative process is given from the old pressure (P_{old}) as follows:

$$P_{new} = P_{old} + F_{rl,under} \times (P_{new} - P_{old}) \qquad (3.41)$$

Generally, if relaxation factor is chosen smaller than one, it is called under-relaxation factor, and if it is chosen larger than one, it is called over-relaxation factor.

To this conjecture, it is briefly mentioned how the partial differential equations can be converted to sets of algebraic equations that can be solved with various numerical methods. For the time discretization, the solver can be defined in the form of explicit scheme or implicit schemes.

In the explicit scheme, an unknown variable is calculated based on known variables in the previous time step. In this way, the boundary conditions (initial values) are used to solve the unknown variable coming from the previous time level. This method is mathematically simple but, requires a sufficiently small time step to be stable. The criterion for having a stable condition is given by the Courant number, *CFL*, which was first discovered by Courant Friedrichs in 1928 (Golub et al., 2007).

In the implicit scheme, estimation of an unknown variable in a certain time level requires information of that variable in its neighboring at the same time level. The implicit method requires more calculations in each time step compared to the explicit method (Johnson, 2012).

Jakobsen (2003) investigated both special and time discretization schemes; in a simple Taylor series analysis of one-dimensional equation, the transient artificial velocity coefficients can be given as (Roach, 1992):

for the explicit scheme:

$$\vartheta_{numerical} = \frac{V_x \Delta x}{2}(1 - CFL) \qquad (3.42)$$

for the implicit scheme:

$$\vartheta_{numerical} = \frac{V_x \Delta x}{2}(1 + CFL) \tag{3.43}$$

where V_x and $\vartheta_{numerical}$ are velocity in the x-direction and numerical diffusion, respectively. As it can be seen, in the case of the explicit scheme, if $CFL = 1$, the numerical error will be zero, and the exact answer (analytical answer) can be achieved. On the other hand, for the implicit method, always a numerical diffusion error will be present. Nevertheless, explicit methods are restricted by stability conditions, which can be aggravated in the multidimensional problems (Jakobsen et al., 1997).

The choice of time discretization scheme depends on the ability of iterative solution (especially for the implicit method), discretized domain, and available computational power.

The solution methods used in this research are explained in Chapters 4 and 5 through Sections 4.2 and 5.2, respectively.

4. Effect of Vertical Internals on the Hydrodynamics and Population Balance Model in Bubble Columns

4.1 Introduction

In this Chapter, the effects of dense vertical internals (rods) on gas holdup and local gas and liquid velocities were investigated using the Eulerian-Eulerian model coupled with the population balance model (PBM). The inclusion of lift and wall lubrication forces was studied by applying different models. Moreover, three circular internals' arrangements were considered to study the effect of wall and core clearance distances on the bubble column hydrodynamics. Also, the turbulence parameters were used to evaluate the capability of the population balance model in the prediction of the bubble size distribution. Then, a modification factor for the breakage and coalescence kernels was proposed.

4.2 CFD Model Development

Figure 4.1a displays the schematic diagram of the experimental set-up. A hollow and an obstructed bubble column with diameters of 0.19 m were considered while the hydrodynamic head of water was kept constant at 1.6 m. Four different internals' configurations comprised of 48 tubes with outer diameters of 0.0127 m were considered. The internals' configurations are depicted in **Figure 4.1b**; all configurations occupied 21.5% of the total cross-section area of the bubble column. Arrangement (A) was considered to mimic the experiment of Youssef et al. (2009) with a slight change in the tubes' arrangement for symmetry. In this arrangement, the tubes were mounted in an equilateral-triangle pitch of 0.024 m. In three other configurations, the tubes were inserted in four concentric bundles. To study the effect of wall clearance distance (d_{wall}), arrangements (B) and (C) with d_{wall}=0.012 m and d_{wall}=0.024 m were designed, respectively. Moreover, configuration (D) was considered to study the effect of core clearance. In this arrangement, the inner bundle diameter was increased by a factor of 1.7 compared to other arrangements. The results are reported along two lines at a height of 0.8 m: line N-N crossing no tubes, and line X-X crossing four tubes, as shown in **Figure 4.1b**.
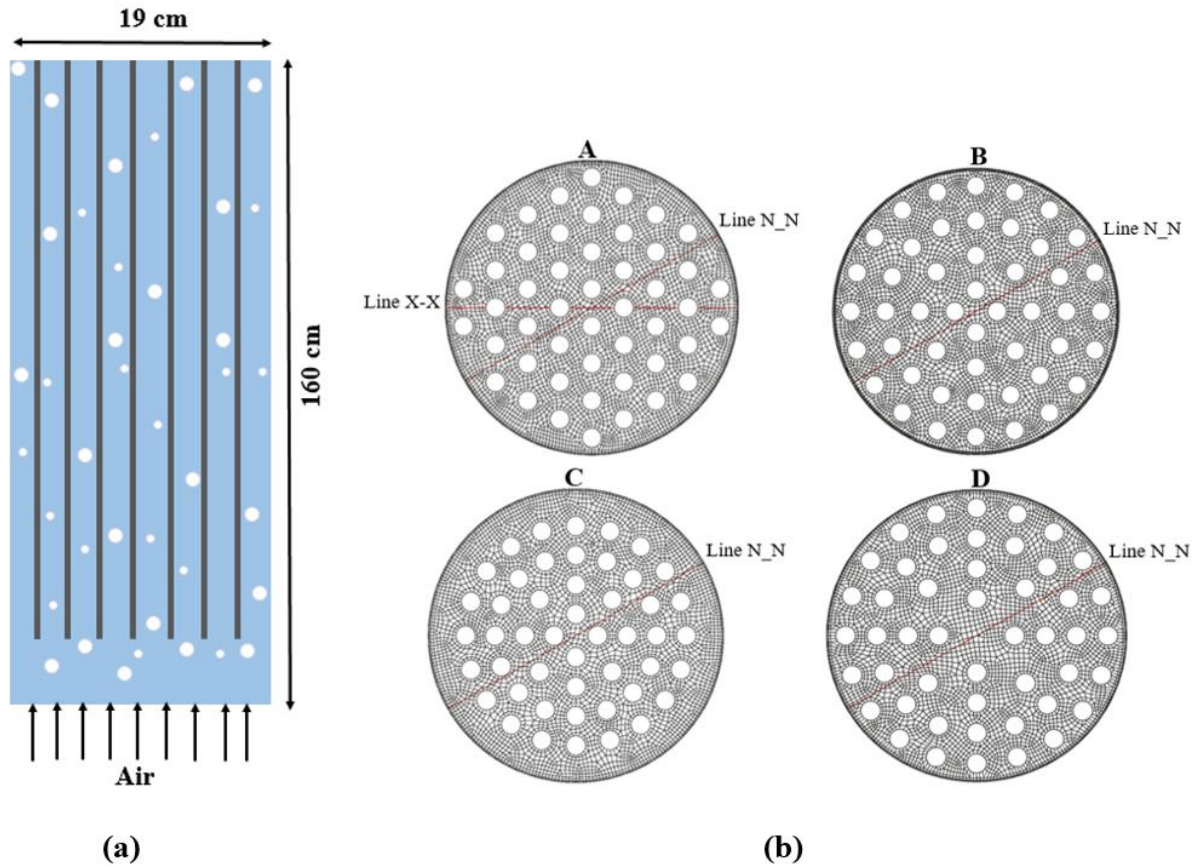
Figure 4.1: (a) Schematic diagram of the experimental set-up; **(b)** Different internals' arrangements with numerical mesh; (A): hexagonal, (B): uniform circular, (C): clear wall region and (D): clear core.

For a better understanding of the effect of internals on the hydrodynamics in the bubble column, the impact of the occupied area on the gas velocity must be considered. To do so, either reducing the gas flow rate (propotrional to area occupied with internals) or increasing the diameter of the column can be applied. In numerical modelings, a larger geometry needs more computational resources, so the former approach was applied in this study. This technique has also been practiced by Kagumba and Al Dahhan (2015), Jasmin (2016), and Al Mesfer et al. (2016). Arrangement (A) was selected to study the effect of interfacial forces and to compare the hydrodynamics of the bubble columns with and without internals. The gas phase (air) with a superficial gas velocity of 0.2 m/s was introduced uniformly at the bottom of the column. The bubble column without internals was named as case H. For the bubble column with internals, two cases were considered: in one case, the superficial gas velocity was assigned based on the free cross-section area CSA (named as case F) and in another case; it was assigned based on the total CSA (named as case T). The specifications of all cases are tabulated in **Table 4.1.** The hexagonal grids were employed to

achieve an acceptable orthogonal quality at reasonable grid sizes. For the hollow bubble column, the grid independence study with 63k, 105k, and 220k grids was conducted. The comparisons of the gas holdup and liquid velocity profiles showed that 105k grids were sufficient to have mesh independence results. For the bubble column with internals, finer grids were created around the tubes while their inside was modeled as space with no grid. The total numbers around 580k cells, depending on the internals' configurations, resulted from the grid sensitivity study; the numerical grids are depicted in **Figure 4.1b**. The mesh study for the bubble column with internals is discussed in Section 4.3. The geometries and discretization were created in ANSYS® Workbench and ANSYS® Meshing (release version 17.2), respectively.

Table 4.1: The specifications of cases.

Arrangement	Superficial gas velocity (V_{sf}, cm/s)
Without internals (case H)	0.2 m/s.
Hexagonal arrangement (A)	Case F: 0.2 m/s based on free cross-section area.
	Case T: 0.2 m/s based on total cross-section area.
Circular arrangements (B, C, D)	0.2 m/s based on total cross section-area.

4.2.1 Numerical Details

The Eulerian-Eulerian model was employed for simulation of the gas-liquid system in this work. Subscript φ is the phase index that can be l for the continuous phase (water) or g for the dispersed phase (air):

$$\frac{\partial}{\partial t}\left(\alpha_\varphi \rho_\varphi\right) + \nabla.\left(\alpha_\varphi \rho_\varphi \vec{u}_\varphi\right) = 0 \tag{4.1}$$

where ρ_φ is density and $\vec{u}_\varphi$ is the velocity vector. The momentum balance for each phase was written as follows:

$$\frac{\partial}{\partial t}\left(\alpha_\varphi \rho_\varphi \overrightarrow{u_\varphi}\right) + \nabla.\left(\alpha_\varphi \rho_\varphi \vec{u}_\varphi \vec{u}_\varphi\right) = -\alpha_\varphi \nabla.P + \nabla.\left(\bar{\bar{\tau}}_{\text{eff}}\right) + \vec{M}_I + \rho_\varphi \alpha_\varphi \vec{g} \tag{4.2}$$

where P is the pressure, $\bar{\bar{\tau}}_{eff}$ is the effective phase stress-strain tensor, $(\rho_\varphi \alpha_\varphi \vec{g})$ is the gravitational force, and $\overrightarrow{M_I}$ is the representation of the interaction forces. In the Eulerian-Eulerian model, two terms are required to close the momentum equation (Equation 4.2): One for interface forces $(\overrightarrow{M_I})$, and one for turbulence $(\bar{\bar{\tau}}_{eff})$:

- Interfacial Forces $(\overrightarrow{M_I})$:

The accuracy of the Eulerian-Eulerian model depends strongly on the modeling of the interfacial closures. These closures can include drag, lift, virtual mass, wall lubricants, Saffman forces, and so on. Sokolichin et al. (2004) entailed the inclusion of each force to experimental verification of its existence, and the degree of its importance for the simulation. Among these forces, the inclusion of the drag force prevails in the numerical modeling, while consideration of others is still under debate. In this study, the drag, lift, and wall-lubrication forces were modeled. The drag force is the predominant force in multiphase flows that can be obtained from the following equation:

$$F_D = \frac{3\alpha_g}{4} C_D \left(\frac{\rho_l}{d_b}\right) |\vec{u}_g - \vec{u}_l| (\vec{u}_g - \vec{u}_l) \tag{4.3}$$

where d_b is the bubble diameter and C_D is the drag coefficient of a bubble in the swarm. Generally, drag coefficients have been derived for an isolated bubble. To account for the effect of the swarm on the drag coefficient, many studies have been conducted (e.g. Simonnet et al., 2008; McClure et al., 2017). However, large discrepancies can be observed among the correlations available in the literature (Rusche, 2003). In this paper, the effect of swarm on the drag coefficient was modeled as follows (McClure et al., 2014):

$$C_D = C_{D\infty} (1 - \alpha_g)^{P_D} \tag{4.4}$$

$C_{D\infty}$ is the drag coefficient for a single bubble in the large fluid. P_D is the volume fraction correction factor, which was considered as 1 (Jiang et al., 2016). The drag coefficient of the isolated bubble ($C_{D\infty}$) was calculated from the modified version of the Schiller and Naumann (1935) model, which can directly read the bubble sizes from population balance models (ANSYS® FLUENT, 2017).

The origin of the lift force is due to the net effect of stress and pressure on the surface of bubbles. The lift force was modeled as follows (Žun, 1980):

$$F_L = -\rho_l C_L \alpha_g (\vec{u}_g - \vec{u}_l) \times (\nabla \times \vec{u}_l) \qquad (4.5)$$

where C_L is the lift force coefficient that can be assumed constant or be estimated based on the local properties. Tomiyama (1998) derived a model based on the Eötvös number (Eo) in order for the coefficient to change in different conditions. In this work, a slightly modified version of the Tomiyama model was used as follows (Frank et al., 2004):

$$C_L = \begin{cases} \min[0.288\tanh(0.121Re_g), f(Eo_d)], & Eo_d < 4 \\ f(Eo_d), & 4 \leq Eo_d \leq 10 \\ -0.27 & Eo_d < 10 \end{cases} \qquad (4.6)$$

where Eo_d is the Eötvös number based on the long axis of the deformable bubble, d_H:

$$f(Eo_d) = 0.00105Eo_d^3 - 0.0159Eo_d^2 - 0.0204Eo_d^2 + 0.474) \qquad (4.7)$$

$$Eo_d = \frac{g(\rho_l - \rho_g)d_H^2}{\sigma}, \qquad d_H = d_b(1 + 0.163Eo)^{1/3} \qquad (4.8), (4.9)$$

$$Eo = \frac{g(\rho_l - \rho_g)}{\sigma} d_b^2 \qquad (4.10)$$

where σ is the surface tension coefficient. In this study, both the constant lift force coefficient and Tomiyama model (Tomiyama, 1998) were considered.

For the modeling of lateral movements of bubbles, Antal et al. (1991) suggested that another force should be included to ensure low volume fractions near walls. They showed that the pressure difference due to the no-slip boundary condition exposes a transverse force on the bubbles near walls. This force is called wall force (or wall-lubrication force):

$$F_{WL} = -C_{WL}\rho_l\alpha_g\left|\vec{u}_g - \vec{u}_l\right|^2\vec{n}_w \tag{4.11}$$

where $\vec{n}_w$ is the outward unit normal vector pointing from the wall, and C_{WL} is the model coefficient which will be discussed later.

- Turbulence Modeling:

The turbulence of the continuous phase was obtained by the Reynolds stress model (RSM). The RSM is superior to the common two-equation models, such as standard $k - \varepsilon$, by considering anisotropy turbulence in the system (Masood et al., 2014). In this model, $\bar{\bar{\tau}}_{eff}$ in Equation (2) is given as

$$\bar{\bar{\tau}}_{eff} = -\rho_l\alpha_l R_{ij} \tag{4.12}$$

The transport equation for the Reynolds stress (R_{ij}) with an extra term ($\Pi_{R,ij}$) for interaction between phases is written as follows (Cokljat et al., 2006):

$$\frac{\partial}{\partial t}(\rho\alpha R_{ij}) + \frac{\partial}{\partial x_k}(\rho\alpha\vec{u} R_{ij})$$
$$= -\rho\alpha\left(R_i\frac{\partial\vec{u}_j}{\partial x_k} + R_j\frac{\partial\vec{u}_i}{\partial x_k}\right) + \frac{\partial}{\partial x_k}\left(\alpha\mu\frac{\partial}{\partial x_k}(R_{ij})\right)$$
$$- \frac{\partial}{\partial x_k}(\rho\alpha u_i'u_j'u_k') + P\alpha\left(\frac{\partial u_i'}{\partial x_j} + \frac{\partial u_j'}{\partial x_i}\right) - \rho\alpha\varepsilon_{ij} + \Pi_{R,ij} \tag{4.13}$$

$$\Pi_{R,ij} = \frac{2}{3}\delta_{ij}\Pi_k \tag{4.14}$$

δ_{ij} is the Kronecker delta. The turbulent interaction term between the liquid and gas phases (Π_k) was solved by the closure proposed by Simonin and Viollet (1990). The turbulence parameters in dispersed phase (i.e. turbulent stress, k, and ε) were estimated by Tchen's theory of dispersion (Hinze, 1975).

- Population Balance Model (PBM)

In the Eulerian-Eulerian model, the size of the bubbles is an important input. Choosing the right size of bubbles is a challenge in the modeling of bubble columns operated at high gas velocities. One method is to choose a constant size for bubbles (known as Sauter mean diameter), which can represent the bubble size distribution. In the other method, two or three bubble sizes are assumed to cover the small and large bubbles (Krishna et al., 1999). Then, the model equations are solved for each bubble size as a separate phase. These two methods might be reasonable at low superficial gas velocities, but their applicability at conditions with a wide range of bubble sizes is under question. Moreover, the need for specifying the Sauter mean diameter prior to running the simulation impairs the predictivity of the methods. In this work, to overcome these difficulties, the discrete population balance model was coupled with the CFD model. The general form of the population balance model (PBM) equation can be written as follows (Ramkrishna, 2000):

$$\frac{\partial N(V_b, t)}{\partial t} + \nabla[U_b N(V_b, t)] = S_N \tag{4.15}$$

The terms on the left-hand side are time variation and transport for the bubble class local number density (N) of a bubble having a volume of V_b. S_N is the source term due to a break up and coalescence which were calculated by the closures of Luo and Svendsen (1996) and Luo (1993), respectively. To solve the PBM equation, the Multiple Sized-Group (MUSIG) method was used. This method is also known as the discrete method that discretized the bubble population into a finite number of size intervals (known as bins). To check the sensitivity of the results to the number of bins, the lognormal probability density function (PDF) of 10, 20, and 30 classes in the range of 1-60 mm were compared to each other. The number of 20 bin classes was found sufficient from the comparision.

The behavior of a bubble column is associated with a high degree of fluctuations making the consideration of an unsteady-state solver with an adequate averaging time inevitable. Although the explicit scheme offers simpler calculations and better handling of the artificial numerical diffusion, it relies strongly on the Courant number, *CFL* (Courant-Friedrichs-Lewy condition) (see Jakobsen, 2003). Therefore, the implicit scheme with a time-step of 0.01 second was applied in this study. The time span of 60 seconds for the pseudo-steady state condition and an extra 100 seconds for

the time averaging were considered. The QUICK discretization schemes were applied to minimize the numerical diffusion errors. The equations were solved by ANSYS$^{©}$ FLUENT (release version 17.2). The convergence criteria were set at 10^{-4} for all residuals except, for the continuity set at 10^{-3} to save computational time. The parallel processing on Inlet Core CPU associating 24 processors was employed; runtime varied 70-90 hours for each case.

4.3 Results and Discussion

Figures 4.2a, **b** show the effect of the number of grids on the volume fractions and gas velocity in the bubble column with internals (arrangement A), respectively. We started our mesh independence study with a coarse mesh of 130k (mesh 1) which results in an unrealistic peak in the gas holdup profile of around $r/r_0 = \pm 0.8$. By increasing the number of cells to 300k (mesh 2) and 580k (mesh 3), the peak decreased while the further increasing of cells to 980k (mesh 4) did not change the gas holdup and velocity profiles. Moreover, the simulations showed less sensitivity to the grid size in the axial direction so a fine grid can be disregarded in that direction. The geometries were discretized into 100 divisions in the axial direction. The results indicated that both volume fraction and gas velocity must be checked to ensure mesh independency. As clearly seen in **Figure 4.2b**, the gas velocity profiles were not largely affected by the grid size. Meanwhile, the gas holdup significantly changed by doubling the number of cells from the coarse size to the medium size (**Figure 4.2a**). The total numbers around 580k cells, depending on the internals' configurations were considered for the bubble columns with the internals.

-Effect of Lift Force:

Modeling of lift force is still premature, and there is no specific guideline for the determination of its coefficient. Due to this ambiguity, it has been completely ignored in such literature as Larachi et al. (2006), Laborde-Boutet et al. (2009), Chen et al. (2005), Pfleger et al. (2001), and Oey et al. (2003). However, our simulations showed that the value of the lift force coefficient plays an important role in the steepness of radial profiles and overall gas holdup. In addition, lift force can be used as a tool to account for other lateral forces (such as turbulent dispersion) where there is no firm formulation for them (Sokolichin et al., 2004). Thakre et al. (1999) suggested a stepwise procedure that is a trial and error method to find the best drag and lift coefficients to fit the drift flux model. In this paper, as the drag coefficient was known from Schiller and Naumann (1935) model, the problem reduced to one unknown coefficient (i.e. lift coefficient). A similar concept was followed, and the gas holdup data reported by (Youssef, 2010) were considered as the benchmark criteria. The procedure resulted in the lift coefficients of 0.08 and -0.06 for the bubble column without and with internals, respectively.
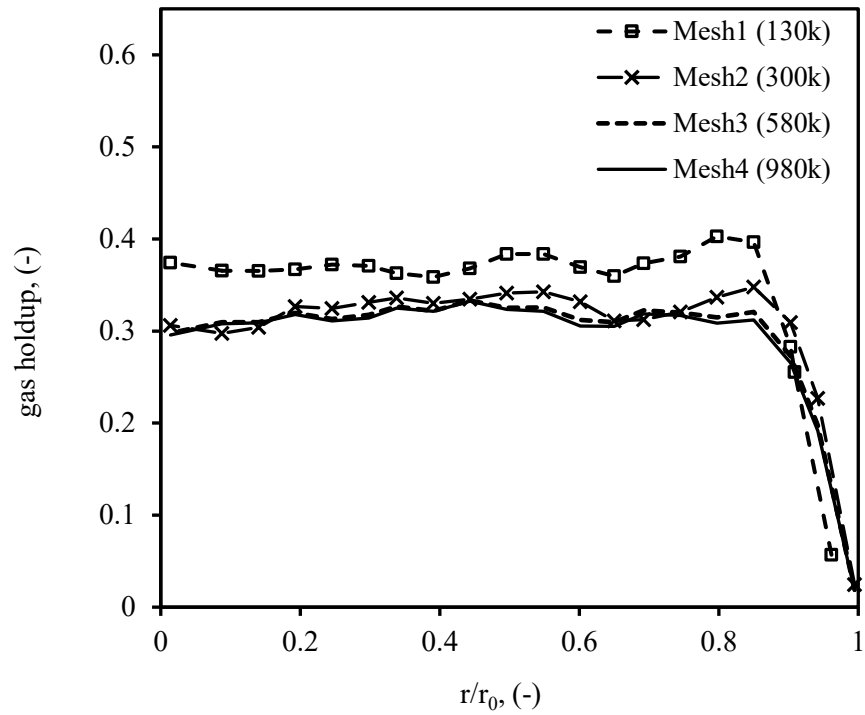
(a)
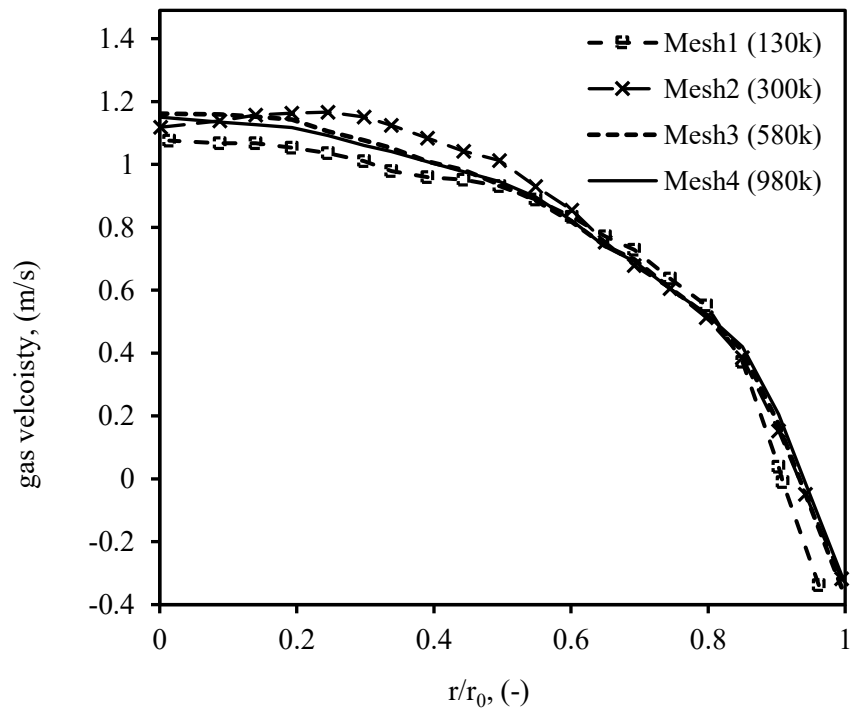
(b)

Figure 4.2: Grid sensitivity study on: **(a)** gas holdup (-); **(b)** gas velocity (m s^{-1}).

Figure 4.3 shows the effect of lift force coefficient on the gas holdup profile in the hollow bubble column. In the exclusion of lift force (C_L=0), the gas holdup profile was found sharp in compared to the experimental data. The positive sign of the lift force coefficient (C_L=+0.08) contributed to a greater dispersion of the bubbles in the radial direction. The positive lift force coefficient caused a significant reduction in the slope of the gas holdup's curve by helping bubbles to move outwards (i.e. towards the column wall) (Tabib et al., 2008). However, the Tomiyama model (Frank et al., 2004) resulted in an unrealistic profile (underestimated in comparison with the experiments) due to the production of large negative values of the lift coefficient for the bubbles with diameters larger than 7mm (C_L=-0.27).

The effect of lift force in the presence of internals are shown in **Figure 4.4**. In the exclusion of lift force (C_L=0), the model resulted in an almost flat gas holdup profile with a peak near the wall region. Because of the existence of liquid circulation in the bubble column, term ($\nabla \times \vec{u}_l$) in the lift force equation (Equation 5) becomes negative. Therefore, the negative lift coefficient can cause a negative force and shift the bubbles to the center of the column (Bhusare et al., 2017). So, a negative value of the lift force coefficient was selected to push the bubbles to the center of the column. Guan and Yang (2017) also employed a small lift coefficient (C_L=-0.02) for simulating bubble columns with sparse internals (5% coverage). Because of the lift force coefficient, the peak of the gas holdup (at $r/r_0 \approx 0.65$) was reduced in **Figure 4.4a**, and the profile got closer to the experimental data of Youssef (2010). In the hollow bubble column, the bubbles were able to move freely in the lateral directions that allowed the parabolic gas holdup profile to be developed easily. However, in the presence of internals, the lateral movement of the bubbles were restricted, so the negative lift force coefficient helped to reproduce the proper radial gas distribution. Comparing **Figures 4.3** and **4.4a,b**, the Tomiyama model (Tomiyama, 1998) performed better in the bubble column with internals as it could predict the sign of the lift force coefficient correctly. In this study, the Tomiyama model was calculated based on the local Sauter mean diameter. The model performance might be enhanced by considering the size of each bubble class as it was originally developed for single bubbles rising in liquid (Tomiyama et al., 2002).
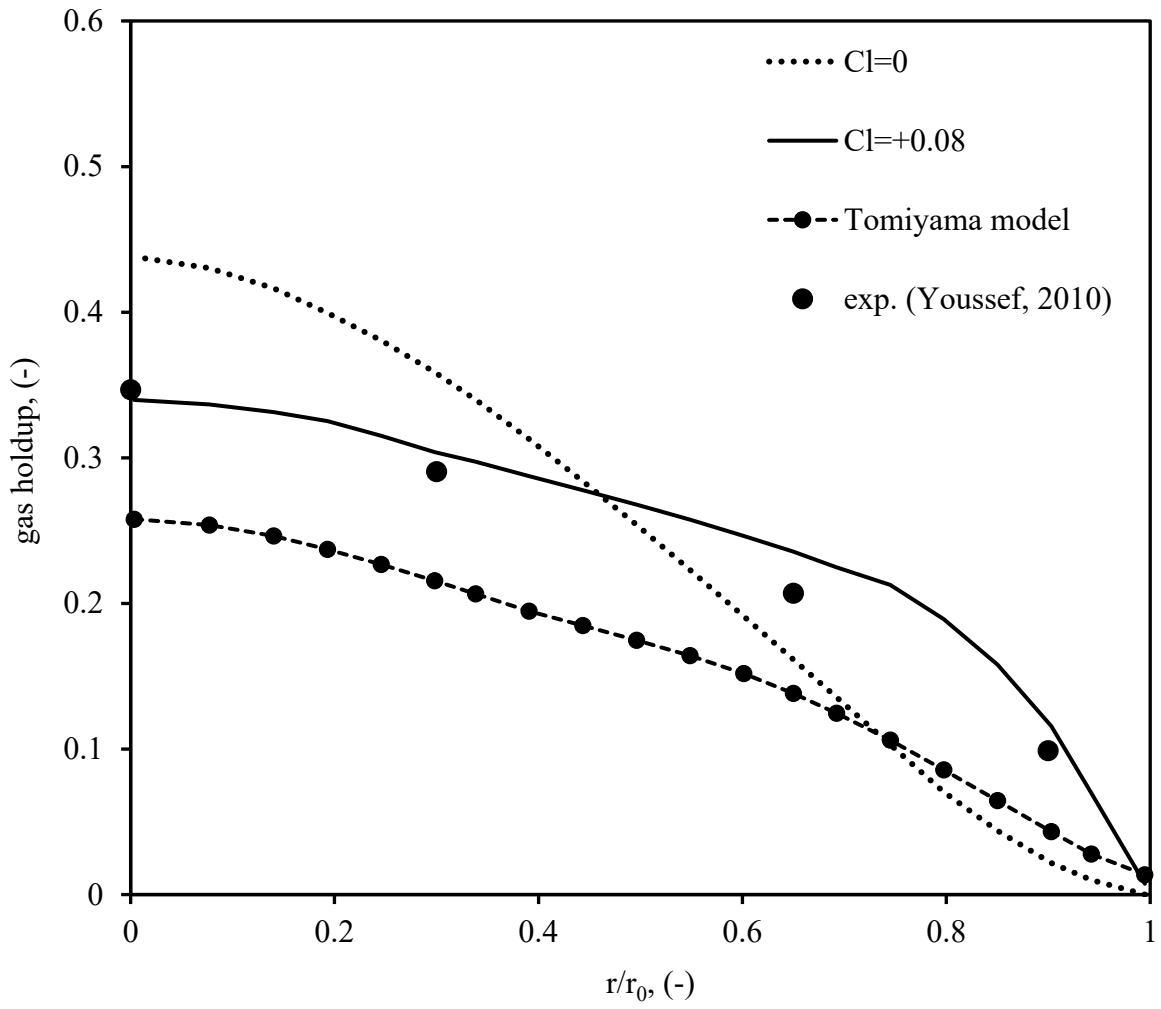
Figure 4.3: The effect of lift force on the gas holdup in the hollow bubble column (case H).

(a)
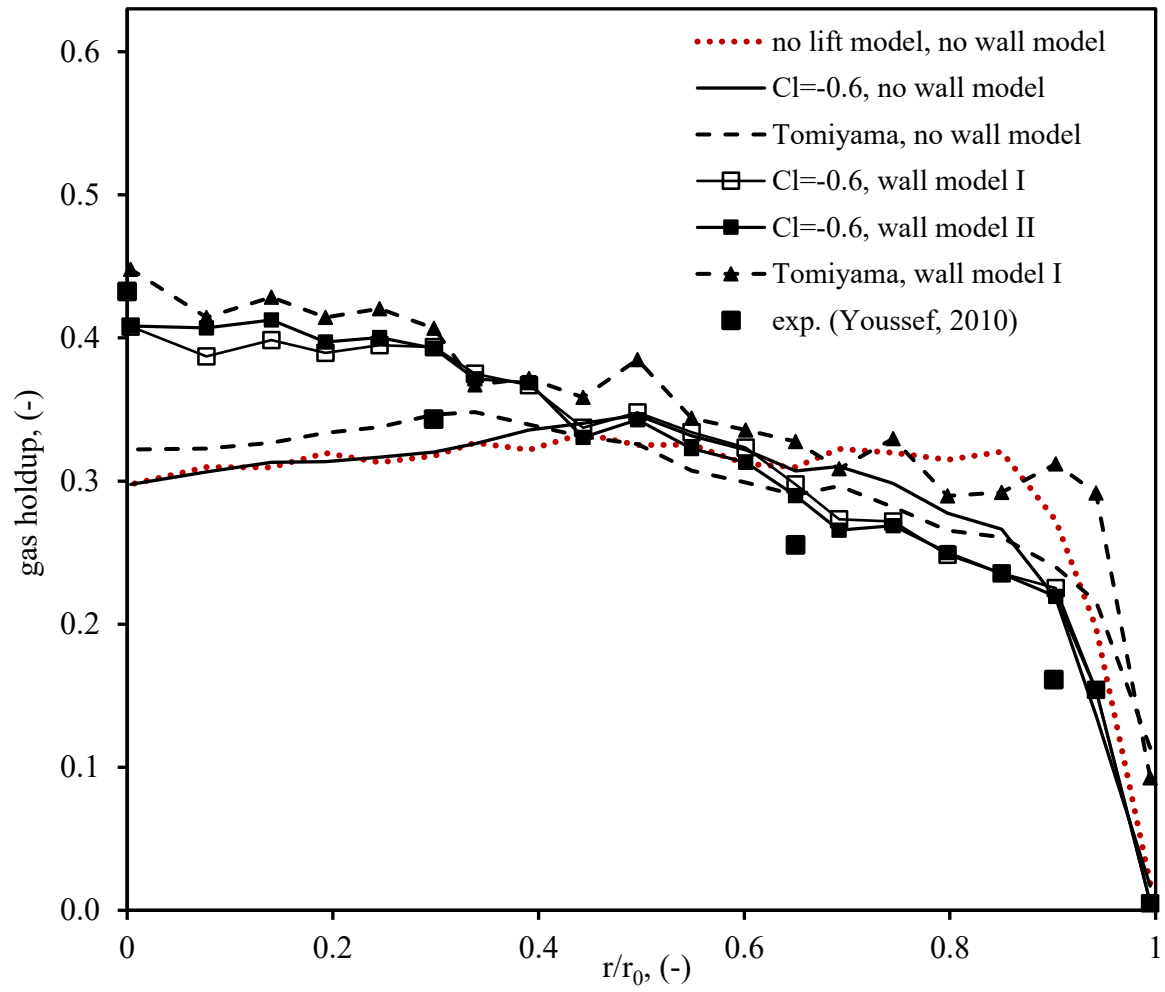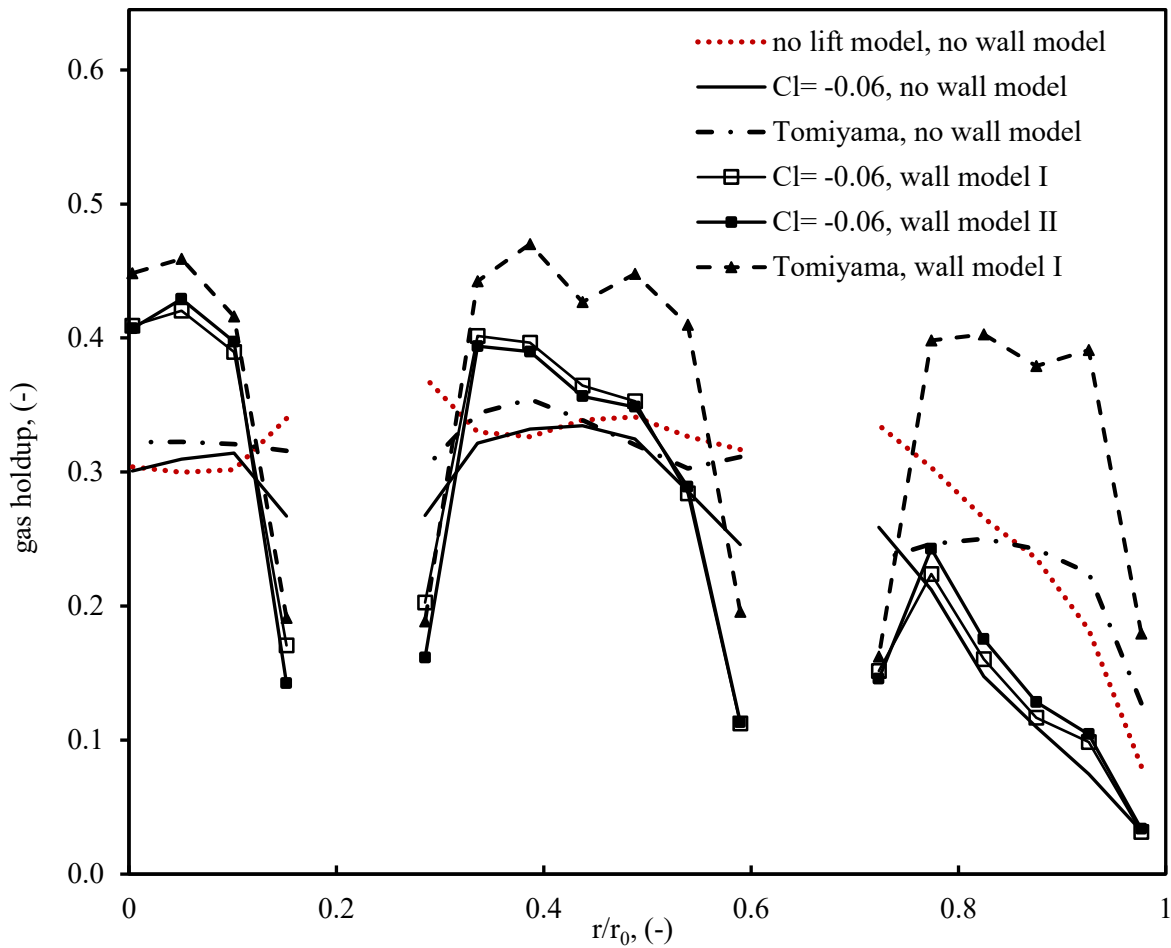
Figure 4.4: The effect of lift and wall force on the gas holdup (-) profile in the bubble column with internals (case T) along **(a)** line N-N; **(b)** line X-X.

-Effect of Wall-lubrication Force:

As mentioned earlier, the negative lift coefficient moved the bubbles away from the column's wall to the center of the column (**Figure 4.4a,b**). However, it could not sufficiently reduce the gas volume fraction near the tubes. This observation contradicts the expectation of very low gas volume fraction near solid walls. To address this issue, the wall-lubrication force was modeled. The wall-lubrication coefficient in Equation (4.11) was calculated by Antal et al. (1991) model as follows:

$$C_{WL} = max(0, \frac{C_{w1}}{d_b} + \frac{C_{w2}}{y_w}) \qquad (4.16)$$

where y_w is the distance from the wall, and C_{w1} and C_{w2} are the model fitting parameters. In this study, the wall force model with two different sets of parameters has been assessed as follows:

parameters I: $C_{w1} = -0.01$, and $C_{w2} = 0.05$ (adapted from Ekambara et al., 2008).

parameters II: $C_{w1} = -0.06U_s - 0.104$ (U_s: slip velocity), and $C_{w2} = 0.147$ (adapted from Antal et al., 1991).

The dependency of the models on d_b and y_w are tabulated in **Table 4.2**. By doubling of y_w, the wall-lubrication coefficients were significantly reduced in both models. However, in parameters I, the small value of C_{w1} made it less sensitive to the bubble size as shown in **Table 4.2**.

The effect of the wall force on the gas volume fraction is shown in **Figure 4.4a,b**. All the cases showed better performance with the wall force model, especially at the center of the column as illustrated in **Figure 4.4a**. The effect of wall force on the value of gas holdup between the rods is shown in **Figure 4.4b**. The local gas holdup significantly reduced near the rods in both cases of the constant lift coefficient and Tomiyama model (Tomiyama, 1998). However, the Tomiyama model over-predicted the values of the gas holdup, especially in the annular region. The comparison of wall force models (I and II) was shown in **Figure 4.4a,b** where almost a similar performance was observed. The two wall models were able to push the bubbles away from the walls sufficiently and enhanced the results. However, as discussed above, parameters I are less reliant on the size of bubbles that would make them more versatile for numerical modeling than parameters II.

As the conclusion, C_l=+0.08 for the hollow bubble column, and C_l=-0.06 with wall-lubrication force parameters I for the bubble columns with internals were found as the best combinations for the interfacial forces. The comparisons of gas holdup profiles in the hollow bubble column (case H) and bubble column with internals (case T) with the experimental data of Youssef (2010) are shown in **Figure 4.3** and **Figure 4.4a**. The models could follow the experimental data very well. The wave-like shape of the gas holdup profile (**Figure 4.4a**) could not be seen in the experimental

data (Youssef 2010) because of the limited number of reported points in the radial direction (four points). In **Figure 4.5**, the gas velocity profiles were compared against the experimental measurements of Hamed (2012) for cases H and F. The most deviation from the experimental data occurred around the liquid inversion point for the hollow bubble column (case H). However, the simulations agreed well with the experimental data both qualitatively and quantitatively.

Table 4.2: The effect of bubble diameter and y_w on the wall force coefficient.

Bubble diameter, m	Wall force coefficient (C_{WL})			
	Parameters I		Parameters II	
	$y_w = 0.002$m	$y_w = 0.004$m	$y_w 0.002$m	$y_w = 0.004$m
0.005	60	23	70	32
0.01	47	10	65	27
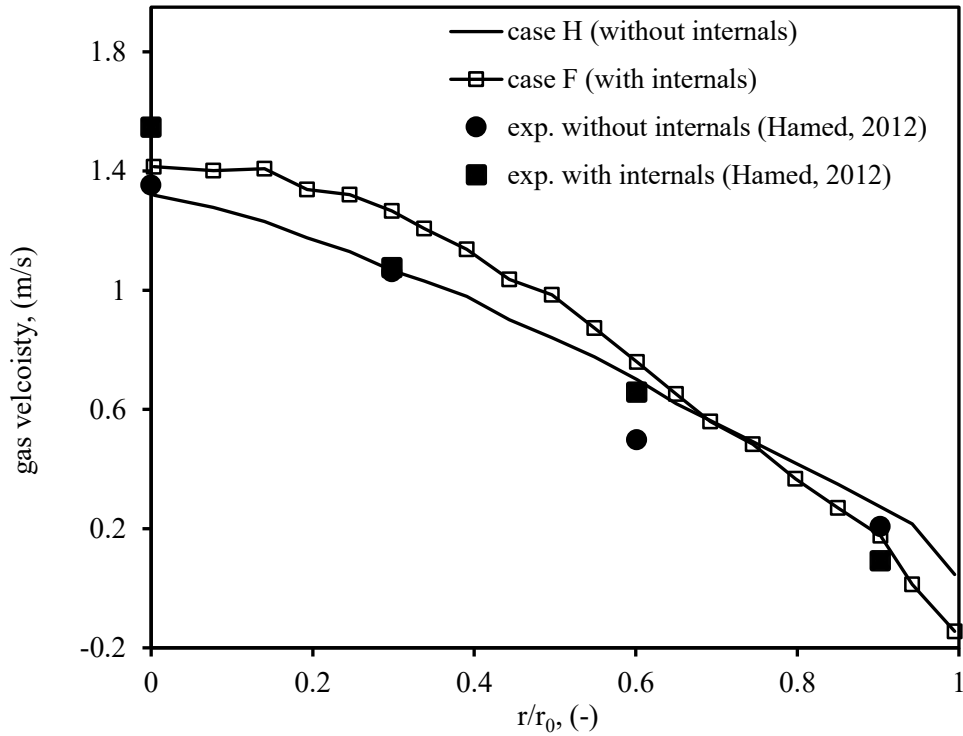
Figure 4.5: The comparison of the gas velocity (m s^{-1}) profiles with the experimental data of Hamed (2012).

-Effect of the Internals (Arrangement A) on Gas Holdup:

The instantaneous and time-averaged gas holdup contours on a vertical plane at the center of the column are depicted in **Figure 4.6**. The instantaneous contours showed chaotic structures in the bubble columns, which is expected because of a high degree of fluctuation in the systems. However, the flow pattern showed up when averaged over time. In the bubble column with internals, the large gas structures in the center broke down through the column.
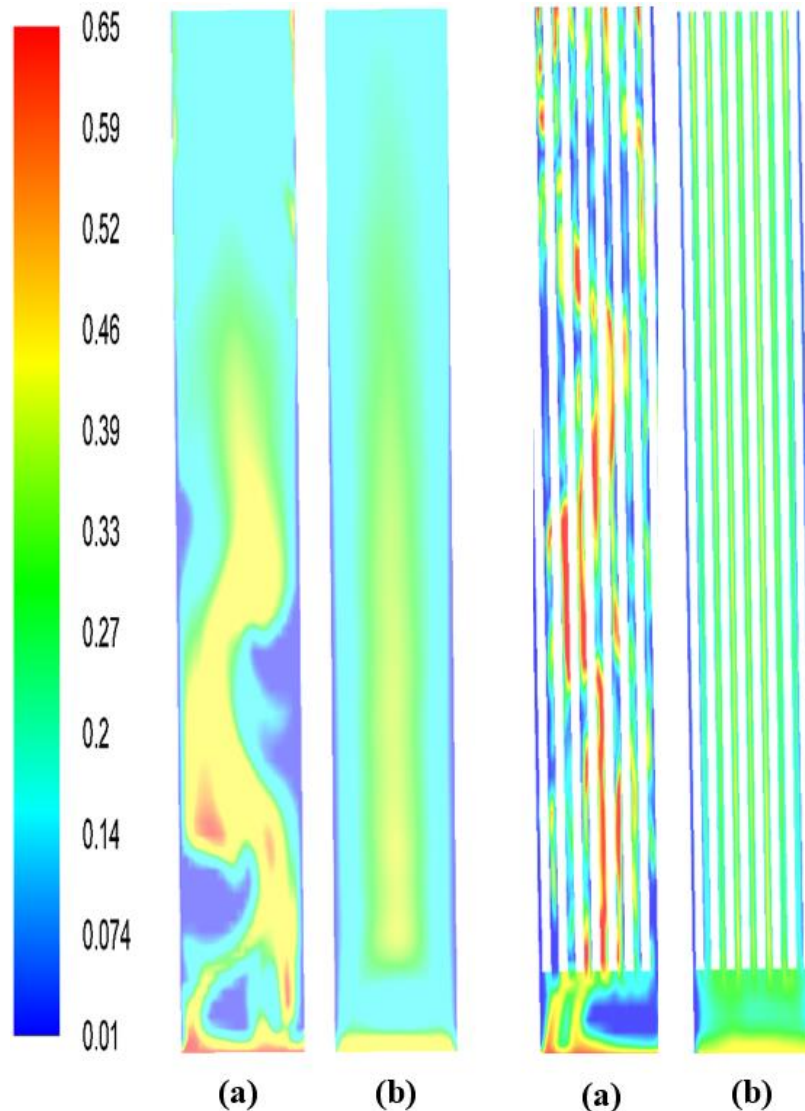
Figure 4.6: The instantaneous and time-averaged contour plots of gas holdup (-) for: **(a)** the hollow bubble column (case H); **(b)** the bubble column with internals (case T).

The gas holdup profiles for the hollow bubble column (case H), and the bubble columns with internals (cases T and F) along the lines of N-N and X-X are illustrated in **Figure 4.7**. The presence of the internals did not alter the core-annular structure where we have the maximum gas holdup values in the core and the minimum values near the walls. However, the internals changed the gas holdup profiles from a smooth curve to wavy-like form because of the intermittently available area for the gas phase. From **Figure 4.7**, the gas holdup profiles became higher and steeper along line N-N in the presence of internals. As the result of internals, the values of the local gas holdup increased by 7% and 20% at the center of the columns in cases F and T, respectively, while no significant change was observed at the walls. This increase of gas non-uniformity in the radial direction makes lateral forces more important in the developing of the flow structure. On the line of X-X, crossing four tubes, the impact of internals became more complicated. The internals increased the gas holdup in the core while reducing its value near the wall of the column, as observed in **Figure 4.7**.

In the hollow bubble column, the overall gas volume fraction was calculated as 0.22, which rose to 0.27 in the presence of internals when the superficial gas velocity was based on the total CSA (case T). On the other hand, when the superficial gas velocity was based on the free CSA (case F), the value of the overall gas holdup just slightly increased by 6%. This finding is in line with previous studies (Jasmin, 2016; Al Mesfer et al., 2016; Kagumba and Al Dahhan, 2015) where the significant increase in the gas holdup was linked to the reduction of the passage area for the gas phase. Hence, as a rule of thumb, one can estimate the overall gas holdup in a bubble column with internals by considering the superficial gas velocity based on the free CSA.
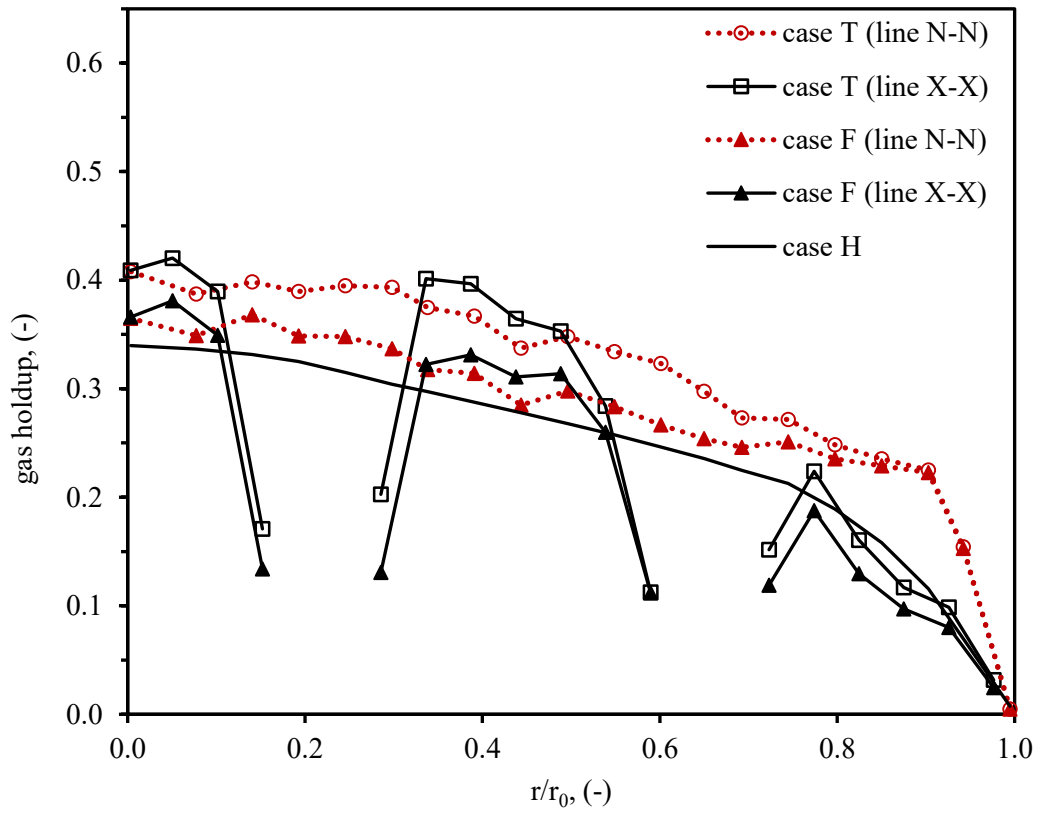
Figure 4.7: The comparison of gas holdup (-) profiles of the hollow bubble column (case H), and the bubble column with internals (cases F and T) along line N-N and line X-X.
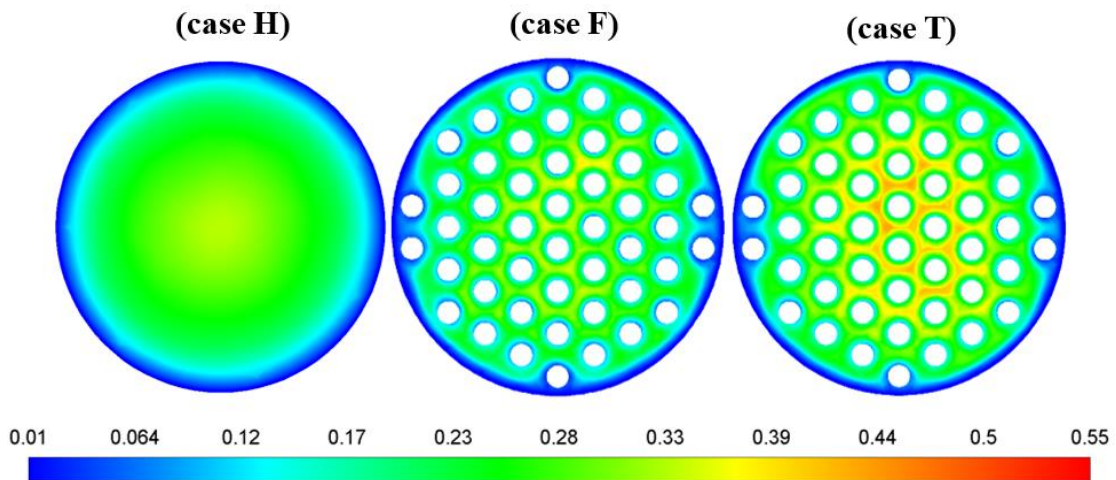

Figure 4.8: The time-averaged gas holdup (-) contours for the hollow bubble column (case H) and the bubble column with internals (case F and case T).

-Effect of the Internals (Arrangement A) on Liquid and Gas Velocities:

The axial liquid velocity profiles are shown in **Figure 4.9**. The positive values of the liquid velocity indicate an upward flow in the core region, and the negative values indicate a downward flow near the walls. The simulations were able to reproduce the well-recognized gulf stream in the bubble columns. In the presence of internals (arrangement A), the maximum of liquid velocities increased 40% and 55% for case F (superficial gas velocity based on free CSA) and case T (superficial gas velocity based on total CSA), respectively. Because of these increases at the centerline, larger negative liquid velocities resulted near the wall of the column.

The liquid velocity behaves differently along the lines of X-X and N-N. From **Figure 4.9**, in case F on the line of X-X, by moving from the core to the wall of the column, the liquid velocity was reduced by 1.6 m/s, which is 18% higher than the one on the line of N-N. These variations in the liquid velocity profiles lead to change the liquid inversion points (where the direction of flow changes). In the bubble columns with internals, the coordinates of the inversion point were interpolated around $r/r_0 = \pm 0.62$ along line X-X. These locations are very close to the inversion point of the hollow bubble column ($r/r_0 = \pm 0.65$). These results are well aligned with the experimental observation of Al Mesfer et al. (2017) where the inversion points took place at $r/r_0 = \pm 0.68$ in both columns with and without internals. One might conclude that internals do not change the inversion points. However, the liquid velocity profiles on the line of N-N revealed that inversion points can be significantly affected by internals. On the line of N-N, the less steep liquid velocity profile (a weaker driver for recirculation), caused inversion points to occur farther from the core ($r/r_0 = \pm 0.8$) compared to line X-X. Still, in the presence of internals, the liquid velocities experienced larger negative values at the wall of the columns, no matter which line was selected.

The behavior of gas and liquid velocities are connected tightly in a way that each one influences the other. Bubbles as the source of the kinetic energy, cause the upward movement of liquid through the center of the column. Consequently, the liquid after being blocked by the free surface carries a portion of the bubbles back downward near-wall regions. The radial gas velocity profiles are depicted in **Figure 4.10**. As can be seen in this figure, the presence of internals increased the gas velocity magnitude at the center of the column by 20% and 30% in cases F and T, respectively. The higher increase in case T was due to its higher gas flow rate, which also intensified the global liquid recirculation. In case H, due to the weaker liquid recirculation, "positive" values for the gas

velocity were obtained at all points. On the other hand, in case T, the great negative magnitude of liquid velocity pulled down the bubbles and created a channel of descending bubbles near the wall of the column. In this case, the gas velocity became negative (downward flow) between $r/r_0= \pm0.8$ to $= \pm1$ along the line of X-X.

Figure 4.9: The comparison of liquid velocity (m s^{-1}) profiles of the hollow bubble column (case H), and the bubble column with internals (cases F and T) along line N-N and line X-X.

The simulations indicated that for a comprehensive understanding of the fluid dynamics in the bubble column with internals, not only different cross-sectional lines, but also the very near-wall regions must be monitored. In case F (**Figure 4.10**), the negative gas velocities can be seen on the 22% of line X-X, although on the line of N-N, it just showed up at a region very close to the wall ($r/r_0\approx \pm0.95$) that wouldn't be easy to capture experimentally. The information about negative gas velocity is very useful in the modeling of reactors where the gas profile largely affects the residence times.
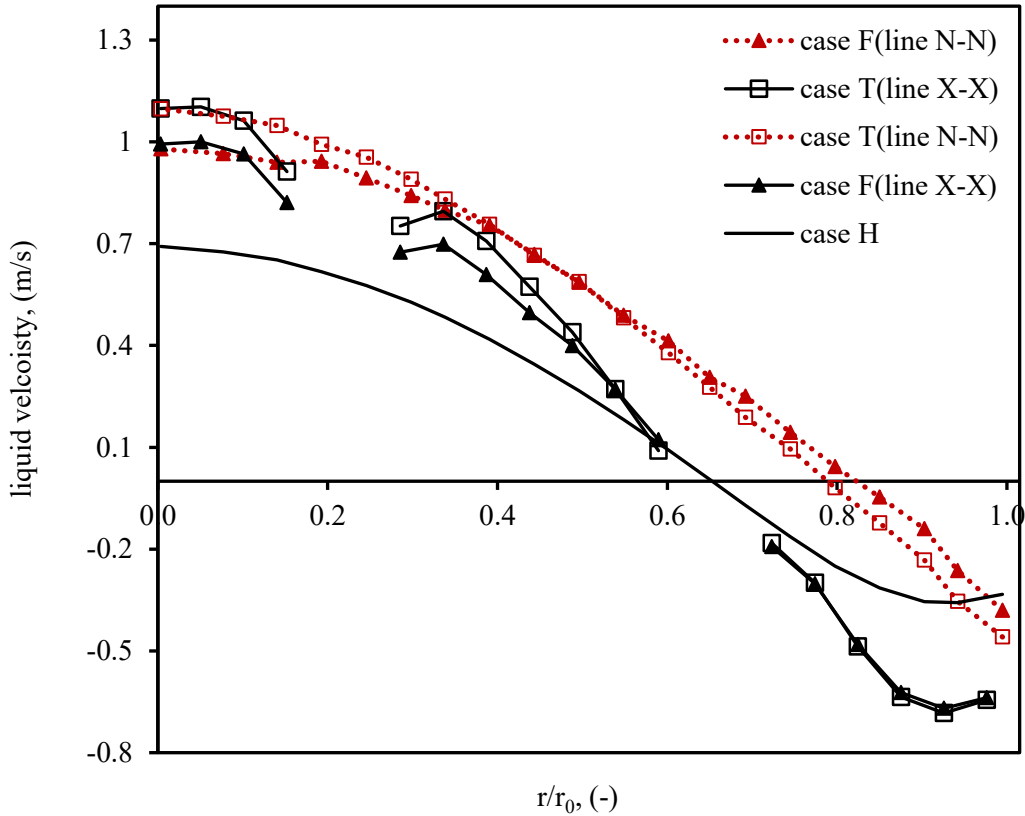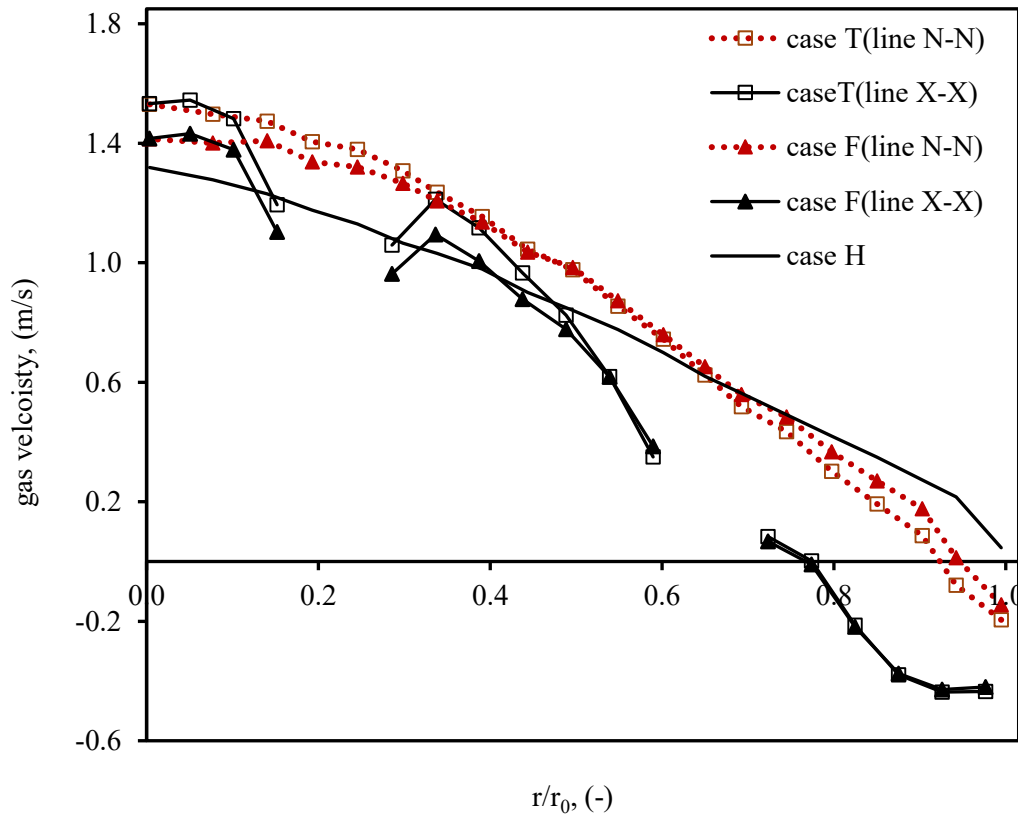
Figure 4.10: The comparison of gas velocity (m s^{-1}) profiles of the hollow bubble column (case H), and the bubble column with internals (cases F and T) along line N-N and line X-X.

-Comparisons of the Different Internals' Configurations (B, C, and D):

Three circular internals' configurations of (B), (C), and (D) were considered to investigate the effect of wall and core clearance distances on the hydrodynamics of bubble columns. **Figure 4.11** shows the contours of gas holdup for the different arrangements on the cross-sectional plane at the middle of the bubble column. As can be seen in **Figure 4.11**, in arrangement (C) (clear wall), the gas volume fraction near the vicinity of the wall is significantly higher than arrangement (B) because of the presence of internals in that region. In arrangement (D) (clear core), a higher concentration of gas phase in the core region is clearly distinguishable compared to the other arrangements. The gas holdup profiles are depicted in **Figure 4.12a**. In arrangement (C), a considerable increase of gas holdup in the near-wall vicinity can be observed. In this case, due to the free space for bubbles in the wall region, a more uniform gas holdup profile could be achieved. On the other hand, in arrangement (B), bubbles were pushed away to the core region that led to 8% of higher central gas holdup compared to arrangement (C). According to **Figure 4.12a**, the

64

core clearance (arrangement D) led to the increase of gas holdup at the center by 8.5% and 18% compared to arrangements (B) and (C), respectively.

Figure 4.12b shows the radial gas velocity profiles of different arrangements. A similar trend to the gas holdup can be observed. Arrangement (C) led to the most uniform gas velocity profile by providing a free space at the wall region. In this case, the bubbles can distribute through the cross-section and scape upward through the wall region. The lowest gas velocity was observed in arrangement (B) where the gas velocity was reduced to -0.48 m/s with the gas inversion points at $r/r_0= \pm0.8$. On the other hand, in arrangement (C) (clear wall), the gas velocity at the wall region was the highest among the cases with the inversion points very close to the wall ($r/r_0= \pm0.97$). **Figure 4.12c** shows the radial liquid velocity profiles of different arrangements. The lower gas velocity gradient in arrangement (C) contributed to the relatively uniform profile of liquid velocity and pushed the liquid inversion points toward the wall of the column. The presence of dense internals near-wall vicinity (arrangements A, B, D) caused the strong liquid circulation and pronounced effects of internals on the bubble column's hydrodynamics. In arrangement (C), the liquid radial velocity gradient and centerline velocity reduced significantly due to the increased the wall clearance distance. These results showed that arrangements of internals might also affect the liquid mixing performance as Krishna et al. (2000) found that the liquid axial dispersion was proportional to the liquid centerline velocity.
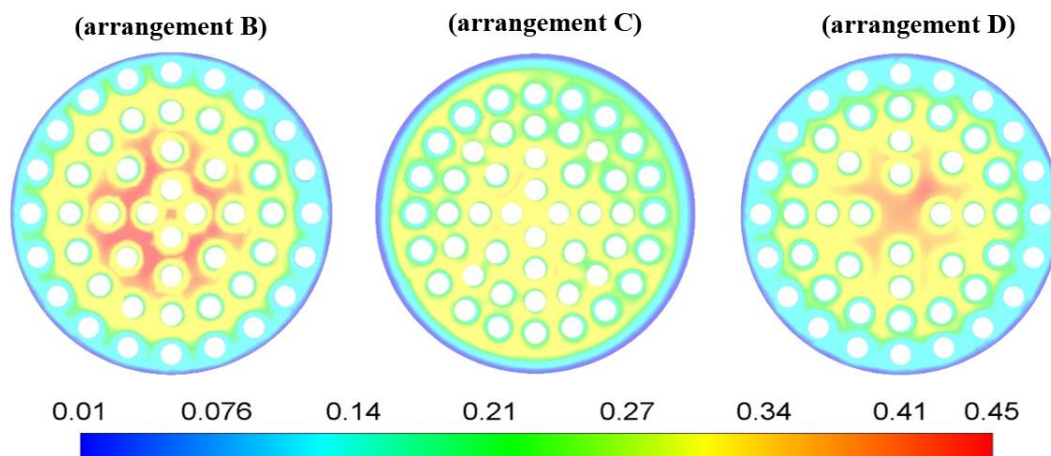
Figure 4.11: The time-averaged gas holdup (-) contours for arrangements B, C (clear wall), and D (clear core).

(a)

(b)

66
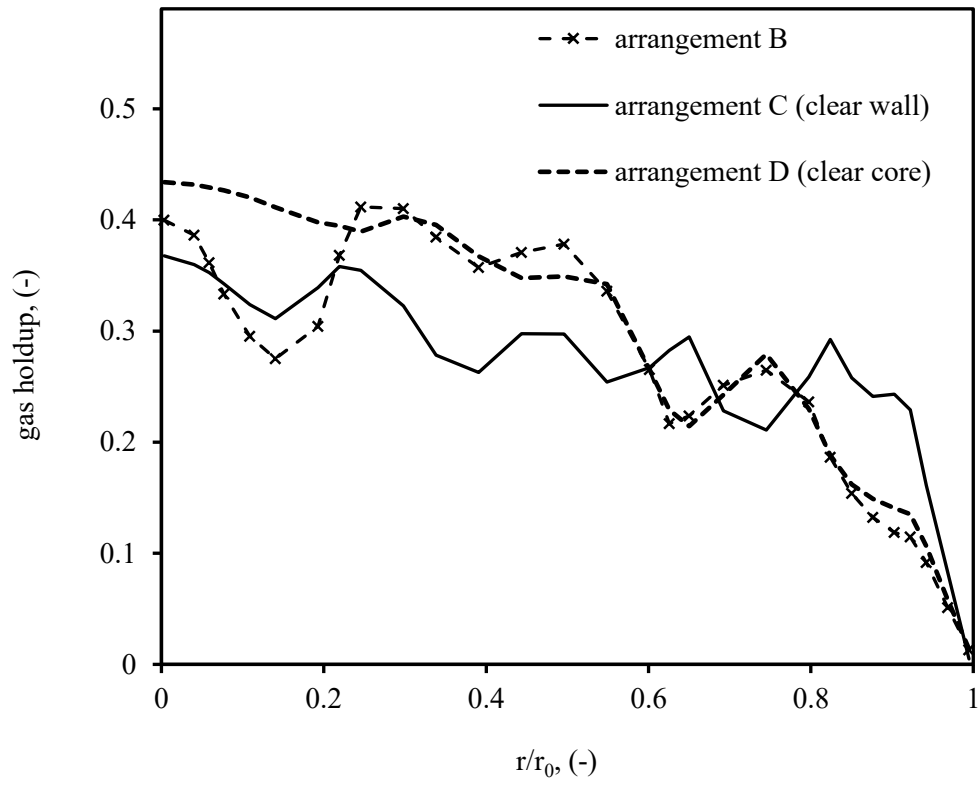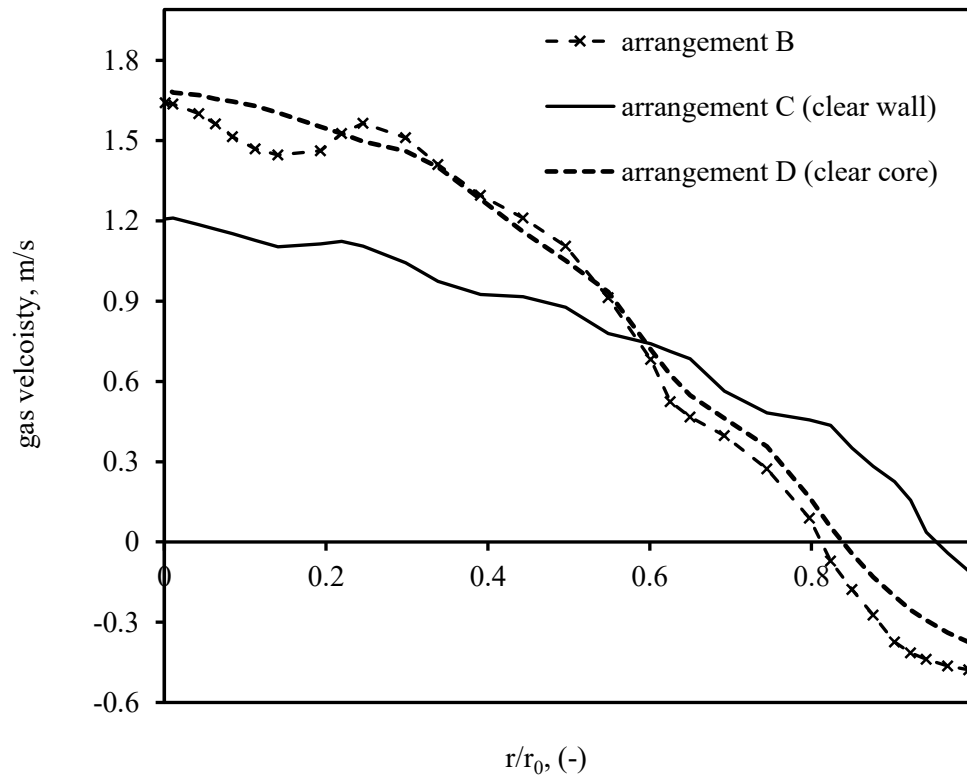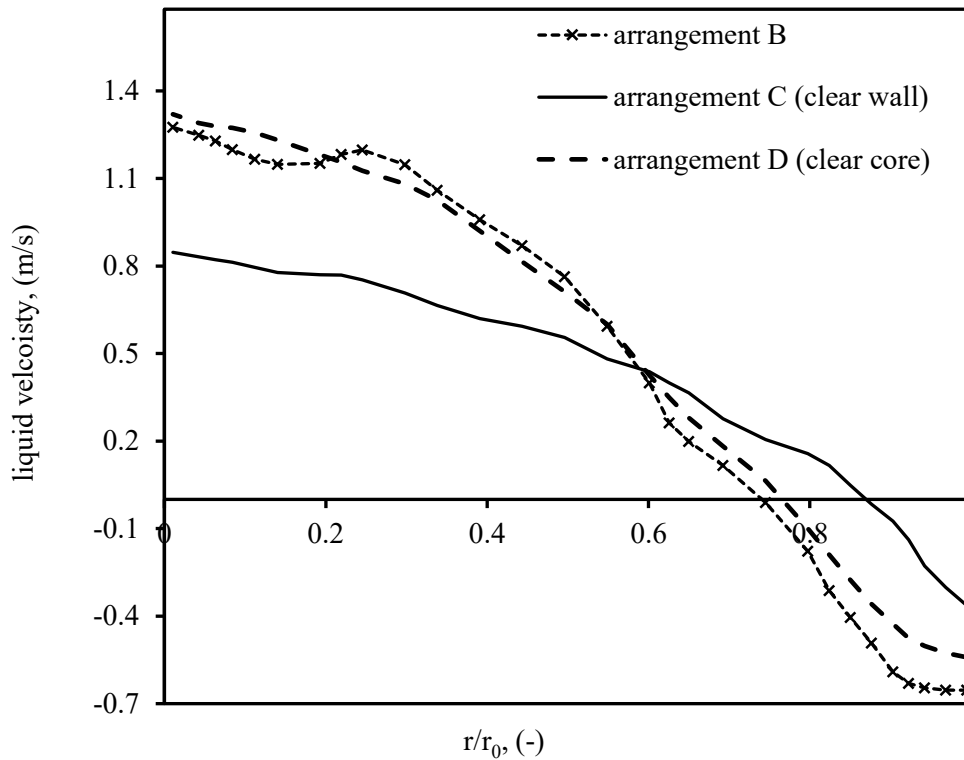
(c)

Figure 4.12: The comparison of **(a)** gas holdup (-) profiles; **(b)** gas velocity (m s^{-1}) profiles; **(c)** liquid velocity (m s^{-1}) profiles of arrangements (B), (C), and (D) alone line N-N.

-Effect of the Internals on the Bubble Size Distribution:

The Luo kernel functions (Luo, 1993; Luo and Svendsen, 1996) relies on both local flow proprieties (e.g. turbulent parameters) and fluid characteristics (e.g. surface tension). Chen et al. (2005) showed that the coalescence rate prevailed the bubble breakage rate in the Luo kernels. They introduced an underestimation of the turbulent dissipation rate (ε) as a possible reason for this malfunctioning. In their study, the breakage rate was timed by ten as a rough engineering estimate. Laborde-Boutet et al. (2009) focused on the effect of turbulent dissipation rate on the mean eddy length scales. They envisaged that by using a turbulence model resulting in smaller length scales, the higher breakage rate would be achieved. Our simulaions showed that the mean eddy length scale was significantly reduced by internals because of geometrical change and the reduction in turbulnt kinetic energy. The turbulent kinetic energy contours are shown in **Figure 4.13a**. Although the mean eddy length scale was reduced by the internals, the breakage rate did

67

not sufficiently increase in our simulation. Therefore, the effects of underestimating the turbulent dissipation rate become pronounce in other terms rather than in eddy length scales. Several studies employed different approaches to address the shortcomings of the population balance kernels, for instance, Bhole et al. (2008) (modified the eddy's energy equation); Yang et al. (2017) (proposed correctors based on the energy minimization), Olmos et al. (2001) (applied a calibration factor of 0.75), etc. Nevertheless, the Luo kernels showed another shortcoming in dealing with the bubble columns with internals as discussed below:

In the breakage rate, the arrival frequency strongly depends on ε (Luo and Svendsen, 1996):

$$w_{br}(d_b) = 0.923(1 - \alpha_l)n(\varepsilon d_b)^{1/3} \frac{(1 + \xi)^2}{d_b^2 \xi^{11/3}} \tag{4.17}$$

where $\xi = \lambda/d_b$. The contour plots of the turbulent dissipation rate (ε) are shown in **Figure 4.13b**. A significant increase in the local turbulent dissipation rate occurred around the internals, which can also be seen in the counter plots reported by Guan and Yang (2017). However, our turbulence model showed a reduction in the mean value of the turbulent dissipation rate in the presence of internals. This reduction can be linked to decreasing the turbulence intensity (due to the decrease in turbulence length scale) and the possible effect of wall shear in the system. As the breakage rate decreases with the decreasing of ε, the PBM resulted in a larger mean bubble diameter. However, this outcome is not consistent with the experimental observations where the mean bubble diameter decreased by internals (Youssef, 2010; Jasmin, 2016). A larger mean bubble diameter despite the increase in the population of smaller eddies, indicated that the collision and breakage efficiencies were not be predicted correctly by the Luo model. In other words, the Luo model resulted in the higher number of smaller eddies whose energy and/or the possibility of collisions are not sufficient for breakage. Therefore, regardless of the accuracy of the turbulence closure in the prediction of ε, the Luo population balance model would fail to decrease the mean bubble diameter in the presence of internals. In our simulation, to address the limitations of the Luo kernels and considering the breakage mechanisms due to the presence of internals, a modification factor "F" was employed. To balance the surface and eddy energies in the breakage kernel, factor F was implemented in the bubble surface energy as follows:

$$\bar{e}(s) = FC_f\pi d_b^2\sigma \qquad (4.18)$$

where σ is the surface coefficient and C_f is the increase coefficient of surface area. Different correctors in coalescence efficiency have been implemented by Nguyen et al. (2013) (based on turbulent suppression) and Xu et al. (2013) (adding factor 0.5), etc., to tune the coalescence kernels. Here, factor F was also applied in the time of drainage formula in the coalescence kernel (Shinnar and Church, 1960) as follows:

$$t_{drainage} = 0.5\frac{u_{12}\rho_l d_{b,eq}^2}{F\sigma} \qquad (4.19)$$

where the $d_{b,eq}$ is the equivalent diameter of colliding bubbles of $d_{b,1}$ and $d_{b,2}$. u_{12} is the charactistic velocity of collision of two particles with the diameter of $d_{b,1}$ and $d_{b,2}$.

In both breakage and coalescence kernels, factor F was imposed on the bubble surface parameters where the internals possibly affect. The value of F was determined in such a way that the mean bubble diameter reaches equilibrium by ascending along the axis of the column. The comparisons of mean bubble diameters on different plates along the height of the columns are shown in **Figure 4.14**. The equilibrium values for the mean bubble diameter could be established by F=0.4 and F=0.7 for bubble columns with and without internals, respectively. The smaller value of F for the bubble column with internals showed that other numerical source terms are needed to balance the breakage and coalescence rates in the presence of internals. The values of the mean bubble diameters from the original model and the modified model have been compared against the experimental data of Youssef (2010) in **Figure 4.15**. The original model largely overestimated the value of mean bubble diameters in both cases H (without internals) and T (with internals). On the other hand, by applying the modification factors, the results agreed well with the experimental data reported by Youssef (2010). Further studies on the possible breakage mechanisms due to the presence of internals (especially the collision of bubbles with internals) are required to develop inclusive kernels for population balance models.
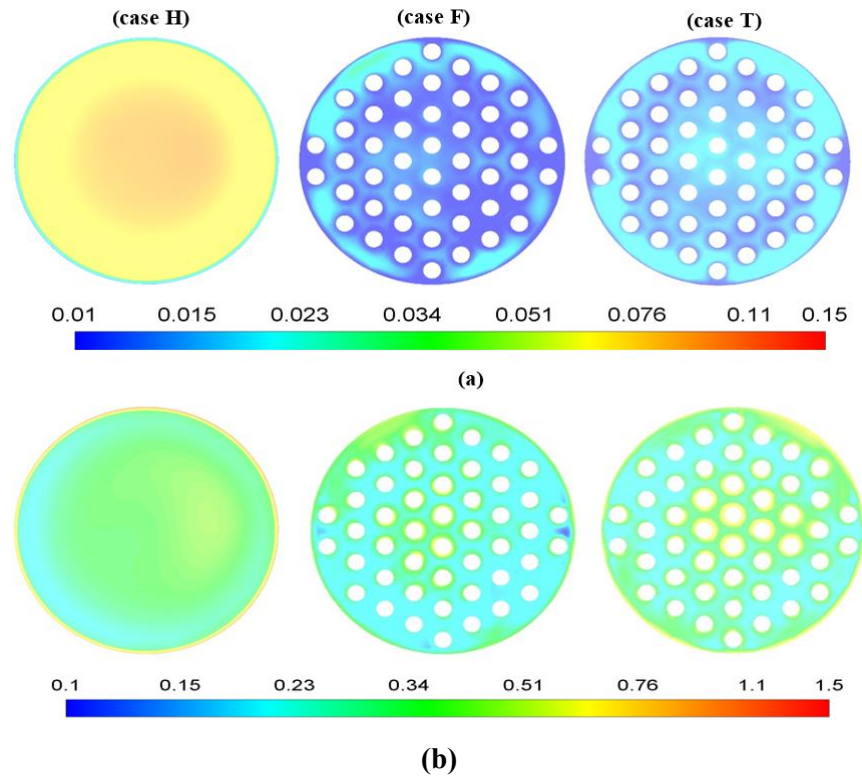
Figure 4.13: The contour plots for the hollow bubble column (case H) and bubble column with internals (case F and case T): **(a):** the turbulent kinetic energy ($m^2 s^{-2}$); **(b)** the turbulent dissipation rate ($m^2 s^{-3}$).
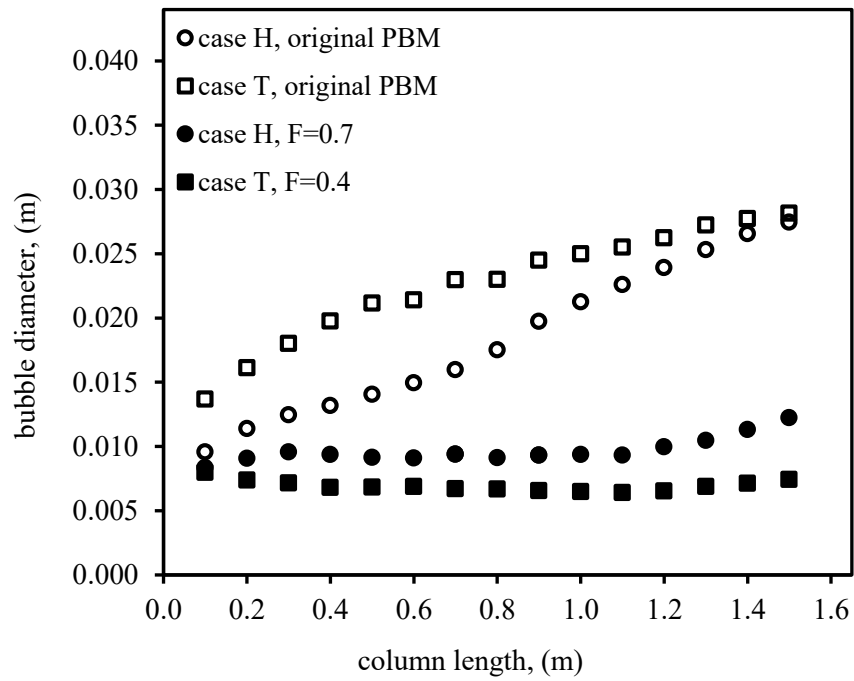
Figure 4.14: The evolution of the mean bubble diameter (m) along the vertical axis (m) of the bubble column.
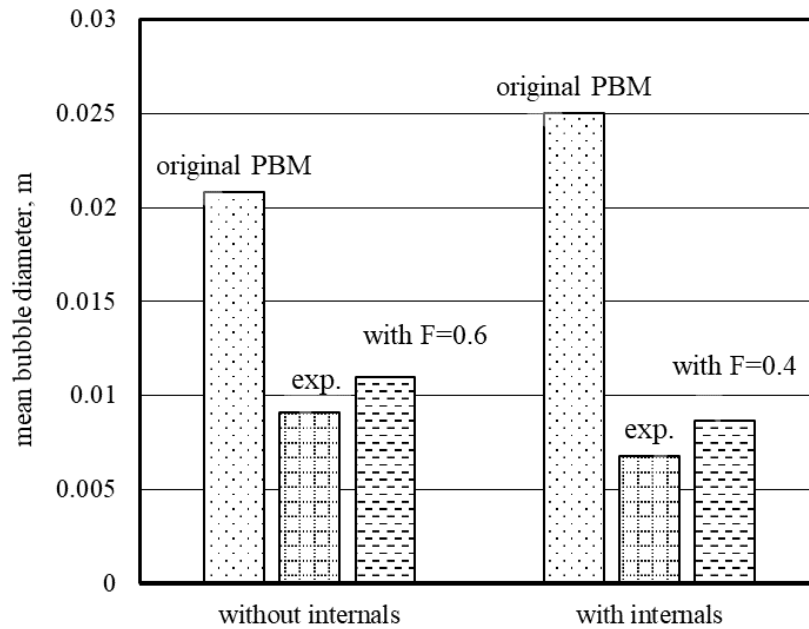
Figure 4.15: The comparison of mean bubble diameters (m) in the bubble columns with and without internals against the experimental data of Youssef (2010).

Figure 4.16 presents the effect of the internals (arrangement A) on the probability distribution function (PDF) profiles. The bubble size distribution can offer valuable information regarding flow regime in bubble columns; a thin range of bubble size distribution and a high ratio of small bubbles to large bubbles can be taken as the characteristics of a bubbly flow regime (see Wang et al., 2005). According to **Figure 4.16**, in the presence of internals, the bubbles were shifted toward the smaller diameters with a narrower range. The internals increased the percentage of small bubbles from 50% to 60% that resulted in the decrease of the mean bubble diameter by 20%. These observations showed that internals can be considered as a hindrance for the flow regime transition in bubble columns. Changing the internals arrangement affected neither the mean value nor the overall bubble size distribution, i.e., all internals' arrangement led to the practically similar PDF profiles and mean bubble diameters. However, the internals arrangement affected the local bubble size; the effect of different arrangements on the local mean bubble diameter is depicted in **Figure 4.17**. The radial profile of mean bubble diameter in the hollow bubble column covered a wider range of bubble sizes compared to the bubble column with internals. Arrangements (B) and (C) resulted in similar radial distributions of bubble sizes while arrangement (D) (clear core) resulted in a slightly higher mean bubble diameter at the core. In arrangement (C), the larger bubble size near the wall's vicinity, in the absence of internals, contributed to a higher gas velocity as reflected in **Figure 4.12b**.

71

Figure 4.16: The comparison of the PDF (mm^{-1}) profiles of bubble sizes (mm) in the bubble column with and without internals.

Figure 4.17: The radial distributions of the mean bubble diameter (m) along line N-N.

4.4 Conclusions

The Eulerian-Eulerian model was employed for the simulation bubble columns with and without internals. The study on the lift force showed that constant lift force coefficients can significantly enhance the results. The lift force coefficients of 0.08 and -0.06 were found th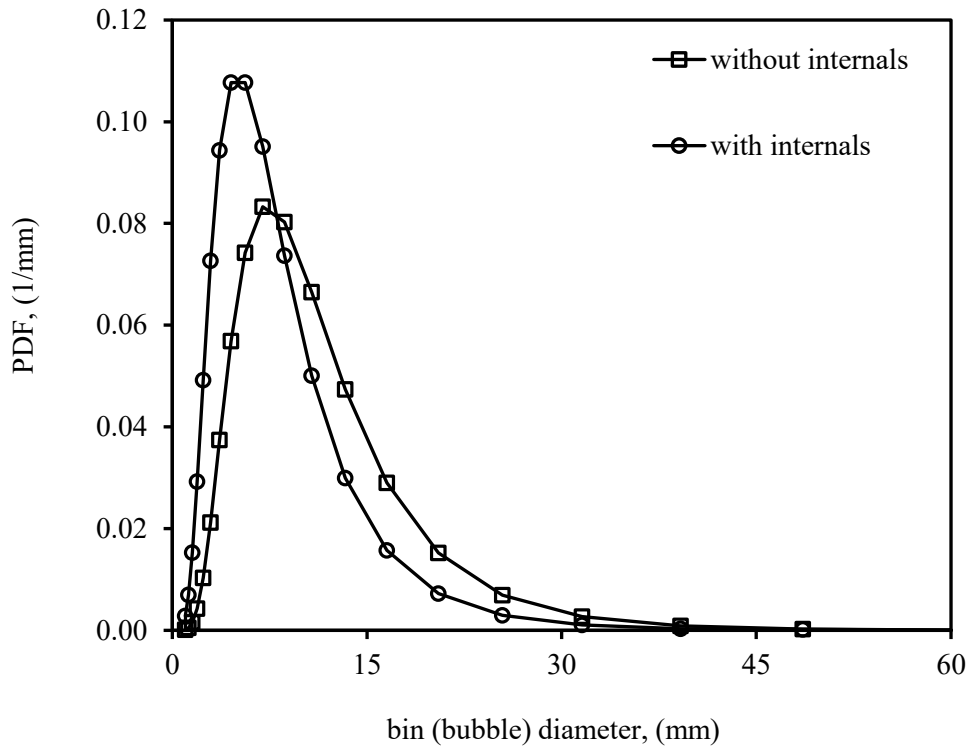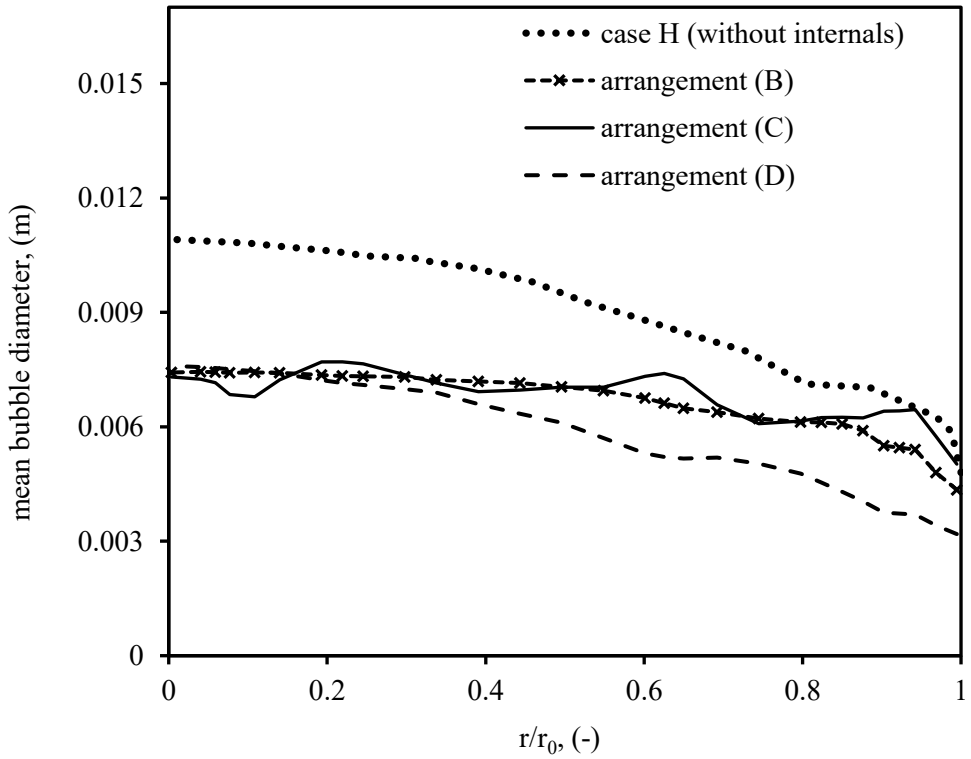e appropriate values for simulation of the bubble column without and with internals, respectively. The inclusion of wall-lubrication force steepened the gas holdup profile and reduced the accumulation of bubbles near the tubes' walls. The model results were validated against the experimental data and then, used to investigate the effect of internals on the bubble column hydrodynamics. The overall gas holdup in case F, the superficial gas velocity based on the free CSA, was slightly higher compared to the hollow bubble column. Meanwhile, in case T, the superficial gas velocity based on the total CSA, the overall gas holdup increased by 23% in respect to the hollow bubble column. In cases F and T, the gas holdup profiles were affected significantly and got steeper by the internals. Also, the gas and liquid phases faced greater velocity gradients in the radial direction. The increase of the gas velocity in the centerline contributed to a strong global liquid recirculation. This liquid recirculation was not uniform and led to the different liquid inversion points on different cross-sectional lines. The effect of wall and core clearance distances were examined by considering three internals circular arrangements. The results indicated that by increasing the wall clearance (arrangement C) the bubbles were able to distribute more uniformly in the cross-section area and, in turn, a less intense liquid recirculation could be established.

The applicability of the widely used breakage kernel of Luo and Svendsen (1996) and the coalescence kernel of Luo (1993) was investigated in the presence of internals. The results indicated that the original models overestimate the value of the mean bubble diameter because of underestimating the breakage rate (or overestimating the coalescence rate). In the presence of internals, the reduction of turbulence led to a further underestimation of breakage rate. It is worthwhile to mention that the impact of reducing turbulence by internals on the breakage rate would not be limited to the Luo kernels as the other population balance kernels (e.g. Lehr et al. 2002, Prince and Blanch, 1990), also, rely strongly on turbulence parameters. In this study, to consider breakage mechanisms caused by internals and balance the breakage and coalescence rates, a modification factor (F) was implemented in the model. By inclusion of this factor, an equilibrium for mean bubble diameters could be achieved.

5. Effect of Vertical Internals on the Gas Dispersion and Liquid Mixing in Bubble Columns

5.1 Introduction

Understanding the effect of internals on the hydrodynamics of bubble columns leads to a reactor design closer to industrial conditions. Liquid mixing and gas dispersion are two important parameters in the design of bubble columns. In this Chapter, the Eulerian-Eulerian simulation coupled with the population balance model was developed for the bubble column with dense vertical internals. The impulse tracer injection was applied to study the gas dispersion. The effect of the gas flow fluctuations, duration of tracer injection, and the presence of internals was analyzed at different superficial gas velocities. To study the liquid mixing, the tracer technique was applied, and the sensitivity of results to the tracer injection and detector points have been discussed.

5.2 Numerical Model Development

The schematic diagram of the model is shown in **Figure 5.1**. A bubble column with a diameter of 0.19 m and hydrodynamic height of 1.6 m at the different superficial gas velocities of 0.01, 0.03, 0.1, and 0.2 m/s was considered. The column was filled with water while air was sparged uniformly from the bottom. The impact of the dense vertical internals on gas dispersion and liquid mixing was investigated by considering a hexagonal internals' bundle with 21.5% of coverage. The number of 48 cylindrical rods with diameters of 0.0127 m was installed whiten the column. The internals' configuration is shown in **Figure 5.1c**. The simulation parameters were chosen to mimic the experiments of Hamed (2012). The results are reported on the cross-sectional line at the middle of the columns (z=0.8 m). For the bubble column with internals, the cross-sectional line was selected in such a way to cross no tubes (the line is shown in red in **Figure 5.1c**).

The Eulerian and Eulerian model was employed to simulate the gas/liquid system as discussed in Section 4-2-1 (Equations 4.1 and 4.2). The drag force was model by Schiller and Naumann (1935) as explained in Section 4.2.1 (Equations 4.3 and 4.4). The lift force was modeled through Equation (4.5). A constant lift force coefficient (C_L) was considered for each case.
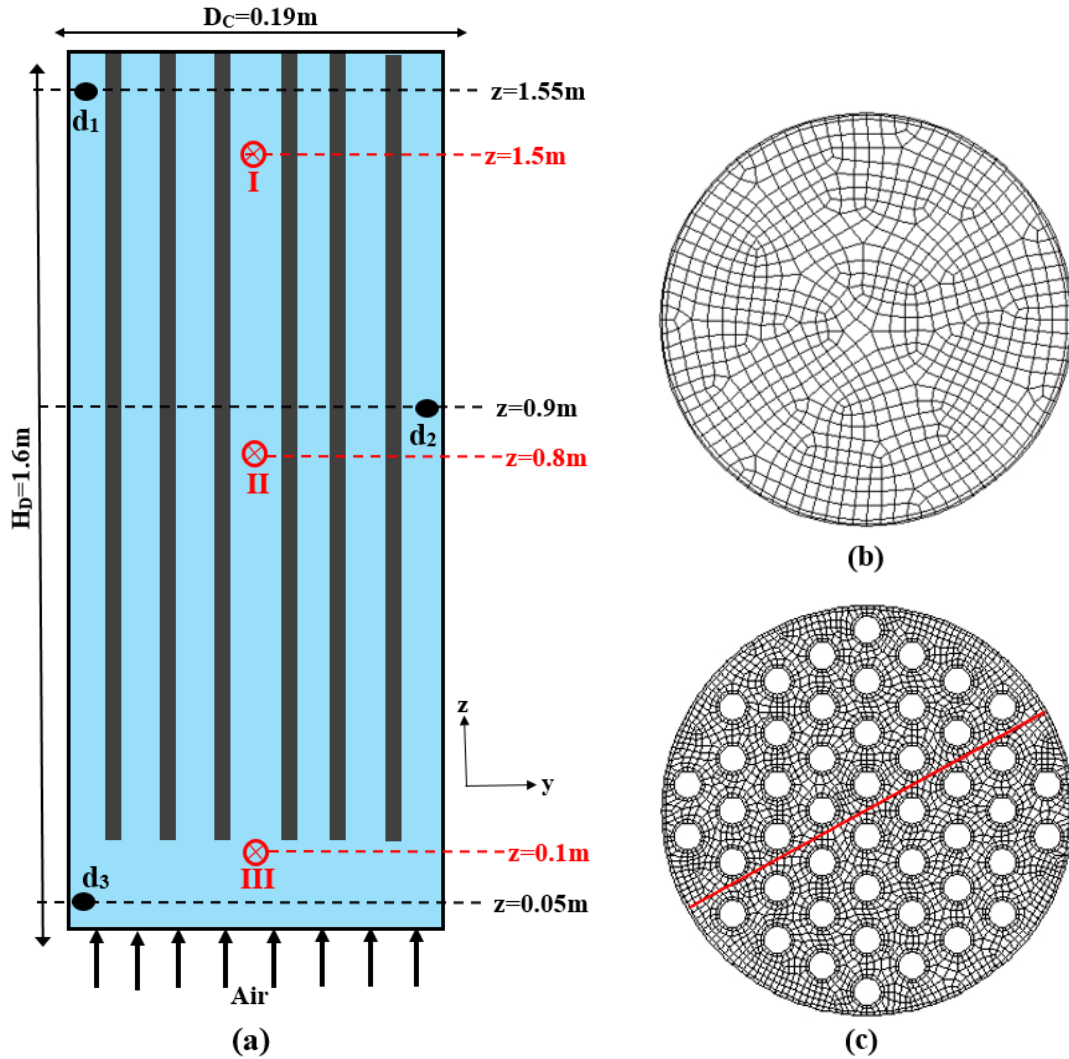
Figure 5.1: (a) The schematic diagram of simulation; **(b)** grid layout for hollow bubble column; **(c)** grid layout for bubble column with internals.

The value of the lift force coefficient was determined in the way to satisfy the desired total gas holdup and radial profile. For the hollow bubble column, the positive lift force was found necessary to reproduce the reasonable velocity profiles. On the other hand, our primary simulation resulted in flat velocity profiles in the presence of internals. Therefore, a negative lift force coefficient was assigned to push the bubbles to the center of the column. A negative lift force coefficient was also practiced by Guan and Yang (2017) in the simulation of bubble columns with internals. The lift force coefficients are tabulated in **Table 5.1**. The wall-lubrication force was modeled by Antal et al. (1991) (Equations 4.11 and 4.16). The model coefficients were adopted from Ekambara et al. (2008) as $C_{w1} = -0.01$ and $C_{w2} = 0.05$.

Table 5.1: The specifications of simulation runs.

Specifications	Hollow	With internals
Superficial gas velocity, (m/s)	0.01 0.03 0.1 0.2	0.01 0.03 0.1 0.2
Lift force coefficient, C_L, (-)	0.03	-0.03
Tubes number, (-)	0	48 (D_o=0.0127m)
Free cross-section area, (m^2)	0.0024	0.0020
Grids number, (-)	98,244	487,315
Bubble size range, (m)	0.0005-0.05 (20bins)	0.0005-0.05 (20bins)
Case F (with internals)	-	Superficial gas velocity based on free cross-section area
Case T (with internals)	-	Superficial gas velocity based on total cross-section area
Column height (H_D), (m)	1.6	
Column diameter, (m)	0.19	

To assign the value of bubble diameter in the model, the population balance model (PMB) proposed by Ramkrishna (2000) was adopted (Equation 4.15). The breakup and coalescence rates were calculated by the closures of Luo and Svendsen (1996) and Luo (1993), respectively. The modification factor *F* was applied as discussed in section 4-3. The bubble range was considered as 0.5-50 mm to cover all bubble sizes could be present in the different superficial gas velocities. To check the sensitivity of the results to the number of bins (bubble classes), the lognormal probability density function (PDF) was considered. The PDF profiles for the bin numbers of 10, 20, and 30 are compared in **Figure 5.2**. As can be seen, by increasing the number of bin classes from 10 to 20, the probability distribution changed significantly while the further increase to 30 bins did not make a considerable change. Therefore, the bin size range of 0.5-50 mm was divided into 20 classes in all simulations. The axial dispersion model (ADM) was considered to study the axial gas dispersion in the bubble column:

$$\frac{\partial c}{\partial t} + V_g \frac{\partial c}{\partial z} = D_{a,g} \frac{\partial^2 c}{\partial z^2} \qquad (5.1)$$

where $V_g = \frac{V_{sf,g}}{\alpha_g}$. The first and second terms in left hand-side are the accumulation rate of the substance by time and the transfer due to convection, respectively and the right hand-side is the dispersion term. To find the axial gas dispersion coefficient $D_{a,g}$, the impulse tracer technique was applied. Then, the residence time distribution (RTD) curves at the outlet of the bubble column were plotted. According to Levenspiel (1999), the variance squared (σ^2) and the mean residence time (t_m) of the RTD curves are given as follows:

$$\sigma_v^2 \cong \frac{\sum(t - t_m)^2 \, C_i \Delta t_i}{\sum C_i \Delta t_i} \qquad (5.2)$$

$$t_m = \frac{\sum t_i C_i \Delta t_i}{\sum C_i \Delta t_i} \qquad (5.3)$$

C_i is the concentration of tracer in the gas phase at the column's exit at a time interval of i. The calculated variance was used to estimate the Peclet number (Pe) and then the axial dispersion coefficient $D_{a,\varphi}$. For $Pe < 100$ we have the following equation (Levenspiel, 1999):

$$\frac{\sigma_v^2}{t_m^2} = \sigma_\theta^2 = 2/Pe - (2/Pe^2)(1 - \exp(-Pe)) \qquad (5.4)$$

$$D_{a,\varphi} = \frac{V_{sf,\varphi} H_D}{\alpha_\varphi Pe} \qquad (5.5)$$

The liquid mixing time was calculated by adding tracer and monitoring the liquid phase to reach the desired homogeneity degree. The transport equation for tracer was modeled as follows:

$$\frac{\partial}{\partial t}\left(\rho C_{i,\varphi}\right) + \nabla.\left(\rho \vec{u}_\varphi C_{i,\varphi}\right) = -\nabla.\vec{J}_{i,\varphi} \qquad (5.6)$$

where $\vec{J_i}$ is flux due to the diffusion that is decomposed of molecular and turbulent diffusions. The molecular diffusion was neglected because of its small magnitude ($\sim 2.88 \times 10^{-5} \frac{m^2}{s}$, ANSYS®️ FLUENT, 2017), and turbulent diffusion was obtained from the turbulence model.

The geometry and discretization were created in ANSYS®️ Workbench and ANSYS®️ Meshing (release version 17.2), respectively. Through the mesh independence study, the mesh number of 98k for the hollow bubble column and 487k for the bubble column with internals were considered. The QUICK schemes were selected to discretize the equations. The implicit solver with a time step of 0.01s was employed for time discretization. A 60s from the initial state was considered to ensure pseudo-steady had been established. The gas tracer was injected into the inlet gas stream, and the liquid tracer was patched on the numerical grids. For the outlet, the degassing boundary condition was assigned to prevent any loss of the tracer inside the liquid phase. The equations were solved by ANSYS©️ FLUENT (release version 17.2). To check the sensitivity of the results to the number of bins (bubble classes), the lognormal probability density function (PDF) with the bin sizes ranging from 0.5 to 50 mm was considered. The PDF profiles for the bin numbers of 10, 20, and 30 are compared in **Figure 5.2**. As can be seen, by increasing the number of bin classes from 10 to 20, the probability distribution changed significantly while the further increase to 30 bins did not make a considerable change. Therefore, the bin size range of 0.5-50 mm was divided into 20 classes in all simulations.
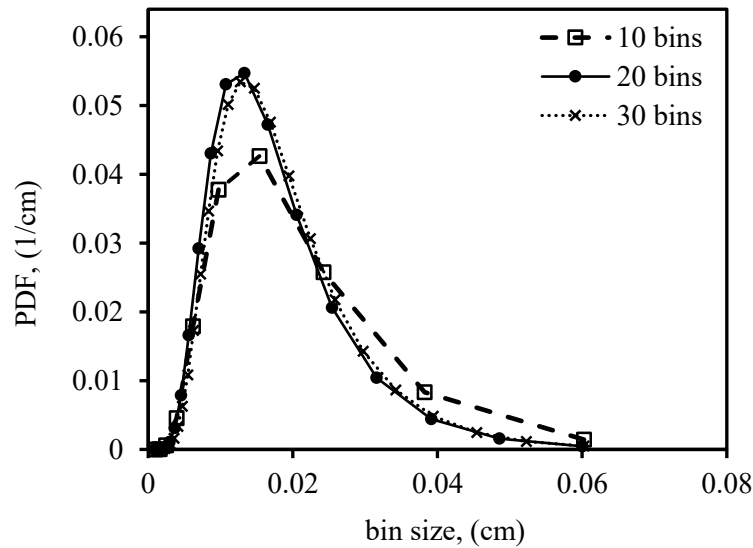

Figure 5.2: The sensitivity study of probability size distribution function (PDF) (cm^{-1}) to the number of bins at the superficial gas velocity of 0.2 m/s.

5.3 Results and Discussion

The overall gas holdup with respect to the superficial gas velocity is depicted in **Figure 5.3**. The simulation results have been compared to several experimental data. Differences in experimental conditions and measuring techniques caused different values to be reported for the gas holdup in the literature. For example, water quality can be a factor by affecting bubble breakage and coalescence rates in systems (Maruyama et al., 1981). However, all the data showed the considerable dependence of gas holdup on superficial gas velocity. The simulation results were well aligned with the data in the literature. In the experimental data, as well as our simulation, in the lower velocities, sharper increases in the gas holdup with increasing superficial gas velocities can be observed. By increasing the superficial gas velocity, the slope of the profile reduced. The change in the slope of gas holdup reflects the regime transition in bubble columns (Krishna et al., 1991).

The gas velocity profiles at the superficial gas velocity of 0.2 m/s are compared with experiments of Hamed (2012) in **Figure 5.4a**. A good agreement was observed between the simulation and experiment. The centerline gas velocity was obtained as 1.26 m/s in the hollow bubble column, which increased to 1.5 m/s in the bubble column with internals. Hence, the presence of internals increased the slopes of the gas velocity profiles compared to the hollow bubble column. Moreover, in the annular region (i.e. close to the column walls), the gas velocity was found lower than in bubble column with internals, compared to the hollow bubble column. It shows that the gas phase, in the annular region, experienced more resistance force in its upward motion in the presence of internals. This resistance force attributed to the existence of more intense liquid recirculation in the bubble column with internals as shown in **Figure 5.4b**. This figure shows the liquid velocity profiles, where the internals caused a higher axial liquid velocity at the center and a stronger downward flow in the annular region. This velocity gradient in the liquid phase produced a strong global recirculation that pulled the bubbles down near the column's wall. In **Figure 5.4b**, also, the liquid velocity profiles were validated against the experiments of Al Mesfer et al. (2017). The simulation results were well aligned with the experimental data. Since in our simulation, the diameter was larger (D_c=0.19m) compared to the experiment (D_c=0.14m in Al Mesfer et al., 2017), a slightly higher liquid velocity profile was obtained. The impacts of the internals on the gas and liquid velocity profiles raise the question of how internals would affect the mixing behavior in bubble columns.
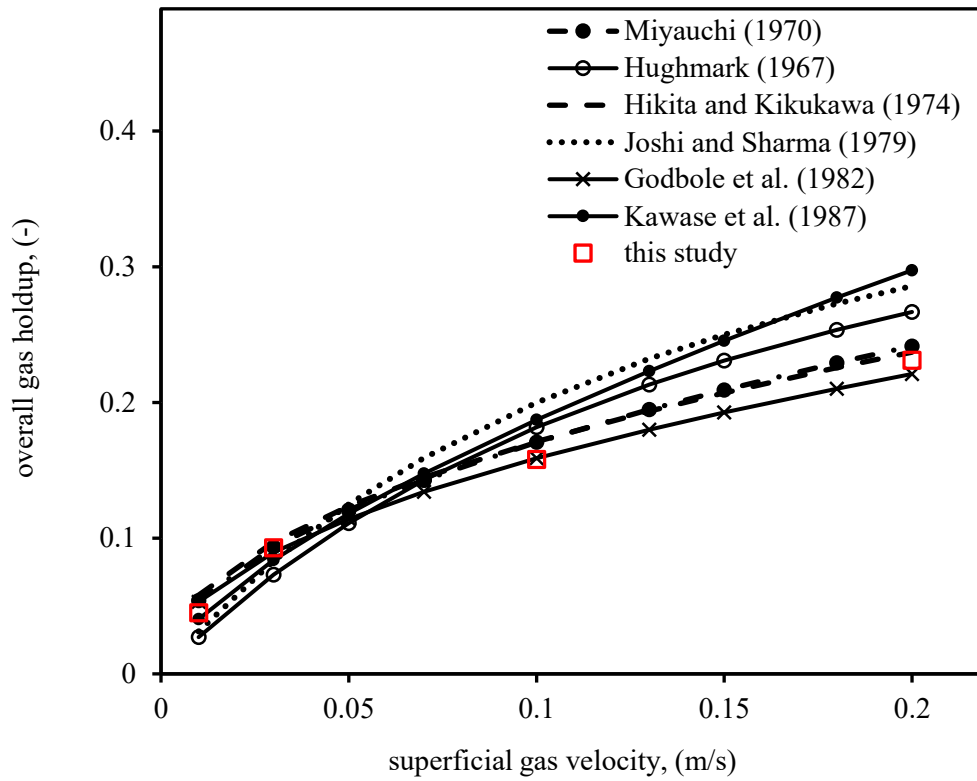
Figure 5.3: Overall gas holdup (-) as a function of the superficial gas velocity (m s^{-1}).
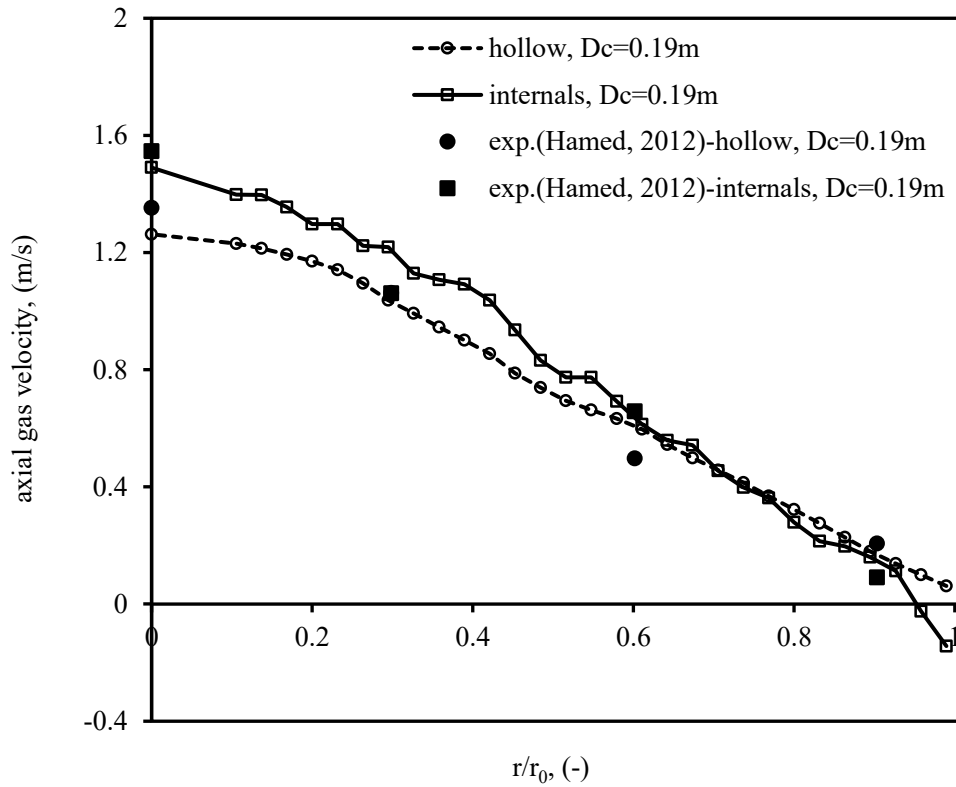
(a)
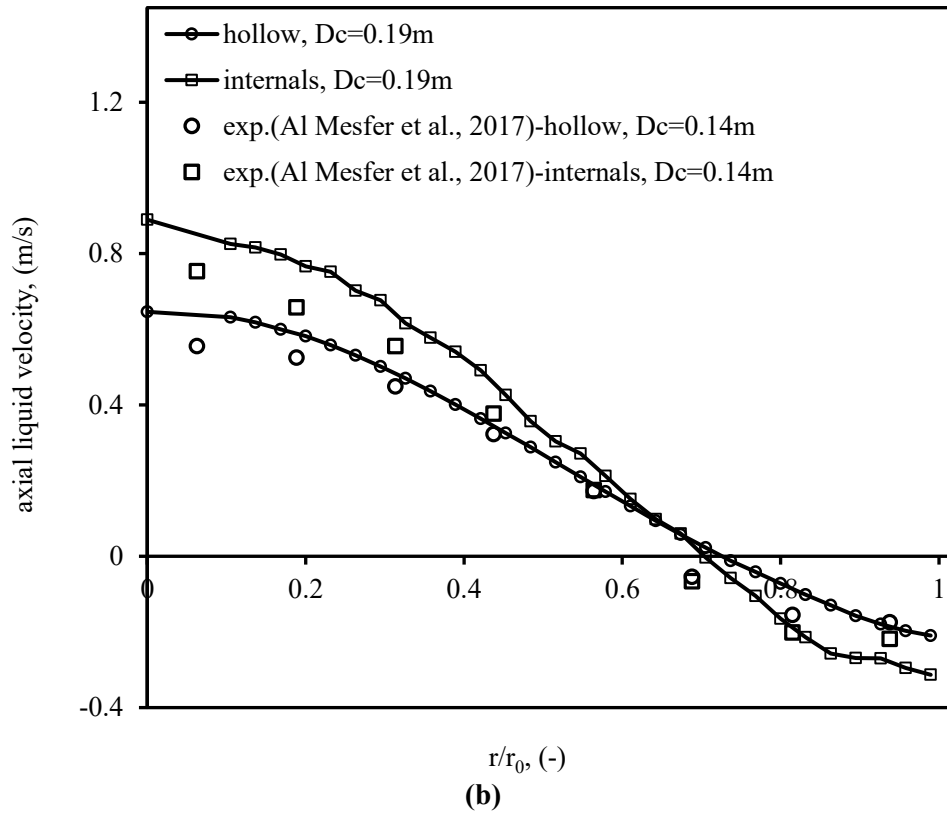
Figure 5.4: (a) The comparison of axial gas velocity profiles in the bubble columns with and without internals versus the experimental data of Hamed (2012); **(b)** The comparison of axial liquid velocity profile in the bubble columns with and without internals versus the experimental data of Al Mesfer et al. (2017).

5.3.1 Gas Dispersion

At the exit of bubble columns, the gas flow rates fluctuate around the mean value because of the turbulence in the system. The fluctuations of gas flow rates are also reflected in the variation of the hydrodynamic height (top free surface). The instantaneous gas flow rates ($m_{g,i}$, kg/s) at the exit of the bubble column are shown in **Figure 5.5**. At the low velocity of 0.03 m/s, the amplitudes of fluctuations are insignificant. However, at the gas velocity of 0.2 m/s, the high intense turbulence led to sever fluctuations in the gas flow rate. In the method for calculating the dispersion coefficient proposed by Levenspiel (1999) (Equations 5.2 and 5.3), a constant flow rate at the outlet was assumed. This assumption has been widely used in the previous experimental studies (e.g. Wachi et al., 1990; Zahradnik et al., 1997). The reason for this assumption is the difficulty in the measuring of the instantaneous gas flow rate at the exit of bubble columns. However, to truly

measure the amount of the tracer exiting the column, the fluctuations in the gas flow rate must be considered. Therefore, in this study, Equations (5.2) and (5.3) are modified by replacing the tracer concentration (c_i) with the tracer flow rate (m_i). If the instantaneous gas flow rate at the column's exit is $m_{g,i}$, the tracer mass flow rate at any given interval can be calculated as follows:

$$m_i = c_i \times m_{g,i} \tag{5.7}$$

Figure 5.6a shows the time-dependence of gas flow rate on the normalized RTD curves. In this figure, the following normalized tracer concentration (C_i) and normalized mass flow rate (M_i) were plotted:

$$C_i = \frac{c_i}{\sum ci} \tag{5.8}$$

$$M_i = \frac{m_i}{\sum m_i} \tag{5.9}$$
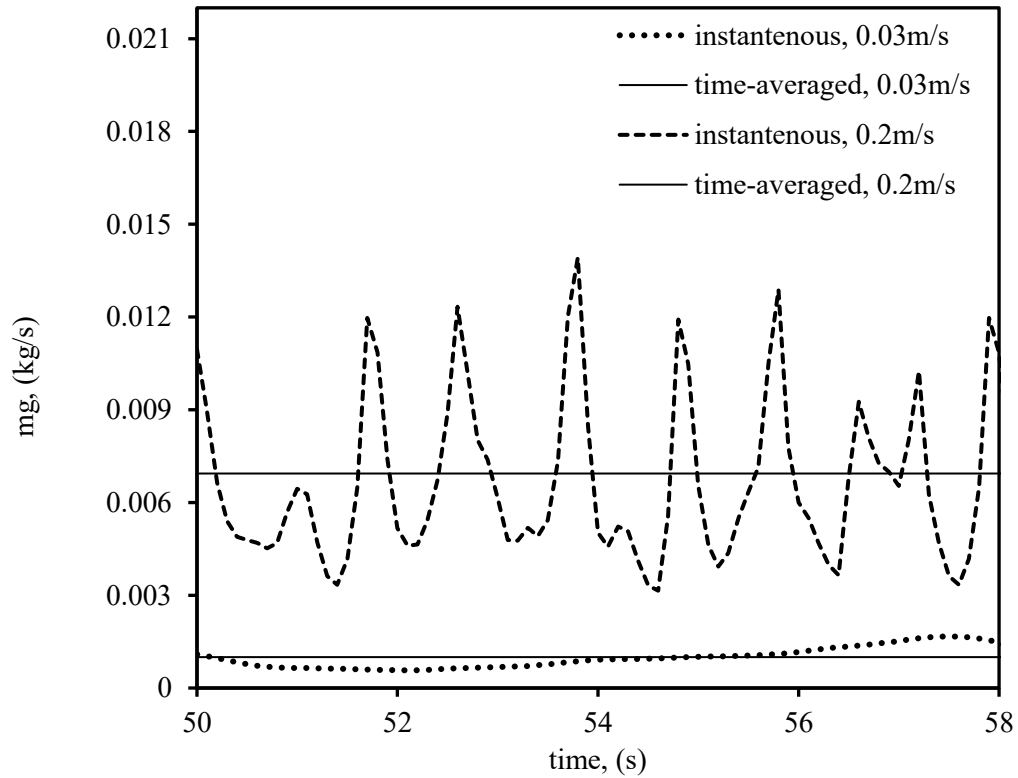
Figure 5.5: The instantaneous and time-averaged gas flow rates at the outlet of the bubble column.

Figure 5.6a shows that at the superficial gas velocity of 0.03 m/s, the difference between results was not considerable since the amplitude of fluctuations in the gas flow rate was small. On the other hand, at the superficial gas velocity of 0.2 m/s, where high fluctuations were present, replacing the tracer concentration with instantaneous gas flow rate changed the Peclet number $(\sigma_\theta^2 = 2/Pe - 2/Pe^2(1 - \exp(-Pe)))$ by 29%. This result shows that in the tracer experiment, the assumption of a constant gas flow rate at the column's exit is a source of error, which gets more pronounced at high superficial gas velocities. In this study, the time dependence of gas flow rates was considered in all cases.

Another parameter in the tracer technique is the time span of tracer injection. For having a reasonable impulse input, Kastánek et al. (1993) proposed the injection time $(\Delta t_{in}) < \left(0.05 \frac{Q_g}{\emptyset_{c,g}}\right)$ (Q_g is the gas flow rate, and $\emptyset_{c,g}$ is the volume of the gas phase in the column). In this study, three $\Delta t_{in} =0.01, 0.1$, and 0.5s were chosen to check the effect of injection time on the numerical results. The results at the superficial gas velocities of 0.03 and 0.2 m/s are compared in **Figure 5.6b**. For 0.03 m/s (low velocity), all three injection times resulted in almost identical RTD (residence time distribution) curves and Peclet numbers. For 0.2 m/s (high velocity), although all injection times satisfied the proposed condition, the results were different. As shown in **Figure 5.6b**, the RTD curves corresponding to Δt_{in} of 0.01 and 0.1s resulted in practically equal Peclet numbers. However, for Δt_{in} of 0.5s a notable change in RTD shape and the value of Peclet number was observed. Therefore, at high superficial gas velocities, the period of tracer injection has to be chosen with more caution. For the rest of the study, the injection time of 0.01s was considered.
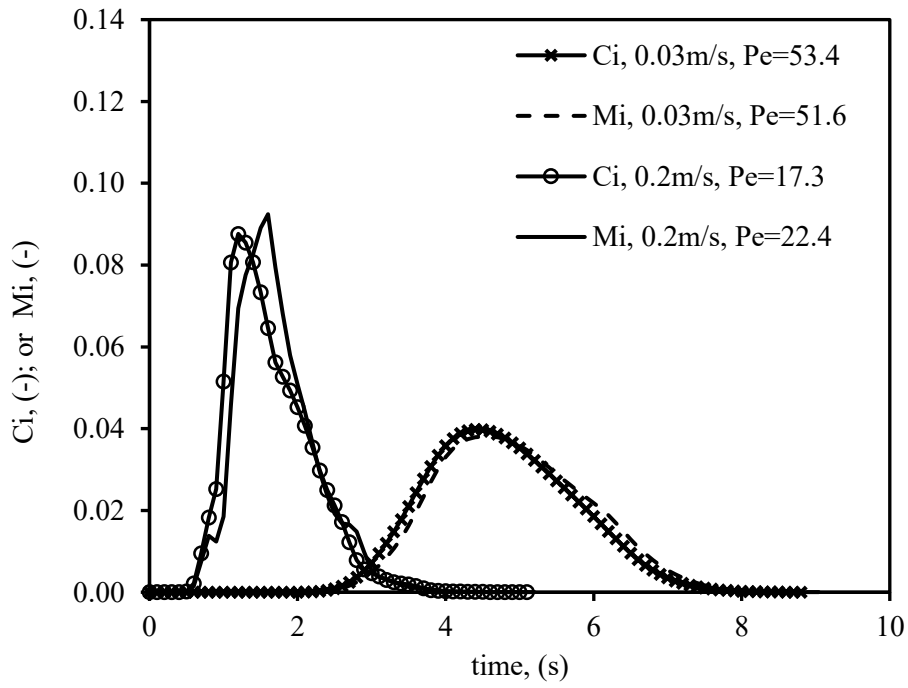
(a)
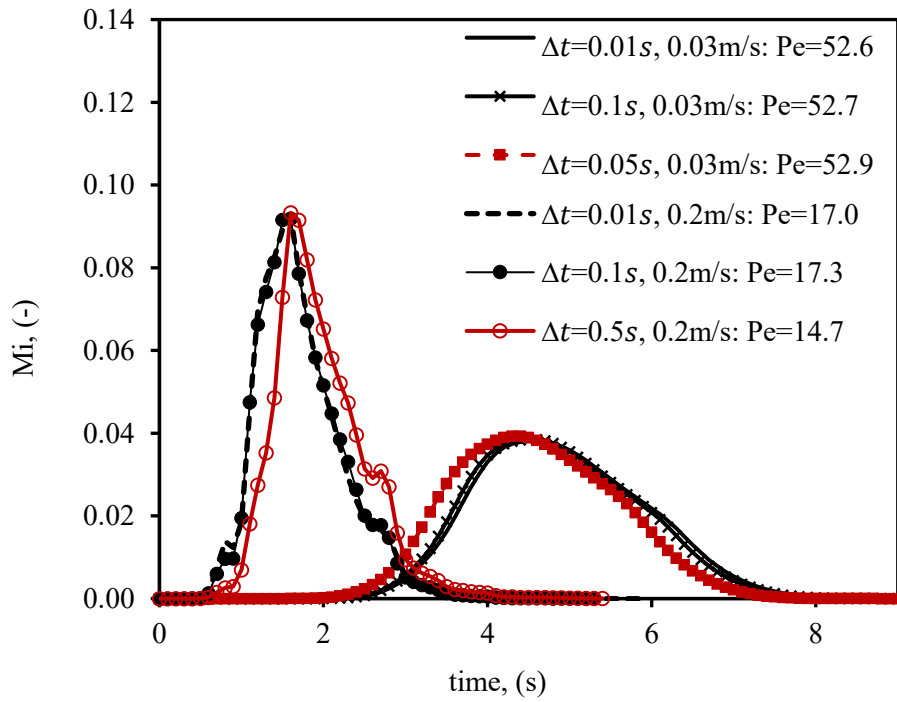
(b)

Figure 5.6: (a) The normalized RDT curves (-) with constant and instantaneous gas flow rates; **(b)** The impact of the tracer injection's time on the RTD curve.

The parameters to estimate the Peclet numbers extracted from the RTD curves are tabulated in **Table 5.2**. Through Equation (20), the estimated Peclet numbers were used to calculate the axial gas dispersion coefficients. **Figure 5.7** shows the axial gas dispersion coefficient as a function of superficial gas velocity. The simulation results are compared with different experimental data and correlations. The considerable discrepancy among the data can be observed since different approaches were used to measure or model the gas dispersion coefficient. Moreover, the measuring tools and experiment's lines could impose different amounts of dispersion on the gas phase, which also explain the lower calculated degree of dispersion in the current simulation. Hamed (2012) showed how an impulse tracer input (at the injection point) could turn to a wide response curve at the entrance of the bubble column because of dispersion imposed by the sampling line and plenum. More discussion on the divergence among the experimental data can be found in Kawase and Young (1989). The simulation results were in alignment most with the experimental data of Zahradnik and Fialova (1996). All data, including this study, show the considerable impact of superficial gas velocity on the gas dispersion. With increasing the superficial gas velocity, more energy transfer to the system and non-uniformity increases, which lead to higher gas dispersion as shown in **Figure 5.7**.

Figure 5.8 compares the RTD curves of the bubble columns with and without internals at the superficial gas velocities of 0.03 and 0.2 m/s. In the presence of internals, the RTD curves slightly shifted to the left-hand side with a larger peak. This observation showed that in the presence of internals, the tracer was sensed sooner at the exit since the internals increased the local gas velocity (as shown in **Figure 5.4a**). For a better representation, the nondiemtional RTD curves were plotted based on the following equation (Levenspiel, 1999):

$$E(\theta) = \frac{1}{\sqrt{4\pi/(Pe)}} \exp[-Pe\frac{(1-\theta)^2}{4}] \qquad (5.10)$$

where θ is the dimensionless time defined as $\theta = t/t_m$, t_m is the mean residence time, and Pe is the Peclet number. The plots of $E(\theta)$ vs. θ at different superficial gas velocities are depicted in **Figure 5.9**. The nondiemtional RTD curves allow us to compare different cases regardless of the size of columns or operating superficial gas velocities. All plots have a single peak at $\theta = 1$ where time and mean residence time are equal. According to **Figure 5.9**, by increasing the superficial gas

velocity, the profiles' peak decreased while wider profiles were observed. This trend illustrates increase in the gas dispersion with increasing superficial gas velocity as already shown in **Figure 5.7**. A wider profile shows more deviation from the impulse curve, i.e., increase in the width and decrease in the peak of the profiles indicate more gas dispersion in the system. **Figure 5.9** also shows the impact of internals at different superficial gas velocities. As can be seen, in the presence of internals, the corresponding curve became thinner with a higher peak, which reflects the reduction of gas dispersion. The reduction of gas dispersion due the presence of internals can also be noticed in the increase of Peclet number in **Table 5.2**. Although at the low superficial gas velocity of 0.01 m/s, the impact of internals was minor, the internals reduced the gas dispersion in all other cases. This results showed that although the internals contributed to more gradients in velocity fields (as already shown in **Figure 5.4a,b**), they caused an overall reduction in the gas dispersion. For a better understanding, another major source of gas dispersion should be studied: the dispersion due to the turbulence.

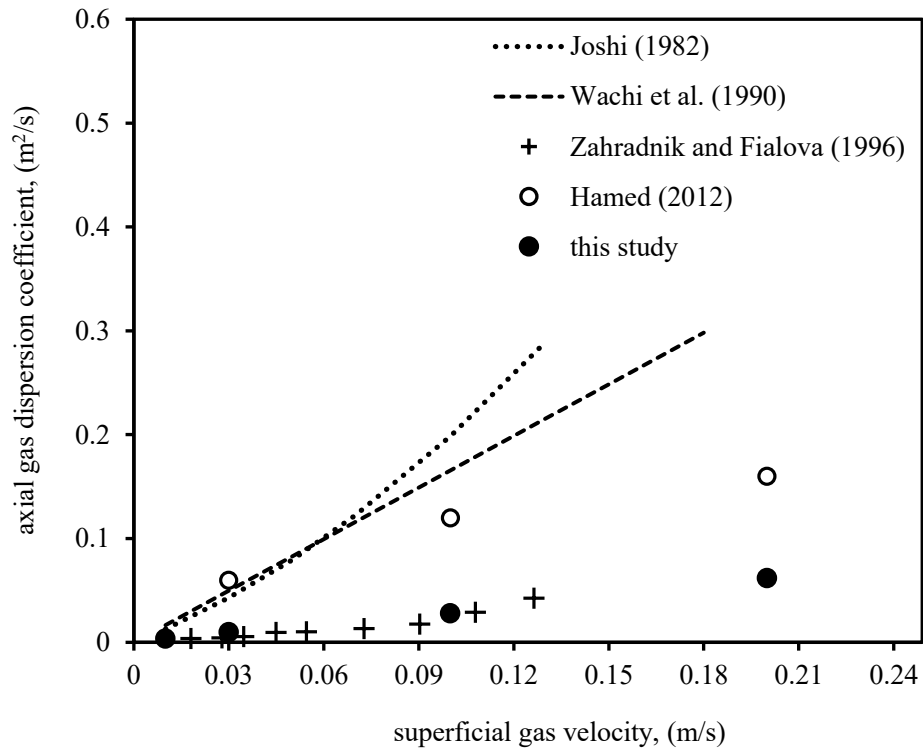**Figure 5.7:** The comparison of the gas dispersion ($m^2 s^{-1}$) obtained from the simulation with the literature data.
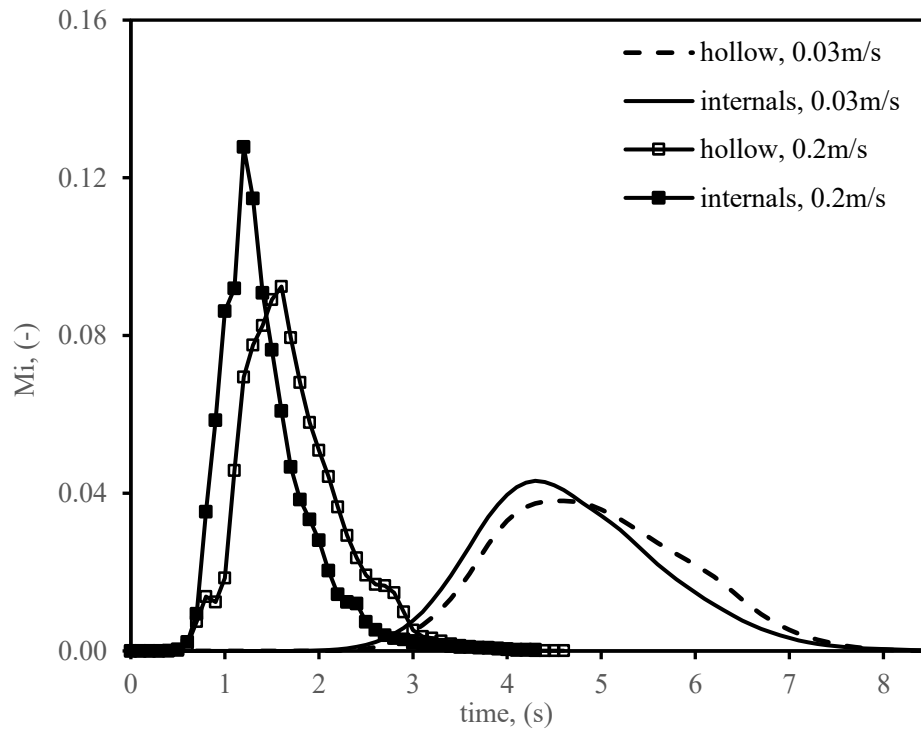
Figure 5.8: The normalized RTD curves (-) for the bubble column with and without internals.
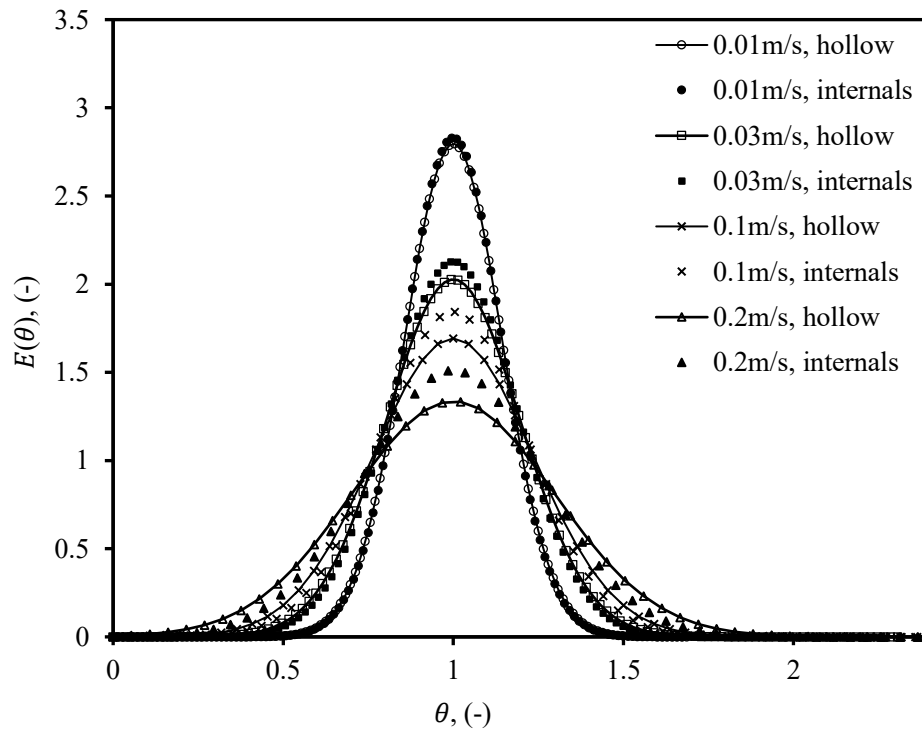
Figure 5.9: The dimensionless RTD curve (-) at different superficial gas velocities.

To study the effect of the internals on the turbulence, the radial profile of fluctuating axial gas velocities and their mean area-averaged values are plotted in **Figures 5.10a** and **5.10b**, respectively. In **Figure 5.10a**, for the hollow bubble column, the fluctuating gas velocities decreased close to the column walls with almost a peak around $r/r_0=7$. The peak is close to the liquid inversion point ($r/r_0=0.73$) where the direction of liquid flow changes; the similar trend for the fluctuating velocities in the liquid phase was reported by Degaleesan (1997). On the other hand, in the bubble column with internals, the profiles became flatter (no peak observed) with a wavy pattern because of the presence of internals. Moreover, the fluctuating velocities were found lower compared to the hollow bubble columns. In the presence of internals, the energy of the gas phase dissipates in the liquid eddies, which leads to a more gradient in the velocity field (Al Mesfer et al., 2017).

The mean area-averaged of fluctuating gas velocities at different superficial gas velocities are depicted in **Figure 5.10b**. The comparison between the bubble columns with and without internals showed a reduction in the mean turbulence by the internals. The internals acted as a dumping agent for the turbulence, i.e., reducing the turbulent kinetic energy and eddies length scales (which also reported by Larachi, 2006; Hamed, 2012; Al Mesfer, 2017). Although the internals intensified the gas circulation in the system, the reduction of turbulence outweighed the effect of circulation and led to a lower degree of gas dispersion. The results are consistent with Hamed (2012). Also, the impact of the internals on the turbulence was found more pronounced at the higher gas velocities.

Figure 5.11 compares the contour plots of tracer mass fraction in the bubble columns with and without internals. The gas tracer had been injected into the gas stream at the bottom of the columns. These contours visualize how the gas phase dispersed and circulated in the bubble columns. The two transfer mechanisms of mean flow (transfer due to the convection) and turbulence (transfer by random motion of eddies) can be seen. From **Figure 5.11**, while the bulk of tracer ascends to the top of the column, some portions of the tracer circulate along the liquid bulk. Also, in the hollow bubble column, a larger cloud of the tracer is formed compared to the bubble column with internals, where the tracer cloud is broken down by internals.
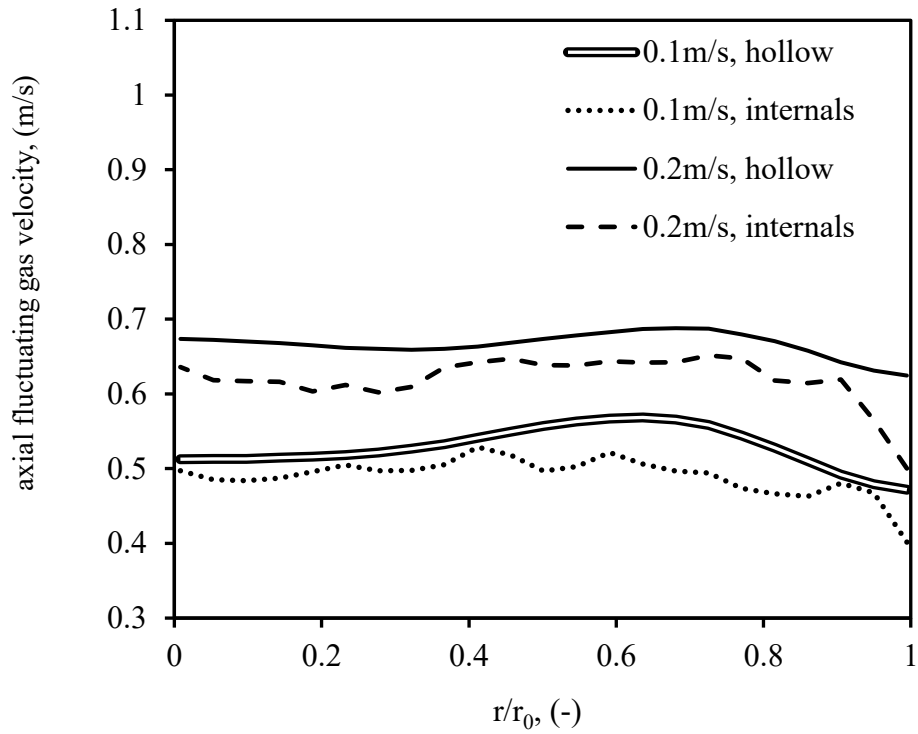
(a)
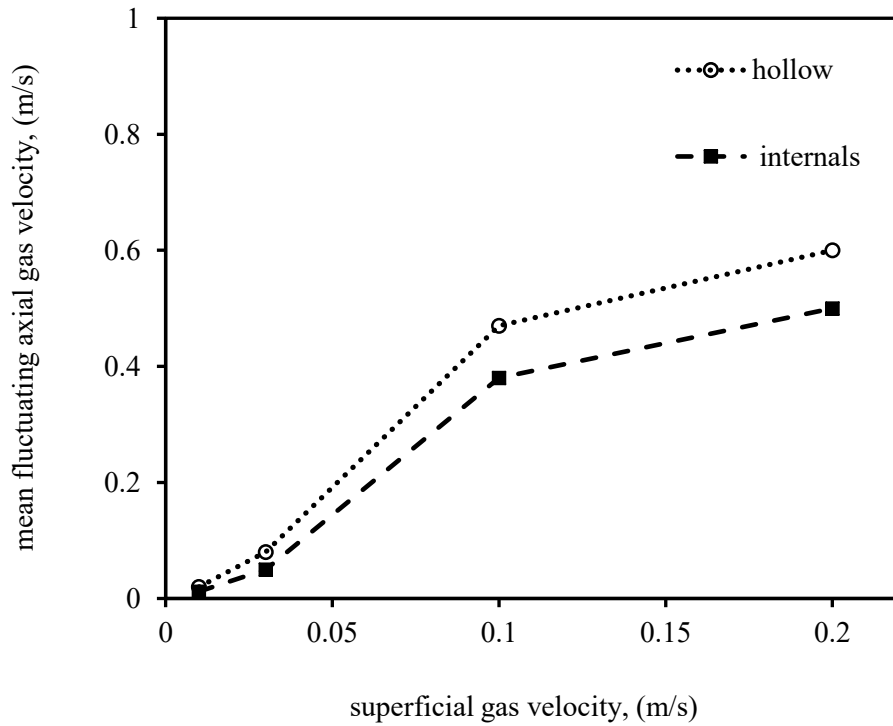
(b)

Figure 5.10: The comparison of the bubble columns with and without internals: (**a**) The axial fluctuating gas velocity profiles (m s^{-1}); (**b**) The area-weighted averages of axial fluctuating gas velocity (m s^{-1}).
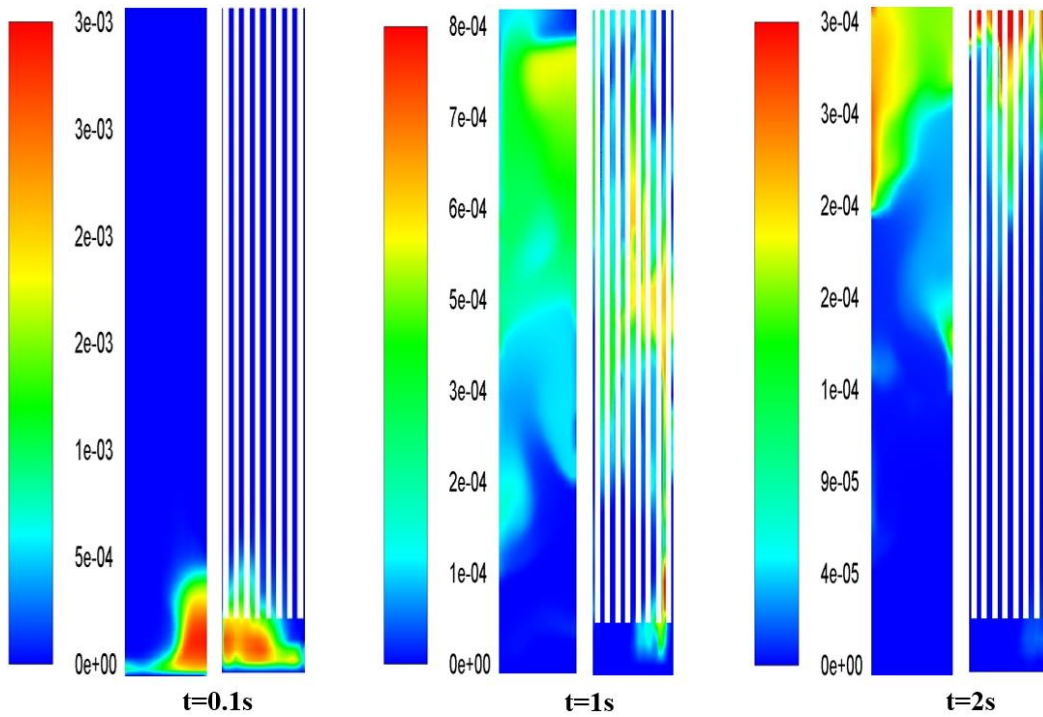
Figure 5.11: The contour plots of the tracer mass fraction (-) (gas phase) in the bubble columns with and without internals.

5.3.2 Liquid Mixing

In order to evaluate mixing in the liquid phase, the tracer technique was applied through patching a certain volume of tracer at the liquid phase. The superficial gas velocity of 0.2 m/s was considered. For the bubble column with internals, in one case, the superficial gas velocity was based on the free CSA (named case F) and in another case, it was based on the total CSA (named case T). Three different detector positions of $d_1(r/r_0 = +0.8,$ z=1.55m), $d_2(r/r_0 = -0.8,$ z=0.9m), and $d_3(r/r_0 = +0.8,$ z=0.05m) were selected to study the sensitivity of mixing time to the detector position. Also, three injection points in the center of the column at the heights of 1.5m (named as I), 0.8m (named as II), and 0.1m (named as III) were tested to study the effect of the injection position. The detector and injection points are shown in **Figure 5.1**.

Figure 5.12 shows the tracer history for the different injection points at the three detector positions in the hollow bubble column. The mixing times were calculated based on two criteria for the degree of homogeneities; i.e., 99% ($T_{99\%}$) and 99.9% ($T_{99.9\%}$). **Figures 5.12a,b,c** show that regardless of injection positions, for the homogeneity of 99% criterion, the calculated mixing times depend on the detector positions. The shortest mixing time was obtained when the tracer had been injected

90

into and monitored at the middle of the column (injecting at II and monitoring at d_2, shown in **Figure 5.12b**). However, by increasing the homogeneity criterion to 99.9%, the differences among the mixing times were almost diminished. This shows that mixing time is practically independent on the detector positions at a high degree of homogeneity in bubble columns.

The dependence of mixing time to injection position can also be observed in **Figure 5.12**. The largest mixing time in each case was considered to compare the results of each tracer injection position. The mixing time calculated for the injection point at the center of the column (point II) was smaller ($T_{99.9\%}= 17.9s$) than the mixing times obtained for the injection points at the top (point I) and the bottom of the column (point III). The mixing times for injection points of (I) and (III) were attained as 21.9s and 23.2s, respectively. At the center of the column, the tracer dispersed in both upward and downward directions causing a faster homogeneity in the system. Moreover, at the top and bottom of the column (points II and III, respectively), the local circulation loops trapping the tracer caused a delay in the overall circulation of tracer throughout the column. The dependence of mixing time on the injection point has also been observed by McClure et al. (2015) and Gholamzadehdevin and Pakzad (2018).
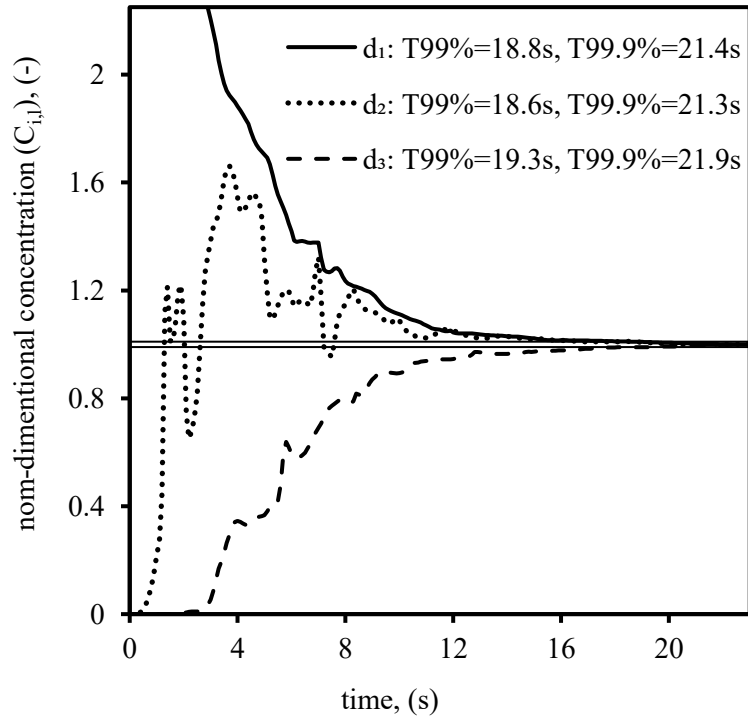
(a)
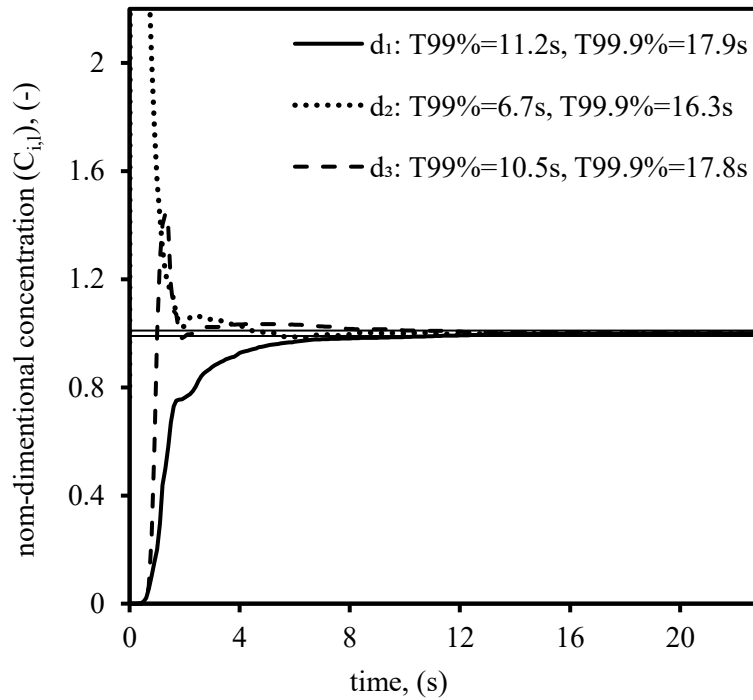
(b)
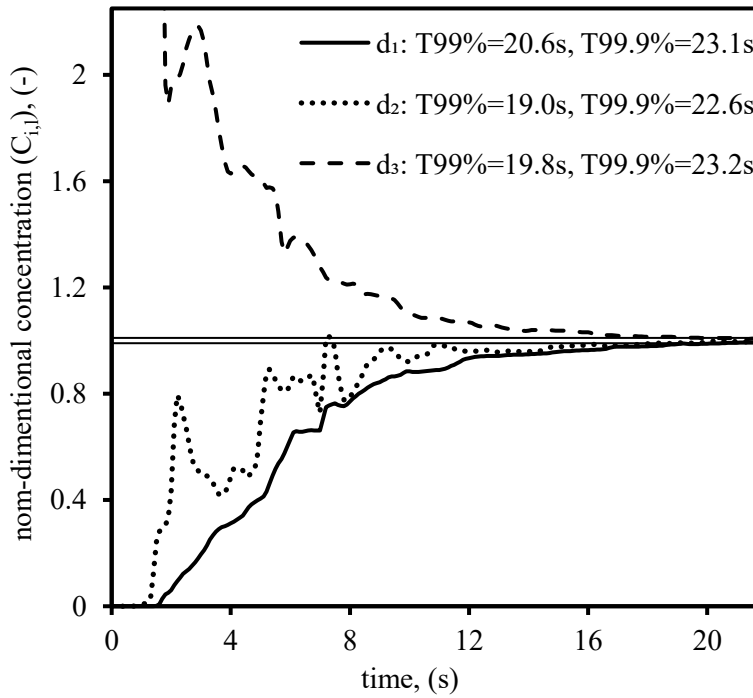
(c)

Figure 5.12: The tracer history recorded at d_1, d_2, and d_3 for the tracer injection point: **(a)** I (top); **(b)** II (center); **(c)** III (bottom). The horizontal lines denote 1% of the normalized equilibrium concentration (-).
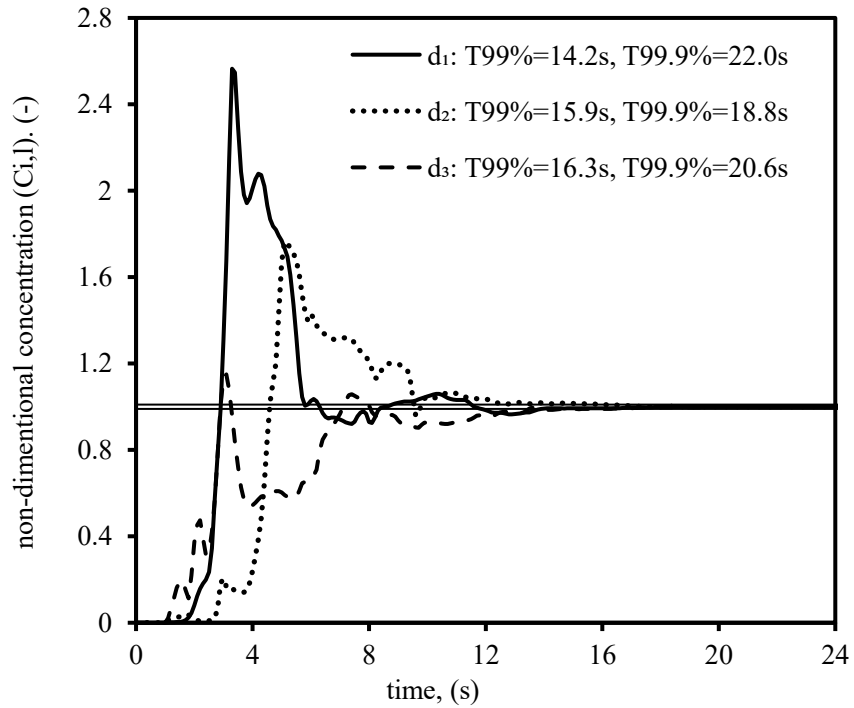
(a)
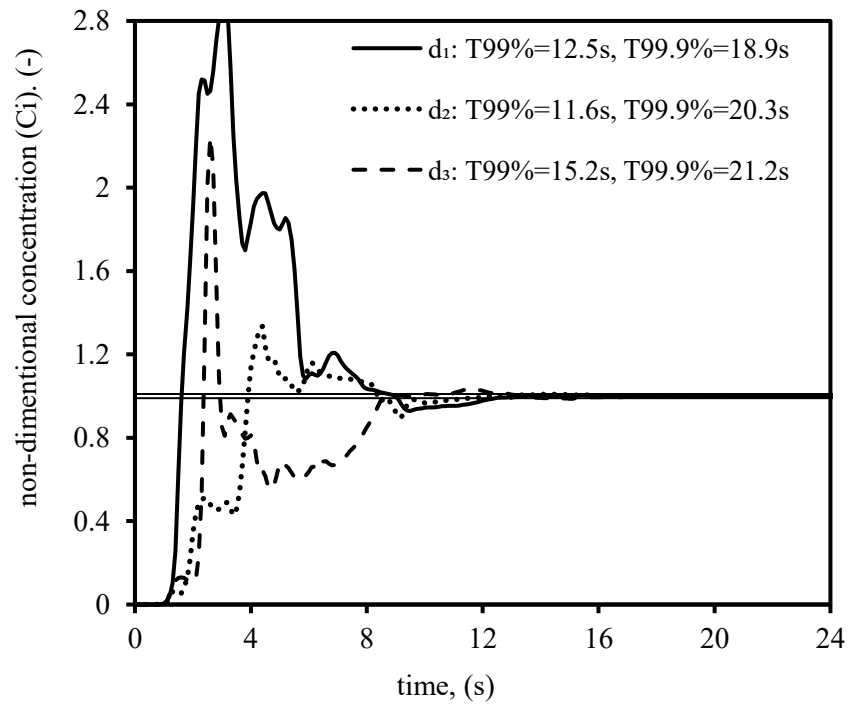
(b)

Figure 5.13: The tracer history at d_1, d_2, and d_3 for tracer injection point II (center) in the bubble column with internals: (**a**) case F; (**b**) case T. The horizontal lines denote 1% of the normalized equilibrium concentration (-).

For the bubble column with internals, the tracer was injected into point II (center), and the concentration was monitored at detectors d_1, d_2, and d_3. The results are shown in **Figure 5.13**. Similarly, to the hollow bubble column, the mixing time was found almost independent upon the detector positions at the higher degree of homogeneity (99.9%). In case F where superficial gas velocity based on the free CSA, a larger mixing time (i.e. $T_{99.9\%}$=22.0s) was observed, compared to the hollow bubble column (i.e. $T_{99.9\%}$=17.9s). Even in case T, by considering the superficial gas velocity based on the total CSA (i.e. increasing gas flow rate), the mixing time just slightly decreased to $T_{99.9\%}$=21.2s.

The reduction of mixing performance in the presence of internals can be linked to the reduction of turbulence in the system. The fluctuating liquid velocity in axial and -y-directions for the bubble column without and with internals (case F) are depicted in **Figure 5.14**. The results showed considerable reductions in the axial and lateral fluctuating liquid velocities by the presence of internals. The internals physically reduced the available space for the turbulent eddies to growth. So, the smaller length scales led to the lower turbulent intensity in the system as also observed in the simulation of Larachi et al. (2006). The results of axial direction were also compared with the experimental data of Forret et al. (2003) in **Figure 5.14**. A good agreement with the experimental data was observed. Both the simulation and the experiment showed a reduction in fluctuating velocities by the internals. However, more radial gradients in the fluctuating velocities can be observed in the experimental data since the column diameter in the experiment (D_c=1m) is much larger than the one simulated in the current study (D_c=0.19m). **Figure 5.15** shows the snapshots of tracer mass fraction one and three seconds after adding the tracer at the injection point of (II) in the bubble column with and without internals. These contours show how the internals imposed a constraint on the tracer dispersion in the lateral direction. Meanwhile, in the hollow bubble column, the tracer could easily disperse across the horizontal cross-sections.
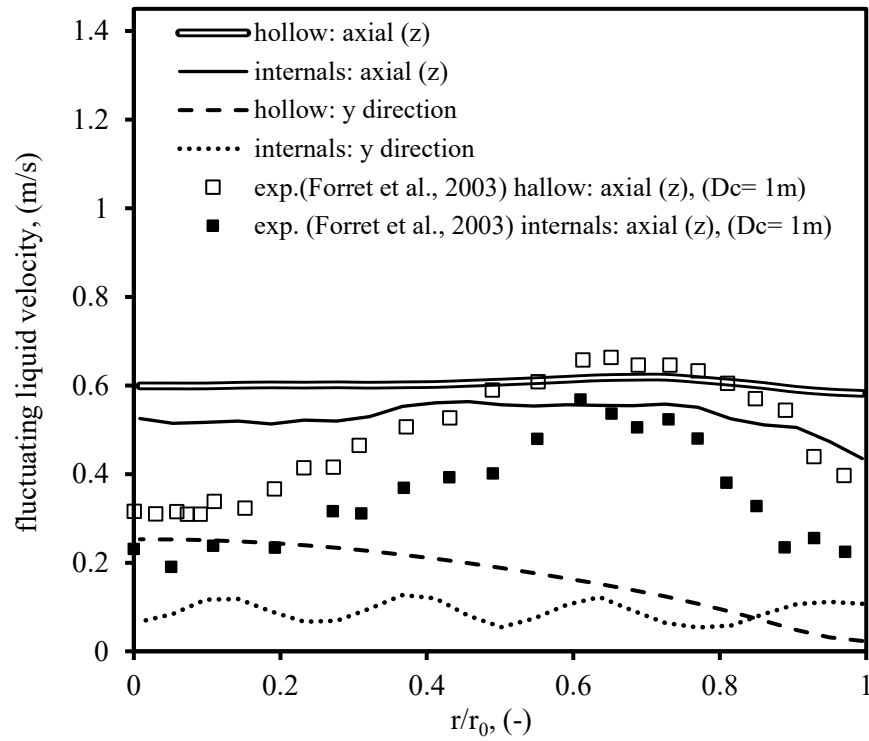
Figure 5.14: The profiles of fluctuating liquid velocity (m s^{-1}) in axial (z) and y directions for the hollow bubble column and bubble column with internals (case F).
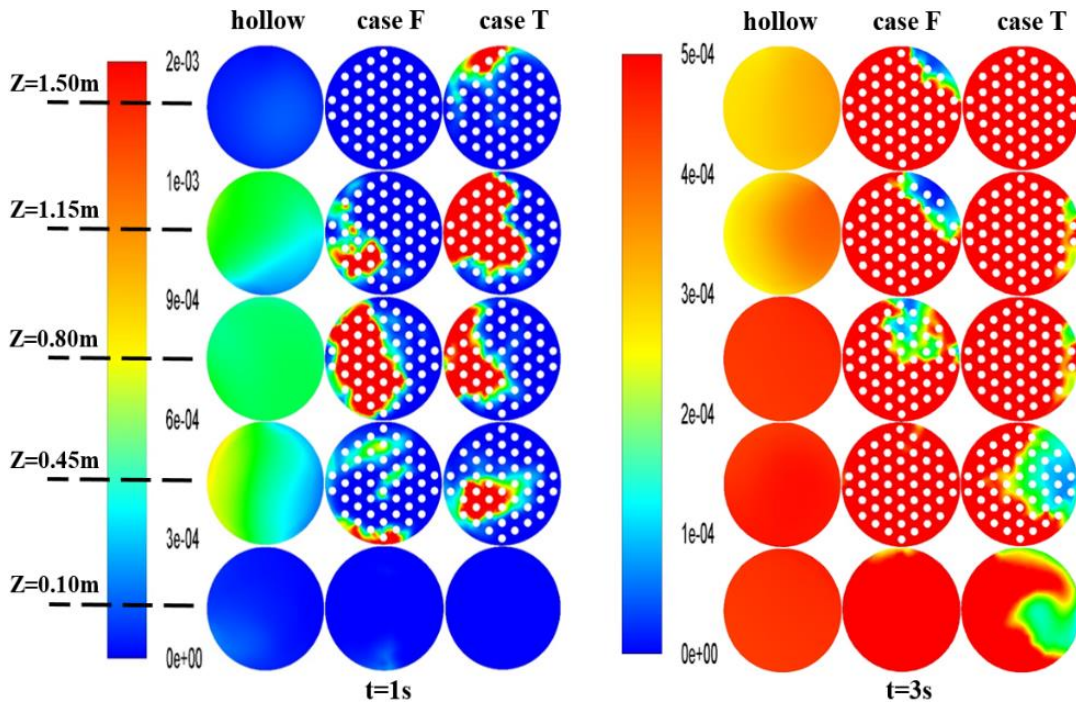
Figure 5.15: The contour plots of tracer mass fraction (-) (liquid phase) in the hollow bubble column and bubble column with internals (case F and case T) (The upper limits in the color bar are limited for a better presentation.).

5.4 Conclusions

In this section, numerical modeling of gas dispersion and liquid mixing in the bubble columns with and without internals were investigated. The impulse tracer technique was applied to investigate dispersion in the gas phase. The results revealed that the fluctuations of gas flow rate must be accounted for to measure the amount of tracer leaving the reactor accurately. Although at low superficial gas velocities, the assumption of the constant gas flow rate (i.e. ignoring the fluctuations in the gas flow rate) was reasonable, it caused a substantial error at the high superficial gas velocities. Moreover, the results showed that deviation from the ideal impulse injection leads to miscalculation of the dispersion degree, especially at high superficial gas velocities.

The gas dispersion increased with increasing the superficial gas velocities because of more turbulence and velocity gradient in the system. The presence of internals contributed to a stronger gas circulation while dumping the turbulence fluctuations. The results show that in compared to the intensified gas circulation, the turbulence was the dominant factor in the determination of gas dispersion. The internals reduced the gas dispersion at all superficial velocities, however, the effect of internals was more pronounced at the higher gas velocities.

The effect of tracer and injection positions on the determination of liquid mixing time was investigated. It was found that the dependence of mixing time upon positions of the detector could be eliminated at high degrees of homogeneities. However, a great dependence to the tracer injection point has been observed. The shortest mixing time was achieved when tracer was patched at the center of the bubble column. The presence of internals significantly reduced the mixing performance, even when the superficial gas velocity was based on the total cross-section area. The internals decreased the fluctuating liquid velocities in both lateral and axial directions and therefore, longer mixing times were obtained.

6. Overall Conclusions and Recommendations

The numerical simulation was developed to study the effect of the dense vertical internals on the hydrodynamics, bubble size distribution, and dispersion in bubble columns. The Eulerian-Eulerian model coupled with population balance model (PBM) was employed. A hexagonal and three circular internals' arrangements were considered. The main findings of this work are summarized as follows:

- The results showed that the inclusion of the lift and wall lubrication forces had noticeable effects on the simulation results. The choice of the lift force coefficient determined the gradient velocities in the system, which consequently affected the gas holdup profiles. For bubble column with internals, a negative lift force coefficient was found necessary to move the bubbles to the center of the column, and reproduce the gas holdup profiles agree with the experiments.

- The presence of hexagonal internals' arrangement in the bubble column, led to a sharper gas holdup, a stronger gas velocity gradient, and more intense liquid recirculation. The internals increased the overall gas holdup when the superficial gas velocity was based on the total cross-section area. However, the impact of the internals on the overall gas holdup when the superficial gas velocity was based on free cross-section area was found minor.

- Three circular internals' arrangements were considered to study the effect of wall and core clearance in the bubble column with internals. The results showed that the internals' arrangement with more free space at the core (clear core), led to a sharper velocities and gas holdup distribution in the column. On the other hand, in the case with larger free space near the column's wall (clear wall), more uniform velocities and gas distributions were achieved.

- The CFD simulation showed a malfunctioning of the Luo population balance kernels (Luo and Svendsen, 1996; Luo, 1993). The results showed that the presence of internals decreased turbulence in the bubble column, and consequently, the population balance model led to the larger bubble sizes. However, in the experimental data, internals was found reducing bubble sizes (Youssef, 2009; Jasmin, 2016). In this study, to address this issue, a

modification factor was introduced. Implementing the modification factor, the population balance model showed a good agreement with the experimental data.

- The presence of internals in the bubble column increased the velocity gradients while reduced the turbulence in the system. The results showed that the effect of turbulence on the gas dispersion was dominant compared to the effect of velocity gradients. The internals reduced gas dispersion at all superficial gas velocities (i.e. 0.01, 0.03, 0.1, and 0.2 m/s).

- The comparison of mixing times in bubble column with and without internals showed that the internals reduced the mixing performance in the liquid phase. Internals decreased turbulence, i.e., reducing liquid fluctuating velocities in axial and lateral directions.

6.1 Recommendations for Future Work

The current study showed that although the simulation results can be improved by applying the appropriate choice of interfacial forces, the lack of robust formulas and procedure for interfacial forces reduce the predictability of the CFD simulations. Therefore, more investigations are needed to derive models for interfacial forces (e.g. lift and wall-lubrication force), especially in the cases of the presence of internals.

This study showed that the presence of internals significantly reduced the turbulence in the system. As the population balance kernels rely strongly on the turbulence parameters, the comparison between bubble columns with and without internals can offer insight to the role of turbulence in the population balance model. Moreover, this study showed the need for other breakage mechanisms when the internals are present in the system. Although the proposed modification factor showed a reasonable performance, even in the different internals' arrangements, it was a tentative attempt to address the presence of internals. Further study on the breakage mechanisms induced by internals is required. Also, different internals specifications (e.g. tube's diameter, tube's type such as plan and pin-fin, etc.) and different types of liquid should be considered in the future studies. For example, the viscosity of non-Newtonian liquids would be affected by severe shear gradients due to the presence of tubes' walls.

The study on the dispersion in the bubble column showed that more mechanisms for gas dispersion must be accounted for to capture all dispersion sources in real bubble columns. In the Eulerian-

Eulerian model, even coupled with the population balance model, the small scales around the bubbles cannot be resolved. Moreover, this study focused on the axial dispersion coefficient that can be expanded by considering radial dispersion. Knowing the weight of each dispersion component can help to improve models for design of bubble columns, especially in the presence of internals.

In the bubble column with internals, generally, a buffer zone is considered between the sparger and the rods bundle. The effect of the height of the buffer zone and the installation of baffles in this region can be a subject for further study (refer to George et al., (2017) for more information).

This study was investigated the vertical internals; the horizontal internals such as perforated trays can also be investigated. The effect of the number of trays, the diameter and number of holes on each tray can be interesting subjects to study. Furthermore, the effect of the trays on the mixing performance would offer valuable information regarding sectionalized bubble columns (refer to Pandit and Joshi, (2005) for more information).

Nomenclature

a constant, (-)

A constant, (-)

A_{12} collision-sectional area of two bubbles, (m^2)

b constant, (-)

b_1 constant, (-)

B_1 constant, (-)

B_{co} birth rate due to coalescence, (s^{-1} m^{-3})

B_{br} birth rate due to the breakage, (s^{-1} m^{-3})

c   concentration, (kg m^3)

c_1 constant, (-)

$C_{1\varepsilon}$ constant, (-)

$C_{2\varepsilon}$ constant, (-)

$C_{3\varepsilon}$ constant, (-)

C_D drag coefficient in swarm, (-)

$C_{D\infty}$ drag coefficient of an isolated bubble, (-)

C_{En} constant, (-)

C_{fi} interfacial friction factor, (-)

C_{fs} increase coefficient of surface area, (-)

C_i dimensionless tracer concentration in the gas phase at a time step of i, (-)

$C_{i,\varphi}$ dimensionless tracer concentration in the phase φ at a time step of i, (-)

C_L lift coefficient, (-)

C_s coefficient for skirt length, (-)

C_{vm} virtual mass coefficient, (-)

C_{w1} wall force coefficient, (-)

C_{w2} wall force coefficient, (-)

C_{wf} constant, (-)

C_{WL} wall force coefficient, (-)

C_{λ} constant, (-)

C_{μ} constant, (-)

C_{γ} constant, (-)

d_1 constant, (-)

d_b local bubble diameter, (m)

$d_{b,1}$ the diameter of colliding bubble, (m)

$d_{b,2}$ the diameter of colliding bubble, (m)

$d_{b,eq}$ equivalent diameter of colliding bubbles, (m)

$d_{b,i}$ bubble class diameter, (m)

d_H long axis of the deformable bubble, (m)

d_{sh} average diameter of sheared-off bubbles, (m)

d_{wall} wall clearance distance, m

$D_{a,\varphi}$ axial dispersion coefficient for phase φ, (m^2 s^{-2})

D_{br} death rate due to breakage, (s^{-1} m^{-3})

D_o tube outer diameter, (m)

D_c diameter of bubble column, (m)

D_{Co} death rate due to coalescence, (s^{-1} m^{-3})

$\bar{e}(s)$ increase of surface energy due to a bubble breakage, (J)

$\bar{e}(\lambda)$ energy of individual eddies, (J)

$E(\theta)$ dimensionless residence time distribution, (-)

E_{int}	interfacial energy, (J)
E_{kin}	kinetic collision energy, (J)
Eo	Eötvös number, (-)
Eo_d	Eötvös number based on the d_H, (-)
f_1	continuous density function, (m^{-6})
f_{BV}	breakage volume fraction, (-)
$fu(x)$	an arbitrary function, (-)
F_A	flux of an arbitrary variable, (unit depends on definition)
F_D	drag force, (N m^{-3})
F_L	lift force, (N m^{-3})
$F_{rl,under}$	under relaxation factor, (-)
F_{WL}	wall-lubrication force, (N m^{-3})
g	referring to gas phase, (-)
$\vec{g}$	gravitational acceleration, (m s^{-2})
h_T	spatial interval, (m)
H_D	hydrodynamic head, (m)
H_S	static head, m
$\vec{J}$	flux due to the diffusion, (kg m^{-3} s^{-1})
k	turbulence kinetic energy, (m^2 s^{-2})
K_1	constant, (-)
K_D	constant, (-)
K_μ	consistency coefficient, $(Pa\ s^{n_\mu})$
l	referring to liquid phase, (-)
l_D	primary length parameter, (m)
m^J	Jth order of moment, (unit depends on J)

m_i	tracer mass flow rate at a time step of i, (kg s^{-1})
$m_{g,i}$	gas mass flow rate at a time step of i, (kg s^{-1})
M_i	dimensionless mass flow rate in the gas phase at a time step of i, (-)
$\vec{M}_I$	interfacial forces, (N m^{-3})
$\vec{n}_w$	outward unit normal vector pointing from the wall, (-)
$\dot{n}_\lambda$	number of eddies in the range of λ to $\lambda + d\lambda$ per unit volume, (m^{-3})
n_μ	power-law index, (-)
$N(r_{ex}, t)$	local average number density in the internal space, (m^{-3})
N_1	constant, (-)
N_φ	number of phases in the system, (-)
P	pressure, (Pa)
$P_{eff,Co}$	coalescence efficiency, (-)
$P_{eff,br}$	breakage efficiency, (-)
P_D	corrector factor of drag coefficient, (-)
P_{new}	new pressure in the iterative process, (Pa)
P_{old}	old pressure in the iterative process, (Pa)
Q	source/sink term within a control volume, (unit depends on definition)
r	radius, (m)
r_{ex}	special (external) coordinate, (-)
R_{ij}	turbulent stress tensor components, (m^2 s^{-2})
Re_φ	Reynolds number of phase φ, (-)
s	referring to liquid phase, (-)
$sdev(V)$	standard deviation of velocity of V, (m s^{-1})
S_A	control surface, (m^2)

S_{f_1}	source/sink term of bubbles, (s^{-1} m^{-6})
S_N	average source/sink term of bubbles, ($m^{-3}s^{-1}$)
St	Stokes number, (-)
t	time, (s)
$t_{contact}$	contact time in the liquid film theory, (s)
$t_{drainage}$	drainage time in the liquid film theory, (s)
t_m	mean residence time for the gas phase, (s)
T	liquid mixing time, (s)
u'	fluctuating velocity, (m s^{-1})
$\vec{u}_\varphi$	velocity of phase φ, (m s^{-1})
U_b	average local bubble velocity, (m s^{-1})
U_C	combined velocity of internal and external coordinate, (m s^{-1})
U_l	liquid velocity, (m s^{-1})
$U_l(0)$	local velocity of liquid at the center of column, (m s^{-1})
U_r	velocity in the external coordinate, (m s^{-1})
U_x	velocity in the internal coordinate, (m s^{-1})
V_b	volume of bubble, (m^3)
$V_{b,1}$	volume of a colliding/daughter bubble, (m^3)
$V_{b,2}$	volume of a colliding bubble, (m^3)
V_i	instantaneous velocity in i direction, (m s^{-1})
V_i'	fluctuation velocity in i direction, (m s^{-1})
$\bar{V}_i$	time-averaged velocity in i direction, (m s^{-1})
$\bar{V}_i'$	time-averaged fluctuation velocity in i direction, (m s^{-1})
$V_{sf,\varphi}$	superficial velocity of phase φ, (m s^{-1})

$V_{trans,g}$	transition superficial gas velocity, (m s^{-1})
w_{br}	collision frequency in breakage, (s^{-1})
w_{co}	collision frequency in coalescence, (s^{-1})
x_{in}	internal coordinate, (-)
y_w	distance from wall, (m)
Y_c	continuous phase vector, (-)
z	axial direction, (-)

Greek letters

α_φ	local volume fraction of phase φ, (-)
α_φ^T	total volume fraction of phase φ, (-)
$\dot{\gamma}$	shear rate, (s^{-1})
δ_{ij}	Kronecker delta, (-)
ε	turbulent dissipation rate, (m^2 s^{-3})
ξ	size ratio between an eddy and a bubble, (-)
θ	dimensionless parameter of time, (-)
$\vartheta_{numerical}$	numerical diffusion, (m^2 s^{-1})
λ	eddies length scale, (m)
$\mu_{k,\varphi}$	kinematic viscosity of phase φ, (m^2 s^{-1})
μ_φ	viscosity of phase φ, (Pa s)
$v_{b,12}$	characteristic velocity of collision of two particles, (m s^{-1})
$v_{b,i}$	discrete absolute mean velocity of bubble, (m s^{-1})
v_{rb}	relative velocity in axial direction of a cap bubble with respect to the liquid at bubble base, (m s^{-1})
v_λ'	turbulent velocity of an eddy with size λ, (m s^{-1})
Π_k	model approximation of $\Pi_{R,ij}$, (kg m^{-1} s^{-3})

$\Pi_{R,ij}$	turbulent phase interaction Reynolds stress source, (kg m^{-1} s^{-3})
ρ_φ	density of phase φ , (kg m^{-3})
σ	surface tension, (N m^{-1})
σ_v^2	variance (squared of standard variation), (t$^{\wedge 2}$)
σ_{ij}^n	normal stress in i and j directions, (m^2 s^{-2})
σ_m^c	conductivity of mixture, (s m^{-1})
σ_φ^c	conductivity of phase φ, (s m^{-1})
$\bar{\bar{\tau}}_{\text{eff}}$	effective stress, (m^2 s^{-2})
τ_f	fluid relaxation time, (s)
τ_{ij}^t	Reynolds turbulent stress in i and j directions, (m^2 s^{-2})
τ_p	particle relaxation time, (s)
τ_w	wall shear stress, (Pa)
φ	phase index, (-)
Φ	arbitrary variable, (unit depends on the definition)
$\emptyset_{c,g}$	the volume of bubble column equipped by gas, (m^3)
Ω	breakage rate, (s^{-1})

Abbreviations

ADM	axial dispersion model
CARPT	computer automated radioactive particle tracking
cdf	cumulative distribution function
CFD	computational fluid dynamics
CFL	Courant-Friedrichs-Lewy condition
CPU	central processing unit
CT	computed tomography

ECT	electrical capacitance tomography
E-E	Eulerian-Eulerian
E-L	Eulerian-Lagrangian
ERT	electrical resistance tomography
FDM	finite difference method
FEM	finite element method
LDA	laser Doppler anemometry
MUSIG	multi-sized group method
PBM	population balance model
PDF	probability density function
PIV	particle image velocimetry
QUICK	quadratic upstream interpolation for convective kinematics
RSM	Reynolds stress model
SIMPLE	semi-implicit method for pressure-linked equations

References

Agahzamin, S., Mirvakili, A., & Rahimpour, M. R. (2016). Investigation and recovery of purge gas streams to enhance synthesis gas production in a mega methanol complex. *Journal of CO₂ Utilization*, *16*, 157-168.

Akosman, C., Orhan, R., & Dursun, G. (2004). Effects of liquid property on gas holdup and mass transfer in co-current downflow contacting column. *Chemical Engineering and Processing: Process Intensification, 43*(4), 503-509.

Al Mesfer, M. K., Sultan, A. J., & Al-Dahhan, M. H. (2016). Impacts of dense heat exchanging internals on gas holdup cross-sectional distributions and profiles of bubble column using gamma ray Computed Tomography (CT) for FT synthesis. *Chemical Engineering Journal*, *300*, 317-333.

Al Mesfer, M. K., Sultan, A. J., & Al-Dahhan, M. H. (2017). Study the effect of dense internals on the liquid velocity field and turbulent parameters in bubble column for Fischer–Tropsch (FT) synthesis by using radioactive particle tracking (RPT) technique. *Chemical Engineering Science*, *161*, 228-248.

Anastasiou, A. D., Passos, A. D., & Mouza, A. A. (2013). Bubble columns with fine pore sparger and non-Newtonian liquid phase: prediction of gas holdup. *Chemical Engineering Science, 98*, 331-338.

ANSYS® FLUENT, User Guide, 2017.

Antal, S. P., Lahey, R. T., & Flaherty, J. E. (1991). Analysis of phase distribution in fully developed laminar bubbly two-phase flow. *International Journal of Multiphase Flow*, 17(5), 635-652.

Avdeev A.A. (2016) Bubble Breakup. In: Bubble Systems. Mathematical Engineering. *Springer, Cham,* Cham, Switzerland.

Azbel, D., & Athanasios, I. L. (1983). A mechanism of liquid entrainment. *Handbook of Fluids in Motion*, 453-482.

Bai, W., Deen, N. G., & Kuipers, J. A. M. (2011). Numerical investigation of gas holdup and phase mixing in bubble column reactors. *Industrial & Engineering Chemistry Research*, *51*(4), 1949-1961.

Baird, M. H. I., & Rice, R. G. (1975). Axial dispersion in large unbaffled columns. *Chemical Engineering Journal, 9*(2), 171-174.

Bando, Y., Kuraishi, M., Nishimura, M., Ando, S., Hattori, M., & Aoyama, K. (1988). Effect of gas-liquid flow mode and column diameter on gas holdup and gas-Liquid Interfacial area in bubble column. *Journal of Chemical Engineering of Japan, 14*(2), 182-188.

Baroni, D. B., Filho, J. S. C., Lamy, C. A., Bittencourt, M. S. Q., Pereira, C. M. N. A., & Motta, M. S. (2011). Determination of size distribution of bubbles in a bubbly column two-phase flows by ultrasound and neural networks. International Nuclear Atlantic Conference, Belo Horizonte, Brazil.

Batchelor, G. K. (2000). An introduction to fluid dynamics. Cambridge University Press, Cambridge, UK.

Besagni, G., Gallazzini, L., & Inzoli, F. (2017). On the scale-up criteria for bubble columns. *Petroleum*.

Besagni, G., Inzoli, F., & Ziegenhein, T. (2018). Two-Phase Bubble Columns: A Comprehensive Review. *ChemEngineering*, *2*(2), 13.

Bhusare, V. H., Dhiman, M. K., Kalaga, D. V., Roy, S., & Joshi, J. B. (2017). CFD simulations of a bubble column with and without internals by using OpenFOAM. *Chemical Engineering Journal*, 317, 157-174.

Buwa, V. V., & Ranade, V. V. (2003). Mixing in bubble column reactors: role of unsteady flow structures. *The Canadian Journal of Chemical Engineering*, *81*(3-4), 402-411.

Carleton, A. J., Flain, R. J., Rennie, J., & Valentin, F. H. H. (1967). Some properties of a packed bubble column. *Chemical Engineering Science, 22*(12), 1839-1845.G. D.

Casanave, D., Galtier, P., & Viltard, J. C. (1999). U.S. Patent No. 5,961,933. Washington, DC: U.S. Patent and Trademark Office.

Chaouki, J., Larachi, F., & Duduković, M. P. (1997). Noninvasive tomographic and velocimetric monitoring of multiphase flows. *Industrial & Engineering Chemistry Research*, *36*(11), 4476-4503.

Chapra, S. C., & Canale, R. (2005). Numerical Methods for Engineers. McGraw-Hill Education, USA.

Chen, J., Jamialahmadi, M., & Li, S. M. (1989). Effect of liquid depth on circulation in bubble columns: a visual study. *Chemical Engineering Research and Design, 67*, 203-207.

Chen, J., Li, F., Degaleesan, S., Gupta, P., Al-Dahhan, M. H., Dudukovic, M. P., & Toseland, B. A. (1999). Fluid dynamic parameters in bubble columns with internals. *Chemical Engineering Science*, *54*(13), 2187-2197.

Chen, P. (2004). Modeling the fluid dynamics of bubble column flows. Doctoral dissertation, Washington University, Saint Louis, Missouri, USA.

Chen, P., Sanyal, J., & Duduković, M. P. (2005). Numerical simulation of bubble columns flows: effect of different breakup and coalescence closures. *Chemical Engineering Science*, *60*(4), 1085-1101.

Clark, K. N. (1990). The effect of high pressure and temperature on phase distributions in a bubble column. *Chemical Engineering Science, 45(8)*, 2301-2307.

Clark, K. N., Foster, N. R., & Weiss, R. G. (1983). Evaluation of the neutron absorption technique for the determination of residence time distributions in coal hydrogenation reactors. In Chemeca 83: Chemical Engineering Today; Coping with Uncertainty; the Eleventh Australian Chemical Engineering Conference (p. 237). Institution of Chemical Engineers.

Cokljat, D., Slack, M., Vasquez, S. A., Bakker, A., & Montante, G. (2006). Reynolds-stress model for Eulerian multiphase. *Progress in Computational Fluid Dynamics, An International Journal*, *6*(1-3), 168-178.

Coulaloglou, C.A., 1975. Dispersed phase interactions in an agitated flow vessel, PhD dissertation, Illinois Institute of Technology, Chicago, USA.

Daly, J. G., Patel, S. A., & Bukur, D. B. (1992). Measurement of gas holdups and sauter mean bubble diameters in bubble column reactors by dynamics gas disengagement method. *Chemical Engineering Science, 47*(13-14), 3647-3654.

Dickin, F., & Wang, M. (1996). Electrical resistance tomography for process applications. *Measurement Science and Technology*, *7*(3), 247.

Deckwer, W. D., Louisi, Y., Zaidi, A., & Ralek, M. (1980). Hydrodynamic properties of the Fischer-Tropsch slurry process. *Industrial & Engineering Chemistry Process Design and Development*, *19*(4), 699-708.

Deen, N. G., Hjertager, B. H., & Solberg, T. (2000, July). Comparison of PIV and LDA measurement methods applied to the gas-liquid flow in a bubble column. In 10th international symposium on applications of laser techniques to fluid mechanics.

Degaleesan, S. (1997). Fluid dynamic measurements and modeling of liquid mixing in bubble columns. D.Sc. Thesis, Washington University, St. Louis.

Degaleesan, S., & Duduković, M. P. (1998). Liquid backmixing in bubble columns and the axial dispersion coefficient. *AIChE Journal, 44*(11), 2369-2378.

Degaleesan, S., Dudukovic, M., & Pan, Y. (2001). Experimental study of gas-induced liquid-flow structures in bubble columns. *AIChE Journal*, *47*(9), 1913-1931.

Delnoij, E., Westerweel, J., Deen, N. G., Kuipers, J. A. M., & van Swaaij, W. P. M. (1999). Ensemble correlation PIV applied to bubble plumes rising in a bubble column. *Chemical Engineering Science, 54*(21), 5159-5171.

Devanathan, N. (1991). Investigation of liquid hydrodynamics in bubble columns via a computer automated radioactive particle tracking (CARPT) facility. Washington University, St. Louis, Missouri, USA.

Devanathan, N., Moslemian, D., & Dudukovic, M. P. (1990). Flow mapping in bubble columns using CARPT. *Chemical Engineering Science, 45*(8), 2285-2291.

Doshi, Y. K., & Pandit, A. B. (2005). Effect of internals and sparger design on mixing behavior in sectionalized bubble column. *Chemical Engineering Journal*, *112*(1-3), 117-129

Eickenbusch, H., Brunn, P. O., & Schumpe, A. (1995). Mass transfer into viscous pseudoplastic liquid in large-diameter bubble columns. *Chemical Engineering and Processing: Process Intensification, 34*(5), 479-485.

Eissa, S. H., & Schügerl, K. (1975). Holdup and backmixing investigations in cocurrent and countercurrent bubble columns. *Chemical Engineering Science, 30*(10), 1251-1256.

Ekambara, K., & Joshi, J. B. (2003). CFD simulation of mixing and dispersion in bubble columns. *Chemical Engineering Research and Design, 81*(8), 987-1002.

Ekambara, K., Nandakumar, K., & Joshi, J. B. (2008). CFD simulation of bubble column reactor using population balance. *Industrial & Engineering Chemistry Research*, 47(21), 8505-8516.

Elgobashi, S. (1991). Particle-laden turbulent flows: direct simulation and closure models. *Applied science Research*, *48*, 301-314.

Field, R. W. and Davidson, J. F. (1980). Axial dispersion in bubble columns, *Transactions of the Institution of Chemical Engineers, 58*(4), 228-236.

Forret, A., Schweitzer, J. M., Gauthier, T., Krishna, R., & Schweich, D. (2003). Liquid dispersion in large diameter bubble columns, with and without internals. *The Canadian Journal of Chemical Engineering*, *81*(3-4), 360-366.

Frank, T., Shi, J., & Burns, A. D. (2004, September). Validation of Eulerian multiphase flow models for nuclear safety application. In Proceeding of the Third International Symposium on Two-Phase Modelling and Experimentation, Pisa, Italy.

Fransolet, E., Crine, M., Marchot, P., & Toye, D. (2005). Analysis of gas holdup in bubble columns with non-Newtonian fluid using electrical resistance tomography and dynamic gas disengagement technique. *Chemical Engineering Science, 60*(22), 6118-6123.

Fu, X. Y., & Ishii, M. (2003a). Two-group interfacial area transport in vertical air–water flow: I. Mechanistic model. *Nuclear Engineering and Design, 219*(2), 143-168.

Fu, X. Y., & Ishii, M. (2003b). Two-group interfacial area transport in vertical air–water flow-II. Model evaluation. *Nuclear Engineering and Design*, *219*(2), 169-190.

Garg, V. K. (1998). Applied computational fluid dynamics. CRC Press, Boca Raton, Florida, USA.

George, K. J. (2015). Investigations in Hydrodynamics and Mixing Pattern in the Bubble Column Equipped with Internals. Electronic Thesis and Dissertation Repository. Paper 3167.

George, K. J., Jhawar, A. K., & Prakash, A. (2017). Investigations of flow structure and liquid mixing in bubble column equipped with selected internals. *Chemical Engineering Science, 170*, 297-305.

Gidaspow, D. (1994). Multiphase flow and fluidization: continuum and kinetic theory descriptions. Academic Press, New York City, New York, USA.

Godbole, S. P., Honath, M. F., & Shah, Y. T. (1982). Holdup structure in highly viscous Newtonian and non-Newtonian liquids in bubble columns. *Chemical Engineering Communications, 16*(1-6), 119-134.

Golub, G., Greenbaum, A., Stuart, A., & Suli, E (2007). Numerical mathematics and scientific computation, Oxford University Press Inc, New York, USA.

Grover, G. S., Rode, C. V., & Chaudhari, R. V. (1986). Effect of temperature on flow regimes and gas hold-up in a bubble column. *The Canadian Journal of Chemical Engineering, 64(3)*, 501-504.

Guan, X., & Yang, N. (2017). CFD simulation of pilot-scale bubble columns with internals: Influence of interfacial forces. *Chemical Engineering Research and Design*, 126, 109-122.

Guan, X., Gao, Y., Tian, Z., Wang, L., Cheng, Y., & Li, X. (2015). Hydrodynamics in bubble columns with pin-fin tube internals. *Chemical Engineering Research and Design*, *102*, 196-206.

Guan, X., Li, Z., Wang, L., Cheng, Y., & Li, X. (2014). CFD simulation of bubble dynamics in bubble columns with internals. *Industrial & Engineering Chemistry Research*, *53*(42), 16529-16538.

Guo, X., & Chen, C. (2017). Simulating the impacts of internals on gas-liquid hydrodynamics of bubble column. *Chemical Engineering Science*, 174, 311-325.

Hamed, M. (2012). *Hydrodynamics, Mixing, and Mass Transfer in Bubble Columns with Internals*. Washington University in St. Louis, USA.

Haque, M. W., Nigam, K. D. P., Viswanathan, K., & Joshi, J. B. (1988). Studies on bubble rise velocity in bubble columns employing non-Newtonian solutions. *Chemical Engineering Communications, 73*(1), 31-42.

Hikita, H., & Kikukawa, H. (1974). Liquid-phase mixing in bubble columns: effect of liquid properties. *Chemical Engineering Journal*, *8*(3), 191-197.

Hikita, H., Asai, S., Tanigawa, K., Segawa, K., & Kitao, M. (1980). Gas hold-up in bubble columns. *The Chemical Engineering Journal, 20*(1), 59-67.

Hills, J. H. (1976). The operation of a bubble column at high throughputs: I. Gas holdup measurements. *The Chemical Engineering Journal, 12*(2), 89-99.

Hinze, J. O. (1955). Fundamentals of the hydrodynamic mechanism of splitting in dispersion processes. *AIChE Journal, 1*(3), 289-295.

Hinze, J. O. (1975). Turbulence. McGraw-Hill, New York City, New York, USA.

Howarth, W. J. (1964). Coalescence of drops in a turbulent flow field. *Chemical Engineering Science, 19*(1), 33-38.

Hughmark, G. A. (1967). Holdup and mass transfer in bubble columns. *Industrial & Engineering Chemistry Process Design and Development*, 6(2), 218-220.

Hulburt, H. M., & Katz, S. (1964). Some problems in particle technology: A statistical mechanical formulation. *Chemical Engineering Science, 19*(8), 555-574.

Ishii, M., & Hibiki, T. (2010). Thermo-fluid dynamics of two-phase flow. Springer Science & Business Media, Berlin, Germany.

Jakobsen, H. A. (2003). Numerical convection algorithms and their role in Eulerian CFD reactor simulations. *International Journal of Chemical Reactor Engineering*, *1*(1).1-15.

Jakobsen, H. A., Sannæs, B. H., Grevskott, S., & Svendsen, H. F. (1997). Modeling of vertical bubble-driven flows. *Industrial & Engineering Chemistry Research*, *36*(10), 4052-4074.

Jasim, A., 2016. The impact of heat exchanging internals on hydrodynamics of bubble column reactor. Missouri University of Science and Technology, Rolla, Missouri, USA.

Jiang, X., Yang, N., & Yang, B. (2016). Computational fluid dynamics simulation of hydrodynamics in the riser of an external loop airlift reactor. *Particuology*, *27*, 95-101

Jin, H., Yuhuan, H., & Suohe, Y. (2009). Gas-Liquid flow characterization in bubble columns with various gas-liquid using electrical resistance tomography. In Journal of Physics: Conference Series (Vol. 147, No. 1, p. 012032). IOP Publishing.

Johnson, C. (2012). Numerical solution of partial differential equations by the finite element method. Courier Corporation, Rolla, Missouri, USA.

Joshi, J. B. (1982). Gas phase dispersion in bubble columns. *The Chemical Engineering Journal*, *24*(2), 213-216.

Joshi, J. B., & Lali, A. M. (1984). Velocity-hold up relationship in multiphase contactors—a unified approach. *Frontiers in Chemical Reaction Engineering*, 1, 330-344.

Kagumba, M., & Al-Dahhan, M. H. (2015). Impact of internals size and configuration on bubble dynamics in bubble columns for alternative clean fuels production. *Industrial & Engineering Chemistry Research*, *54*(4), 1359-1372.

Kalaga, D. V., Pant, H. J., Dalvi, S. V., Joshi, J. B., & Roy, S. (2017a). Investigation of Hydrodynamics in Bubble Column with Internals using Radioactive Particle Tracking (RPT). *AIChE Journal*.

Kalaga, D. V., Yadav, A., Goswami, S., Bhusare, V., Pant, H. J., Dalvi, S. V., Joshi, J. B.& Roy, S. (2017b). Comparative analysis of liquid hydrodynamics in a co-current flow-through bubble column with densely packed internals via radiotracing and Radioactive Particle Tracking (RPT). *Chemical Engineering Science*, *170*, 332-346.

Kantak, M. V., Hesketh, R. P., & Kelkar, B. G. (1995). Effect of gas and liquid properties on gas phase dispersion in bubble columns. *The Chemical Engineering Journal and the Biochemical Engineering Journal, 59*(2), 91-100.

Kastánek, F., Zahradník, J., Kratochvíl, J., & Cermák, J. (1993). Chemical reactors for gas-liquid systems, Ellis Horwood, Chichester.

Kawase, Y., Halard, B., & Moo-Young, M. (1987). Theoretical prediction of volumetric mass transfer coefficients in bubble columns for Newtonian and non-Newtonian fluids. *Chemical Engineering Science, 42*(7), 1609-1617.

Kawase, Y., & Moo-Young, M. (1989). Mixing time in bioreactors. *Journal of Chemical Technology & Biotechnology*, *44*(1), 63-75.

Kazakis, N. A., Mouza, A. A., & Paras, S. V. (2008). Experimental study of bubble formation at metal porous spargers: effect of liquid properties and sparger characteristics on the initial bubble size distribution. *Chemical Engineering Journal*, *137*(2), 265-281.

Kennard, E. H. (1938). Kinetic theory of gases, with an introduction to statistical mechanics.

Kitscha, J., & Kocamustafaogullari, G. (1989). Breakup criteria for fluid particles. *International Journal of Multiphase Flow*, *15*(4), 573-588.

Kolmogorov, A. N. (1941, February). The local structure of turbulence in incompressible viscous fluid for very large Reynolds numbers. *Dokl. Akad. Nauk SSSR 30(4).* 299-303.

Komabayasi, M., Gonda, T., & Isono, K. (1964). Life time of water drops before breaking and size distribution of fragment droplets. *Journal of the Meteorological Society of Japan. Ser. II*, *42*(5), 330-340.

Kölbel, H., Langemann, H., & Platz, J. (1962). Eigenschaften des Blasensäulen-Reaktors-Das Verweilzeitspektrum der gasförmigen Phase. *Dechema Monographien, 41*, 225-243.

Krishna, R., & Ellenberger, J. (1996). Gas holdup in bubble column reactors operating in the churn-turbulent flow regime. *AIChE Journal, 42*(9), 2627-2634.

Krishna, R., Baten, J. V., & Urseanu, M. I. (2001). Scale effects on the hydrodynamics of bubble columns operating in the homogeneous flow regime. *Chemical Engineering & Technology, 24*(5), 451.

Krishna, R., De Swart, J. W., Ellenberger, J., Martina, G. B., & Maretto, C. (1997). Gas holdup in slurry bubble columns: effect of column diameter and slurry concentrations. *AIChE Journal, 43*(2), 311-316.

Krishna, R., & Sie, S. T. (2000). Design and scale-up of the Fischer–Tropsch bubble column slurry reactor. *Fuel Processing Technology*, *64*(1-3), 73-105.

Krishna, R., Urseanu, M. I., Van Baten, J. M., & Ellenberger, J. (1999). Influence of scale on the hydrodynamics of bubble columns operating in the churn-turbulent regime: experiments vs. Eulerian simulations. *Chemical Engineering Science*, *54*(21), 4903-4911.

Krishna, R., Van Baten, J. M., & Urseanu, M. I. (2000). Three-phase Eulerian simulations of bubble column reactors operating in the churn-turbulent regime: a scale up strategy. *Chemical Engineering Science*, *55*(16), 3275-3286.

Krishna, R., Wilkinson, P. M., & Van Dierendonck, L. L. (1991). A model for gas holdup in bubble columns incorporating the influence of gas density on flow regime transitions. *Chemical Engineering Science, 46*(10), 2491-2496.

Kuboi, R., Komasawa, I., & Otake, T. (1972a). Behavior of dispersed particles in turbulent liquid flow. *Journal of Chemical Engineering of Japan, 5*(4), 349-355.

Kuboi, R., Komasawa, I., & Otake, T. (1972b). Collision and coalescence of dispersed drops in turbulent liquid flow. *Journal of Chemical Engineering of Japan, 5*(4), 423-424.

Kumar, S. B., Dudukovic, M. P., & Toseland, B. A. (1997). Measurement techniques for local and global fluid dynamic quantities in two and three phase systems. *Non-Invasive Monitoring of Multiphase Flows*, 1-45.

Kundu, P. K, Cohen, I. M (2004) Fluid Mechanics, Third edition, Elsevier Academic Press, San Diego, California, USA.

Laborde-Boutet, C., Larachi, F., Dromard, N., Delsart, O., & Schweich, D. (2009). CFD simulation of bubble column flows: Investigations on turbulence models in RANS approach. *Chemical Engineering Science*, *64*(21), 4399-4413.

Larachi, F., Desvigne, D., Donnat, L., Schweich, D., (2006). Simulating the effects of liquid circulation in bubble columns with internals. *Chemical Engineering Science*, 41, 4195–4206.

Lee, J. C., & Hodgson, T. D. (1968). Film flow and coalescence-I Basic relations, film shape and criteria for interface mobility. *Chemical Engineering Science, 23*(11), 1375-1397.

Lee, Y. H., Kim, Y. J., Kelkar, B. G., & Weinberger, C. B. (1985). A simple digital sensor for dynamic gas holdup measurements in bubble columns. *Industrial & Engineering Chemistry Fundamentals, 24*(1), 105-107.

Lehr, F., & Mewes, D. (2001). A transport equation for the interfacial area density applied to bubble columns. *Chemical Engineering Science, 56*(3), 1159-1166.

Lehr, F., Millies, M., & Mewes, D. (2002). Bubble-Size distributions and flow fields in bubble columns. *AIChE Journal, 48*(11), 2426-2443.

Levenspiel, O. (1999). Chemical reaction engineering. *Industrial & Engineering Chemistry Research*, *38*(11), 4140-4143.

Li, H., & Prakash, A. (2000). Influence of slurry concentrations on bubble population and their rise velocities in a three-phase slurry bubble column. *Powder Technology, 113*(1), 158-167.

Liao, Y., & Lucas, D. (2009). A literature review of theoretical models for drop and bubble breakup in turbulent dispersions. *Chemical Engineering Science, 64*(15), 3389-3406.

Liao, Y., & Lucas, D. (2010). A literature review on mechanisms and models for the coalescence process of fluid particles. *Chemical Engineering Science, 65*(10), 2851-2864.

Leifer, I., De Leeuw, G., & Cohen, L. H. (2003). Optical measurement of bubbles: system design and application. *Journal of Atmospheric and Oceanic Technology*, *20*(9), 1317-1332.

Lin, J. S., Chen, M. M., & Chao, B. T. (1985). A novel radioactive particle tracking facility for measurement of solids motion in gas fluidized beds. *AIChE Journal, 31*(3), 465-473.

Lin, T. J., Tsuchiya, K., & Fan, L. S. (1998). Bubble flow characteristics in bubble columns at elevated pressure and temperature. *AIChE Journal, 44*(3), 545-560.

Luo, H. (1993). Coalescence, Breakup and Liquid Circulation in Bubble Column Reactors, Department of Energy. Norges Tekniske Hoegskole, Trondheim.

Luo, H., & Svendsen, H. F. (1996). Theoretical model for drop and bubble breakup in turbulent dispersions. *AIChE Journal, 42*(5), 1225-1233.

Majumder, S. K. (2008). Analysis of dispersion coefficient of bubble motion and velocity characteristic factor in down and upflow bubble column reactor. *Chemical Engineering Science, 63(*12), 3160-3170.

Makkawi, Y. T., & Wright, P. C. (2002). Fluidization regimes in a conventional fluidized bed characterized by means of electrical capacitance tomography. *Chemical Engineering Science*, *57*(13), 2411-2437.

Mangartz, K. H., & Pilhofer, T. (1981). Interpretation of mass transfer measurements in bubble columns considering dispersion of both phases. *Chemical Engineering Science, 36*(6), 1069-1077.

Maruyama, T., Yoshida, S., & Mizushina, T. (1981). The flow transition in a bubble column. *Journal of Chemical Engineering of Japan, 14*(5), 352-357.

Masood, R. M. A., Rauh, C., & Delgado, A. (2014). CFD simulation of bubble column flows: An explicit algebraic Reynolds stress model approach. *International Journal of Multiphase Flow, 66*, 11-25.

Mathieu, J., & Scott, J. (2000). An introduction to turbulent flow. Cambridge University Press, Cambridge, UK.

Maxwell, J. C. (1873). A treatise on electricity and magnetism, Clarendon Press, Oxford, UK.

McClure, D. D., Aboudha, N., Kavanagh, J. M., Fletcher, D. F., & Barton, G. W. (2015). Mixing in bubble column reactors: experimental study and CFD modeling. *Chemical Engineering Journal*, 264, 291-301.

McClure, D. D., Kavanagh, J. M., Fletcher, D. F., & Barton, G. W. (2014). Development of a CFD model of bubble column bioreactors: part two–comparison of experimental data and CFD predictions. *Chemical Engineering & Technology*, *37*(1), 131-140.

McClure, D. D., Kavanagh, J. M., Fletcher, D. F., & Barton, G. W. (2017). Experimental investigation into the drag volume fraction correction term for gas-liquid bubbly flows. *Chemical Engineering Science*, *170*, 91-97.

Merchuk, J. C., & Stein, Y. (1981). Local hold-up and liquid velocity in air-lift reactors. *AIChE Journal, 27*(3), 377-388.

Men'shchikov, V. A., & Aerov, M. E. (1968). Measuring the local gas content in a bubbling layer. *Journal of Engineering Physics, 15*(2), 697-700.

Nguten, T. V., Song, C. H., Bae, B. U., & Euh, D. J. (2013). Modeling of bubble coalescence and break-up considering turbulent suppression phenomena in bubbly two-phase flow. *International Journal of Multiphase Flow*, *54*, 31-42.

Mirón, A. S., García, M. C. C., Camacho, F. G., Grima, E. M., & Chisti, Y. (2004). Mixing in bubble column and airlift reactors. *Chemical Engineering Research and Design*, *82*(10), 1367-1374.

Mirvakili, A., Bakhtyari, A., & Rahimpour, M. R. (2018). A CFD modeling to investigate the impact of flow mal-distribution on the performance of industrial methanol synthesis reactor. *Applied Thermal Engineering*, *128*, 64-78.

Mitsutake, T., Morooka, S., Suzuki, K., Tsunoyama, S., & Yoshimura, K. (1990). Void fraction estimation within rod bundles based on three-fluid model and comparison with X-ray CT void data. *Nuclear Engineering and Design*, *120*(2-3), 203-212.

Miyauchi, T. (1970). Flow of fluid in gas-bubble columns. *Kagaku Kogaku, 34*, 958-964.

Muharam Y., Dianursanti, Pramadana A.B., Wirya A.S., 2017, Modelling and simulation of a bubble column photobioreactor for the cultivation of microalgae nannochloropsis salina, *Chemical Engineering Transactions, 56*, 1555-1560.

Maurer, S., Wagner, E. C., van Ommen, J. R., Schildhauer, T. J., Teske, S. L., Biollaz, S. M., ... & Mudde, R. F. (2015). Influence of vertical internals on a bubbling fluidized bed characterized by X-ray tomography. *International Journal of Multiphase Flow*, *75*, 237-249.

Moslemian, D., Devanathan, N., & Dudukovic, M. P. (1992). Radioactive particle tracking technique for investigation of phase recirculation and turbulence in multiphase systems. *Review of Scientific Instruments, 63*(10), 4361-4372.

Mudde, R. F., Groen, J. S., & Van Den Akker, H. E. A. (1997). Liquid velocity field in a bubble column: LDA experiments. *Chemical Engineering Science, 52*(21-22), 4217-4224.

Myers, K. J., Duduković, M. P., & Ramachandran, P. A. (1987). Modelling churn-turbulent bubble columns—I. Liquid-phase mixing. *Chemical Engineering Science*, *42*(10), 2301-2311.

Nishikawa, M., Kato, H., & Hashimoto, K. (1977). Heat transfer in aerated tower filled with non-Newtonian liquid. *Industrial & Engineering Chemistry Process Design and Development, 16*(1), 133-137.

Oakley, T. R., Loth, E., & Adrian, R. J. (1997). A two-phase cinematic PIV method for bubbly flows. *Journal of Fluids Engineering, 119*(3), 707-712.

Oey, R. S., Mudde, R. F., & Van den Akker, H. E. A. (2003). Sensitivity study on interfacial closure laws in two-fluid bubbly flow simulations. *AIChE Journal*, *49*(7), 1621-1636.

Pakzad, L., Ein-Mozaffari, F., & Chan, P. (2008). Using electrical resistance tomography and computational fluid dynamics modeling to study the formation of cavern in the mixing of pseudoplastic fluids possessing yield stress. *Chemical Engineering Science*, *63*(9), 2508-2522.

Pandit, A. B., Varley, J., Thorpe, R. B., & Davidson, J. F. (1992). Measurement of bubble size distribution: an acoustic technique. *Chemical Engineering Science*, *47*(5), 1079-1089.

Park, J. Y., & Blair, L. M. (1975). The effect of coalescence on drop size distribution in an agitated liquid-liquid dispersion. *Chemical Engineering Science, 30*(9), 1057-1064.

Patankar, S. V., & Spalding, D. B. (1983). A calculation procedure for heat, mass and momentum transfer in three-dimensional parabolic flows. In *Numerical Prediction of Flow, Heat Transfer, Turbulence and Combustion* (pp. 54-73).

Peiró, J., & Sherwin, S. (2005). Finite difference, finite element and finite volume methods for partial differential equations. In *Handbook of materials modeling* (2415-2446). Springer, Dordrecht. Netherlands.

Pfleger, D., & Becker, S. (2001). Modelling and simulation of the dynamic flow behaviour in a bubble column. *Chemical Engineering Science*, *56*(4), 1737-1747.

Pradhan, A. K., Parichha, R. K., & De, P. (1993). Gas hold-up in non-Newtonian solutions in a bubble column with internals. *The Canadian Journal of Chemical Engineering, 71(3)*, 468-471.

Prakash, A., Margaritis, A., Li, H., & Bergougnou, M. A. (2001). Hydrodynamics and local heat transfer measurements in a bubble column with suspension of yeast. *Biochemical Engineering Journal, 9*(2), 155-163.

Prince, M. J., & Blanch, H. W. (1990). Bubble coalescence and break-up in air-sparged bubble columns. *AIChE Journal, 36*(10), 1485-1499.

Ramkrishna, D. (2000). Population balances: Theory and applications to particulate systems in engineering. Academic Press, New York City, New York, USA.

Rampure, M. R., Kulkarni, A. A., & Ranade, V. V. (2007). Hydrodynamics of bubble column reactors at high gas velocity: experiments and computational fluid dynamics (CFD) simulations. *Industrial & Engineering Chemistry Research, 46*(25), 8431-8447.

Ranade, V. V., & Tayalia, Y. (2001). Modelling of fluid dynamics and mixing in shallow bubble column reactors: influence of sparger design. *Chemical Engineering Science, 56*(4), 1667-1675.

Reese, J., Chen, R. C., & Fan, L. S. (1995). Three-dimensional particle image velocimetry for use in three-phase fluidization systems. *Experiments in fluids, 19*(6), 367-378.

Richardson, L. F. (1922). Weather Prediction by Numerical Process. Cambridge: Cambridge University Press, Cambridge, UK.

Roache, P. J. (1992). A flux-based modified method of characteristics. *International Journal for Numerical Methods in Fluids*, *15*(11), 1259-1275.

Rollbusch, P., Becker, M., Ludwig, M., Bieberle, A., Grünewald, M., Hampel, U., & Franke, R. (2015). Experimental investigation of the influence of column scale, gas density and liquid properties on gas holdup in bubble columns. *International Journal of Multiphase Flow, 75*, 88-106.

Ross, S. L. (1971). Measurements and models of the dispersed phase mixing process, PhD dissertation, The University of Michigan, USA.

Roy, S., & Joshi, J. B. (2008). CFD study of mixing characteristics of bubble column and external loop airlift reactor. *Asia-Pacific Journal of Chemical Engineering, 3*(2), 97-105.

Rusche, H. (2003). Computational fluid dynamics of dispersed two-phase flows at high phase fractions. Doctoral dissertation, Imperial College London (University of London), London, UK.

Ruzicka, M. C., Drahoš, J., Mena, P. C., & Teixeira, J. A. (2003). Effect of viscosity on homogeneous–heterogeneous flow regime transition in bubble columns. *Chemical Engineering Journal, 96*(1-3), 15-22.

Salas, M. D., Hefner, J. N., & Sakell, L. (Eds.). (1999). Modeling complex turbulent flows. Springer Science & Business Media, B.V, Berlin, Germany.

Salehi, K., Jokar, S. M., Shariati, J., Bahmani, M., Sedghamiz, M. A., & Rahimpour, M. R. (2014). Enhancement of CO conversion in a novel slurry bubble column reactor for methanol synthesis. *Journal of Natural Gas Science and Engineering*, *21*, 170-183.

Saffman, P. G. F., & Turner, J. S. (1956). On the collision of drops in turbulent clouds. *Journal of Fluid Mechanics*, *1*(1), 16-30.

Saxena, S. C., Rao, N. S., & Saxena, A. C. (1990). Heat-transfer and gas-holdup studies in a bubble column: air-water-glass bead system. *Chemical Engineering Communications, 96*(1), 31-55.

Saxena, S. C., Rao, N. S., & Thimmapuram, P. R. (1992). Gas phase holdup in slurry bubble columns for two-and three-phase systems. *The Chemical Engineering Journal*, *49*(3), 151-159.

Shiller, *L.* and *Naumann*, A. (*1935*). A *Drag* Coefficient Correlation. *Zeitschrift des Vereins Deutscher Ingenieure,* 77, 318-320.

Seher, A., & Schumacher, V. (1979). Determination of residence times of liquid and gas phases in large bubble columns with the aid of radioactive tracers. *German Chemical Engineering, 2*(2), 117-122.

Schumpe, A., & Grund, G. (1986). The gas disengagement technique for studying gas holdup structure in bubble columns. *The Canadian Journal of Chemical Engineering, 64*(6), 891-896.

Shah, Y. T., Kelkar, B. G., Godbole, S. P., & Deckwer, W. D. (1982). Design parameters estimations for bubble column reactors. *AIChE Journal, 28*(3), 353-379.

Shah, Y. T., Stiegel, G. J., & Sharma, M. M. (1978). Backmixing in gas-liquid reactors. *AIChE Journal, 24*(3), 369-400.

Shetty, S. A., Kantak, M. V., & Kelkar, B. G. (1992). Gas-phase backmixing in bubble-column reactors. *AIChE Journal, 38*(7), 1013-1026.

Shinnar, R., & Church, J. M. (1960). Statistical theories of turbulence in predicting particle size in agitated dispersions. *Industrial & Engineering Chemistry, 52*(3), 253-256.

Simonnet, M., Gentric, C., Olmos, E., & Midoux, N. (2008). CFD simulation of the flow field in a bubble column reactor: Importance of the drag force formulation to describe regime transitions. *Chemical Engineering and Processing: Process Intensification*, *47*(9-10), 1726-1737.

Simonin, C., & Viollet, P. L. (1990). Predictions of an oxygen droplet pulverization in a compressible subsonic coflowing hydrogen flow. *Numerical Methods for Multiphase Flows*, 91, 65-82.

Sivasubramanian, V., & Prasad, B. N. (2009). Effects of superficial gas velocity and fluid property on the hydrodynamic performance of an airlift column with alcohol solution. *International Journal of Engineering, Science and Technology, 1*(1), 245-253.

Sokolichin, A., Eigenberger, G., & Lapin, A. (2004). Simulation of buoyancy driven bubbly flow: established simplifications and open questions. *AIChE Journal*, *50*(1), 24-45.

Sovova, H. (1981). Breakage and coalescence of drops in a batch stirred vessel—II comparison of model and experiments. *Chemical Engineering Science*, *36*(9), 1567-1573.

Sriram, K., & Mann, R. (1977). Dynamic gas disengagement: A new technique for assessing the behaviour of bubble columns. *Chemical Engineering Science, 32*(6), 571-580.

Sultan, A. J., Sabri, L. S., Shao, J., & Al-Dahhan, M. H. (2017). Overcoming the gamma-ray computed tomography data processing pitfalls for bubble column equipped with vertical internal tubes. *The Canadian Journal of Chemical Engineering*.

Sun, X. (2001). Two-group interfacial area transport equation for a confined test section. Purdue University, West Lafayette, Indiana, USA.

Sun, X., Kim, S., Ishii, M., & Beus, S. G. (2004). Modeling of bubble coalescence and disintegration in confined upward two-phase flow. *Nuclear Engineering and Design, 230(*1-3), 3-26.

Sutor, A., Heining, M., Lindenberger, C., & Buchholz, R. (2014). Method for optimizing the field coils of internally illuminated photobioreactors. *IEEE Transactions on Magnetics*, *50*(11), 1-4

Tabib, M. V., Roy, S. A., & Joshi, J. B. (2008). CFD simulation of bubble column—an analysis of interphase forces and turbulence models. *Chemical Engineering Journal*, *139*(3), 589-614.

Tang, C., & Heindel, T. J. (2004). Time-dependent gas holdup variation in an air–water bubble column. *Chemical Engineering Science, 59*(3), 623-632.

Tang, C., & Heindel, T. J. (2006). Estimating gas holdup via pressure difference measurements in a cocurrent bubble column. I*nternational Journal of Multiphase Flow, 32(7)*, 850-863.

Tarmy, B. L., Chang, M., Coulaloglou, C. A., & Ponzi, P. R. (1984). The Three-Phase Hydrodynamic Characteristics of the EDS Coal Liquefaction Reactors; Their Development and Use in Reactor Scale-up. International Symposium on Chemical Reaction Engineering, Edinburgh, UK.

Thakre, S. S., Phanikumar, D. V., Khare, A. S., & Joshi, J. B. (1999). CFD modeling of flow, macro-mixing and axial dispersion in a bubble column. *The Canadian Journal of Chemical Engineering, 77*(5), 826-837.

Thaker, K., & Rao, D. P. (2007). Effects of gas redispersion and liquid height on gas–liquid hydrodynamics in a multistage bubble column. *Chemical Engineering Research and Design, 85*(10), 1362-1374.

Taylor, G. I. (1953). Dispersion of soluble matter in solvent flowing slowly through a tube. *Proceedings of the Royal Society*, *219*(1137), 186-203.

Tomiyama, A. (1998). Struggle with computational bubble dynamics. *Multiphase Science and Technology*, 10(4), 369-405.

Tomiyama, A., Tamai, H., Zun, I., & Hosokawa, S. (2002). Transverse migration of single bubbles in simple shear flows. *Chemical Engineering Science, 57*(11), 1849-1858.

Toye, D., Fransolet, E., Simon, D., Crine, M., L'Homme, G., & Marchot, P. (2005). Possibilities and limits of application of electrical resistance tomography in hydrodynamics of bubble columns. *The Canadian Journal of Chemical Engineering*, *83*(1), 4-10.

Towell, G. D. and Ackermann, G. H., (1972). Axial mixing of liquid and gas in large bubble reactors, Proceedings of Fifth European/ Second International Symposium on Chemical Reaction Engineering, Amsterdam, New York, USA.

Tsuchiya, K., & Nakanishi, O. (1992). Gas holdup behavior in a tall bubble column with perforated plate distributors. *Chemical Engineering Science, 47*(13-14), 3347-3354.

Van Baten, J. M., & Krishna, R. (2001). Eulerian simulations for determination of the axial dispersion of liquid and gas phases in bubble columns operating in the churn-turbulent regime. *Chemical Engineering Science, 56*(2), 503-512.

Vera, M. U., Saint-Jalmes, A., & Durian, D. J. (2001). Scattering optics of foam. *Applied Optics*, *40*(24), 4210-4214.

Varma, R. (2008). Characterization of anaerobic bioreactors for bioenergy generation using a novel tomography technique. Washington University in St. Louis, Missouri, USA.

Vermeer, D. J., & Krishna, R. (1981). Hydrodynamics and mass transfer in bubble columns in operating in the churn-turbulent regime. *Industrial & Engineering Chemistry Process Design and Development, 20*(3), 475-482.

Versteeg, H. K., & Malalasekera, W. (2007). An introduction to computational fluid dynamics. Pearson Education Limited, London, UK.

Wachi, S., & Nojima, Y. (1990). Gas-phase dispersion in bubble columns. *Chemical Engineering Science, 45*(4), 901-905.

Wang, T. (2011). Simulation of bubble column reactors using CFD coupled with a population balance model. *Frontiers of Chemical Science and Engineering*, *5*(2), 162-172.

Wang, T., Wang, J., & Jin, Y. (2005). Theoretical prediction of flow regime transition in bubble columns by the population balance model. *Chemical Engineering Science*, *60*(22), 6199-6209.

Wilkinson, P. M., Spek, A. P., & van Dierendonck, L. L. (1992). Design parameters estimation for scale-up of high-pressure bubble columns. *AIChE Journal*, *38*(4), 544-554.

Xu, L., Yuan, B., Ni, H., & Chen, C. (2013). Numerical simulation of bubble column flows in churn-turbulent regime: comparison of bubble size models. *Industrial & Engineering Chemistry Research*, *52*(20), 6794-6802.

Xue, J., Al-Dahhan, M., Dudukovic, M. P., & Mudde, R. F. (2003). Bubble Dynamics Measurements Using Four-Point Optical Probe. *The Canadian Journal of Chemical Engineering, 81*(3-4), 375-381.

Yang, Y. B., Devanathan, N., & Duduković, M. P. (1993). Liquid backmixing in bubble columns via computer-automated radioactive particle tracking (CARPT). *Experiments in Fluids, 16*(1), 1-9.

Yang, W. Q., Xie, C. G., Gamio, J. C., & Beck, M. S. (1995). Design of a capacitance tomographic imaging sensor with uniform electric field-Process tomography-implementation for industrial processes, UMIST Publications, Manchester, UK.

Yamashita, F. (1987). Effects of vertical pipe and rod internals on gas holdup in bubble columns. *Journal of Chemical Engineering of Japan*, *20*(2), 204-206.

Yeh, Y., & Cummins, H. Z. (1964). Localized fluid flow measurements with an He–Ne laser spectrometer. *Applied Physics Letters*, *4*(10), 176-178.

Yeoh, G. H., Cheung, C. P., & Tu, J. (2013). Multiphase flow analysis using population balance modeling: bubbles, drops and particles. Butterworth-Heinemann, UK.

Yin, J., Li, J., Li, H., Liu, W., & Wang, D. (2015). Experimental study on the bubble generation characteristics for an venturi type bubble generator. *International Journal of Heat and Mass Transfer*, *91*, 218-224.

Yoshida, F., & Akita, K. (1965). Performance of gas bubble columns: Volumetric liquid-phase mass transfer coefficient and gas holdup. *AIChE Journal, 11*(1), 9-13.

Youssef, A. A. (2010). Fluid dynamics and scale-up of bubble columns with internals. Washington University in St. Louis, Missouri, USA.

Youssef, A. A., & Al-Dahhan, M. H. (2009). Impact of internals on the gas holdup and bubble properties of a bubble column. *Industrial & Engineering Chemistry Research*, *48*(17), 8007-8013.

Youssef, A. A., Al-Dahhan, M. H., & Dudukovic, M. P. (2013). Bubble columns with internals: a review. *International Journal of Chemical Reactor Engineering*, *11*(1), 169-223.

Zahradnik, J., & Fialova, M. (1996). The effect of bubbling regime on gas and liquid phase mixing in bubble column reactors. *Chemical Engineering Science, 51*(10), 2491-2500.

Zahradnik, J., Fialova, M., Ru, M., Drahos, J., Kastanek, F., & Thomas, N. H. (1997). Duality of the gas-liquid flow regimes in bubble column reactors. *Chemical Engineering Science*, *52*(21-22), 3811-3826.

Zhang, Y., L, J., Wang, L., & Li, X. (2009). Studies on hydrodynamics of turbulent slurry bubble column (III) Effect of vertical pipe bundles. *Journal of the Chemical Industry and Engineering Society of China*, *5*.

Zhang, Z. (2010). LDA application methods: laser Doppler anemometry for fluid dynamics. Springer Science & Business Media. Berlin, Germany.

Zou, R., Jiang, X., Li, B., Zu, Y., & Zhang, L. (1988). Studies on gas holdup in a bubble column operated at elevated temperatures. *Industrial & Engineering Chemistry Research, 27*(10), 1910-1916.

Zufiria, J. A. (1988). Bubble competition in Rayleigh–Taylor instability. *The Physics of Fluids, 31*(3), 440-446.

Žun, I. (1980). The transverse migration of bubbles influenced by walls in vertical bubbly flow. *International Journal of Multiphase Flow*, *6*(6), 583-588.